



**UNIVERSITY
OF BRASILIA**

Chemistry Institute
Graduate Program in Chemistry
LabPoIN



**UNIVERSITÉ
DE LORRAINE**

Ecole doctorale SIMPEE Laboratoire
LERMAB

Doctoral thesis

**Production of biomaterials composed of
polyurethane foam and heat treated wood fibers**

**Produção de biomateriais compostos por
espuma de poliuretano e fibras de madeira
tratadas termicamente**

Rodolfo ANDRADE BREVES

Advisors: Prof. Maria José ARAÚJO SALES and
Prof. Mathieu PÉTRISSANS

Co-advisor: Prof^a. Roseany de V. Vieira Lopes

Brasília, DF
2024



**UNIVERSITY
OF BRASILIA**

Chemistry Institute
Graduate Program in Chemistry
LabPoIN



**UNIVERSITÉ
DE LORRAINE**

Ecole doctorale SIMPEE Laboratoire
LERMAB

Doctoral thesis

Production of biomaterials composed of polyurethane foam and heat treated wood fibers

Produção de biomateriais compostos por espuma de poliuretana e fibras de madeira tratadas termicamente

Doctoral thesis presented for the Chemistry Grad School Program (PPGQ) of University of Brasília, as a requirement for obtaining the Doctor title, with the guidance of Prof^a. Maria José Araújo Sales & Prof. Dr. Mathieu Petrissans and co-advisor of Prof^a. Roseany de V. Vieira Lopes.

Rodolfo Andrade Breves

Brasília, DF
2024

I dedicate this work to my family, friends, professors, advisors,
and technicians for all the patience and
continued support during all this journey.
It would not have been possible without all your help.

THANKS

Too many people helped me throughout this long and challenging journey who deserve special thanks. First, I would like to thank my parents, Mario Batista Breves and Maria Divina Xavier Andrade Breves, for having supported and given me the opportunity I needed to have reached this far.

To my Advisor from Brazil, Prof^a. Dr^a. Maria José Araújo Sales, for accepting me into her laboratory and allowing me to work with her since I was an inexperienced undergraduate student and for allowing us to work together since then.

To my co-advisor Prof^a. Dr^a. Roseany de Vasconcelos Vieira Lopes for her unending patience and support whenever I needed, investing countless hours in helping me realize this work always filled with optimism.

To Professor Rafael Quirino for not only presenting me with this co-tutorship opportunity, but also for constantly helping me when I had doubts about the results of my work and for the DMA analysis.

To my French advisor Prof. Dr. Mathieu Pétrissans, for accepting me into his lab and providing me with all the support I needed for the development of this work.

To Dr. Baptiste Colin, who readily helped me all the times I needed since my very first day at the IUT and for the help with the preparation of the wood samples I used in this work.

To Professor Dr. Anelie Pétrissans who, despite not being in my direct leadership, always supported me when I needed with care and patience.

To Professor Dr. Adail de Castro Carvalheiro and the UnB farm Água Limpa, for providing me the samples of Carvoeiro.

To the ANP and Dr. Paulo Mattos, for allowing me to run viscosity and oxidative stability in their lab, even though this line of work was discontinued.

To the CAIQ (Analytical Central from the Chemistry Institute) for the FTIR, TGA/DTG and NMR analysis.

To the college in my PhD group for sharing this experience with me.

To former undergraduate student Tayane Alencar Marques Serafim who collaborated in the initial stages of this work.

To the undergrad student Letícia Valença, for helping me with the final steps of this work.

To all the technicians who helped me in so many ways to count and name

Special thanks to CAPES, CNPq, IQ-UnB, IUT Épinal- Hubert Curien and the French Embassy from Brazil, for the financial support.

ABSTRACT

The search for renewable materials with low production costs stimulated this work, where composites were prepared from vegetable oil (VO) and wood sawdust. The polyol used to obtain polyurethanes (PU) was prepared by epoxidation of the Macauba seed oil (MKO) followed by opening the rings with glycerol, increasing the amount of hydroxyl groups in the fatty acid chains, which is an innovative method. The wood powder was used to reinforce the PU polymeric matrix to add value to the final product. Amounts of reagents used for epoxidation of the MKO with formic acid and H₂O₂ were calculated based on the unsaturation per mole of the MKO, determined by integrating the peaks into its ¹H NMR spectrum. The epoxide ring opening (EPKO) reaction occurred with 1:1 ratio, glycerin and EPMKO. BF₃(Et₂O) was used at 10% as catalyst. PU were prepared in different [NCO]/[OH] molar ratio. Composites were obtained by adding wood powder to the PU matrices. The wood species used were beech (*Fagus sylvatica*), fir (*Albies alba*) and charcoal (*Tachigali vulgaris*) (CV). Before getting the PU, the woods were pre-treated and its samples dried at 103 °C, until the mass stabilized. All the woods were treated for 2 °C·min⁻¹ heating rate until a set temperature, followed by a 30 min isothermal. By analyzing the DTG deconvolution data and wood fractionation, the treatment temperatures chosen were: 275 °C, 310 °C, and 290 °C, for beech, fir, and CV, respectively. The delignification of the CV was closer to that of spruce than that of beech, with small increments in the cellulose/hemicellulose ratio until cellulose degradation. The formation of epoxide and polyol was confirmed by FTIR and ¹H NMR. The calculated OH index, 85.57 mg KOH/g, was low for a polyol from VO with few unsaturation. PU were produced at three different [NCO]/[OH] ratios and showed similar FTIR spectra, especially PU 1.0 and 1.2, indicating that after the 1.0 ratio, the added isocyanate remains in excess. It was observed that the FTIR spectra of the composites with the C-N peak almost identical in samples with 1.0 and 1.2 [NCO]/[OH], being lower for PU 0.8. Composites with raw wood showed differences in the C-N peak in PU 1.0 and 1.2 and did not exhibit as much residual -OH as the other samples. TG and DTG curves of PU 1.0 showed three usual degradation peaks. PU 0.8 and 1.2 showed 4 peaks, suggesting that different proportions of NCO and OH may have caused crosslinks that result in segments of intermediate stiffness and softness. FTIR spectra indicated that the addition of wood to PU favors the formation of hard and soft segments. 5% wood influenced TG analyses, comparing composite samples with raw and treated wood. The DVS for PU showed very similar results, with less than 2% water absorption. The addition of 2% raw wood barely changed water absorption, but composites with treated wood showed greater water absorption. All samples with 5% raw wood displayed much higher water absorption than the composites with 2%. DMA analysis was used to calculate the crosslink density of the samples and help explain their thermo-mechanical behavior. The PU obtained in this research are excellent candidates as matrices for bio-based composites.

Key words: macauba; glycerol; polyurethane; wood; thermal stability; composite.

RESUMO

A busca por materiais renováveis e com baixo custo de produção estimulou este trabalho, onde foram preparados compósitos a partir de óleo vegetal (OV) e serragem de madeira. O polioliol utilizado para obtenção das poliuretanas (PU) foi obtido por epoxidação do óleo da semente de macaúba (OAM), com abertura dos anéis usando glicerol maior quantidade de grupos hidroxila nas cadeias de ácidos graxos, que é um método inovador. O pó de madeira foi usado para reforçar a matriz polimérica de PU e agregar valor ao produto. As quantidades de reagentes para epoxidação do OAM com ácido fórmico e H_2O_2 foram calculadas com base na insaturação por mol do OAM, obtida pela integração dos picos em seu espectro de RMN 1H . A reação de abertura do anel epóxido (EPOAM) ocorreu na proporção 1:1, glicerina e EPOAM. $BF_3(Et_2O)$ a 10% foi utilizado como catalisador. As PU foram preparadas em diferentes razões molares $[NCO]/[OH]$. Os compósitos foram obtidos adicionando pó de madeira às matrizes de PU. As espécies de madeira utilizadas foram faia (*Fagus sylvatica*), abeto (*Albies alba*) e carvoeiro (*Tachigali vulgaris*) (CV). As madeiras foram pré-tratadas e suas amostras secadas a 103 °C, até a estabilização da massa. Todas as madeiras foram tratadas a 2 °C·min⁻¹, até atingir a temperatura definida, seguida de tratamento isotérmico de 30 min. Ao analisar os dados de deconvolução do DTG e fracionamento da madeira, as temperaturas de tratamento escolhidas foram: 275 °C, 310 °C e 290 °C, para faia, abeto e CV, respectivamente. A deslignificação do CV foi mais próxima da do abeto do que da faia, com poucos incrementos na relação celulose/hemicelulose, até a degradação da celulose. A formação de epóxido e polioliol foi confirmada por FTIR e RMN 1H . O índice OH calculado, 85,57 mg KOH/g, foi baixo para um polioliol de OV com pouca insaturação. As PU foram produzidas em três razões $[NCO]/[OH]$ diferentes e apresentaram espectros no FTIR semelhantes, especialmente PU 1,0 e 1,2, indicando que após a razão 1,0, o isocianato adicionado permanece em excesso. Os picos C-N nos espectros FTIR dos compósitos 1,0 e 1,2 $[NCO]/[OH]$ foram quase idênticos, sendo menores para o 0,8. Os compósitos com madeira crua exibiram diferenças no pico C-N nas PU 1,0 e 1,2 e não exibiram tanto -OH residual como as demais amostras. As curvas TG e DTG da PU 1,0 mostraram três picos de degradação e as PU 0,8 e 1,2 4 picos, sugerindo que diferentes razões de NCO e OH podem formar ligações cruzadas resultando em segmentos rígidos e macios intermediários. Os espectros no FTIR indicaram que a madeira favorece a formação de segmentos duros e moles. 5% de madeira mudaram as análises de TG, comparando amostras compostas com madeira crua e tratada. O DVS para PU mostrou resultados semelhantes com menos de 2% de absorção de água. A adição de 2% de madeira crua mudou pouco a absorção de água, mas a adição de madeira tratada mostrou maior absorção de água. Todas as amostras com 5% de madeira crua apresentaram absorção de água muito maior que os compósitos com 2%. A análise por DMA foi usada para calcular a densidade de reticulação das amostras e ajuda a explicar seu comportamento termomecânico. As PU obtidas nesta pesquisa são excelentes candidatos como matrizes para compósitos de base biológica.

Palavras-chave: macaúba; glicerol; poliuretana; madeira; estabilidade térmica; compósito.

INDEX

List of Figures.....	XXII
List of Tables.....	XXVIII
List of Acronyms.....	XXX
Chapter 1.....	1
<i>Introduction</i>	1
1.1 Introduction.....	2
1.2 Justification.....	5
1.3 General Objectives.....	6
1.4 Specific Objectives.....	6
Chapter 2.....	8
<i>Bibliographic Review</i>	8
2.1 Wood and vegetable fibers (VF).....	9
2.2 Thermal treatment.....	17
2.3 Biocomposites.....	21
2.3.1 Vegetable oils.....	21
2.3.2 Macauba and its oils.....	24
2.3.3 Polyurethanes.....	27
2.3.4 Glycerol.....	31
2.3.5 Composites.....	35
2.3.6 Additional work.....	38
2.3.6.1 Lubricants.....	38
2.3.6.2 Biolubricants.....	41
2.3.6.3 Vitamin E.....	43
2.3.6.4 α -tocopherol acetate.....	45
Chapter 3.....	46
<i>Materials and methods</i>	46
3.1 Materials.....	47

3.2 Methods	47
3.2.1 Wood samples and vegetable oils.	47
3.2.2 Sampling.....	48
3.3 Pretreatment.....	48
3.4 Wood density	48
3.5 Thermal treatment	49
3.6 Grinding	50
3.7 Thermogravimetric analysis/Derived thermogravimetry analysis (TGA/DTG)	50
3.7.1 DTG Deconvolutions.....	51
3.8 Wood Fractioning.....	52
3.9 Epoxide synthesis.....	53
3.10 Polyol synthesis	55
3.11 OH index.....	57
3.12 Polyurethane/composites synthesis	57
3.13 Fourier transform infrared spectroscopy (FTIR).....	57
3.14 Dynamic vapor sorption (DVS)	57
3.15 Dynamic mechanical analysis (DMA)	58
3.16 Additional work	58
3.16.1 Other attempts at polyol synthesis.....	58
3.16.2 α -tocopherol acetate additivation.....	59
Chapter 4.....	60
<i>Production of modified wood fibers by thermal treatment.....</i>	<i>60</i>
4.1 Wood's density	61
4.2.1 Thermal treatments.....	61
4.2.2 Deconvolutions DTG.....	65
4.3 Wood fractioning	70
4.3.1 Delignification	70

4.3.2 α -Cellulose gravimetry	75
4.4. Conclusion	76
Chapter 5.....	78
<i>Production of polyurethane foams and bio composite with thermally modified wood fibers</i>	78
5.1 ¹ H NMR spectrum of the MKO.....	79
5.2 MKO, EPMKO and GlyMKO, synthesis and FTIR spectra	80
5.3 MKO, EPMKO and GLyMKO ¹ H NMR spectra.....	81
5.4 OH Index	83
5.5 Free NCO ratio	84
5.6 Synthesis of PU foam.....	84
5.7 Composites.....	86
5.7.1 FTIR, characterizations of the materials	88
5.7.1.2 Preparation of PU	91
5.8 Thermogravimetric Analysis (TGA).....	97
5.8.1 PU.....	97
5.8.2 Beech 2%, NCO/OH 0.8	99
5.8.3 Beech 2%, NCO/OH 1.0	101
5.8.4 Beech 2%, NCO/OH 1.2	102
5.8.5 Fir 2%, NCO/OH 0.8	104
5.8.6 Fir 2%, NCO/OH 1.0	106
5.8.7 Fir 2%, NCO/OH 1.2	107
5.8.9 Beech 5%, NCO/OH 0.8	109
5.8.10 Beech 5%, NCO/OH 1.0	111
5.8.11 Beech 5%, NCO/OH 1.2	112
5.8.12 Fir 5%, NCO/OH 0.8	114
5.8.13 Fir 5%, NCO/OH 1.0	115

5.8.14 Fir 5%, NCO/OH 1.2	116
5.8.15 CV 2%, NCO/OH 0.8	117
5.8.16 CV 2%, NCO/OH 1.0	119
5.8.17 CV 2%, NCO/OH 1.2	120
5.8.18 CV 5%, NCO/OH 0.8	121
5.8.19 CV 5%, NCO/OH 1.0	122
5.8.20 CV 5%, NCO/OH 1.2	123
5.9 Dynamic mechanical analysis (DMA)	124
5.10 Dynamic vapor sorption (DVS)	125
5.10.1 PU	126
5.10.2 Beech 2% 0.8	127
5.10.3 Beech 2% 1.0	129
5.10.4 Beech 2% 1.2	130
5.10.5 Fir 2% 0.8	130
5.10.6 Fir 2% 1.0	131
5.10.4 Fir 2% 1.2	132
5.10.5 Beech 5% 0.8	133
5.10.6 Beech 5% 1.0	134
5.10.7 Beech 5% 1.2	134
5.10.8 Fir 5% 0.8	135
5.10.9 Fir 5% 1.0	136
5.10.10 Fir 5% 1.2	136
5.11 Conclusions	137
Chapter 6	141
General Conclusions	141
6.1 General Conclusions	142
Chapter 7	145

<i>Future works perspectives</i>	145
Chapter 8.....	147
<i>References</i>	147
Chapter 9.....	159
Discontinued work results.....	159
9.1 Polyol T1 Synthesis.....	160
9.2 Polyol using zinc as a catalyst.....	160
9.3 α -tocopherol acetate additivation	161

List of Figures

Figure 1. Molecular structures of glucose, cellobiose and cellulose (15).	9
Figure 2. Hemicelluloses monomers, their symbols are show on the top right of the molecules (21).	11
Figure 3. Fragment of a hemicellulose chain bonded to a lignin monomer (highlighted) (19).	12
Figure 4. Lignin precursors (15).	12
Figure 5. Proposed structure for a fragment of lignin (19).	13
Figure 6. Organization of the biopolymers in a vegetable (22).	14
Figure 7. Structure of a vegetable cell wall (15).	14
Figure 8. A) A vessel element (ve), a tracheid (t) and a fiber (f), another structure present in hardwoods, B) The stacking of two vessel elements and C) the opening at an end of a vessel element (15).	16
Figure 9. A softwood (A) and its microscopy (C); a hardwood (B) and its microscopy (D) (15).	17
Figure 10. (a) Old one-step pyrolysis model, and (b) the model proposed by Shafizadeh (31), Adapted figure.	19
Figure 11. Multiple steps pyrolysis of wood (33).	20
Figure 12. Experimental and calculated thermal degradation profile of a rubberwood sample, showing also the deconvolution for each individual biopolymer (34).	20
Figure 13. Glycerol, FA and triglyceride. R represents the rest of the FA molecules in a triglyceride and are not all necessarily the same (36).	21
Figure 14. Lauric acid, saturated; oleic acid, cis unsaturated and basic acid, trans unsaturated (39).	22
Figure 15. Reactive sites found in a triglyceride (40).	22
Figure 16. Example of possible reactions with vegetable oils (7).	23
Figure 17. Intact macauba fruits (left) (48), and a cut fruit (right) (49). Adapted figure.	24
Figure 18. Parts of the macauba fruit and their main commercial usages (50). Adapted figure.	25
Figure 19. Example of possible ways to form polyols (4).	29
Figure 20. Some commercially available kinds of isocyanates (4).	30

Figure 21. Formation of an urethane group (63). The rest of the polyol and isocyanate have been omitted for better visual clarity.	31
Figure 22. Rigid and soft segments in a PU (64).	31
Figure 23. Transesterification of a Triglyceride (65). The fatty ester molecules represent the biofuel produced by the transesterification.	33
Figure 24. Growth in the world production of biodiesel and glycerol (67).	33
Figure 25. Main usages of glycerol in 2019 (67).	34
Figure 26. Bonding between an isocyanate and a chain of hemicellulose in the synthesis of a polyurethane composite. (71) Adapted figure.	37
Figure 27. Effects of alkaline treatment on the cellulose chains (16).	38
Figure 28. Zoom in a region between two non-lubricated surfaces (up) and two lubricated surfaces (down). Adapted figure (73).	39
Figure 29. Shearing of lubricant layers (74).	39
Figure 30. Comparison between (a) a Triglyceride and (b) hydrocarbons (74).	41
Figure 31. Formation of a protecting lubricant film of Triglyceride over a metallic surface (79).	42
Figure 32. Molecular structures of some tocochromanols (85).	43
Figure 33. Antioxidant action of α -tocopherol, where P means phythyl and L means lipid.	44
Figure 34. Dimensions of the wood samples used in this work (up), and a piece of wood sample (down).	48
Figure 35. Representation of the reaction used in the thermal treatment of the wood samples.	49
Figure 36. Thermal profile of the thermal treatments done on the wood samples.	49
Figure 37. Temperature profile used in the TG/DTG analyses done in this work.	51
Figure 38. Comparison between (a) the deconvolution made by Carrier et al. (2011) (35), and (b) this work.	51
Figure 39. Apparatus used in the MKO epoxidation.	54
Figure 40. Suggested mechanism for the formation of peracid (91).	54
Figure 41. Epoxide formation (92).	55
Figure 42. Apparatus used for GLMKO synthesis.	56

Figure 43. Proposed mechanism for the epoxide ring opening and formation of polyol. Cat represents catalyst, R ¹ and R ² represent the rest of the Triglyceride molecule.....	56
Figure 44. Mass loss as a function of treatment temperature. All samples were treated for 30 min (not counting the time needed to reach each target temperature).....	63
Figure 45. Common kinds of hemicelluloses found in hardwoods and softwoods (96).....	64
Figure 46. Deconvolution DTG curves of the (a) raw beech sample, and of the beech samples treated at (b) 260 °C, and (c) 270 °C.....	65
Figure 47. Cel/Hemi ratio for samples of beech treated at different temperatures.	66
Figure 48. Cel/Hemi ratio for samples of fir treated at different temperatures.	67
Figure 49. Deconvolution DTG curves of the raw fir.	68
Figure 50. Cel/Hemi ratio for samples of CV treated at different temperatures.	69
Figure 51. Deconvolutions DTG curves of the raw CV.....	70
Figure 52. Wet pulp resulting from the delignification of the F270 sample.	71
Figure 53. Dried delignified samples of fur treated at different temperatures. .	71
Figure 54. Delignification gravimetry of the fir samples.	72
Figure 55. F305 and F310 after delignification.	72
Figure 56. Delignification gravimetry of the CV samples.	73
Figure 57. "Jam" resulting from the delignification of the CV 295 sample.	73
Figure 58. Delignification gravimetry of the beech samples.	74
Figure 59. α-Cellulose obtained.....	75
Figure 60. Mass loss by α-Cellulose gravimetry in samples of fir treated at different temperatures.	75
Figure 61. ¹ H NMR spectrum for MKO (105).....	79
Figure 62. FTIR spectra of the MKO, EPMKO and GlyMKO samples (105,107).	80
Figure 63. ¹ H NMR spectra of the MKO, EPMKO and GlyMKO (105).....	82
Figure 64. Digital images of the three produced samples of PU. Do notice they have stains from markers from the first attempt to label them.	84

Figure 65. FTIR spectra of the three produced PU samples (107), (105). The CO ₂ peaks have been omitted for better visual clarity.	85
Figure 66. (a) PU 1.2, showing some the digital image of the PU crystals seen in its underside and their FTIR spectrum (105) (107).....	86
Figure 67. Digital images of all samples produced in this work.	88
Figure 68. How particle size affects the polymeric matrix of a composite (117).	89
Figure 69. FTIR spectra of beech treated at 275 °C (B275) in different particle sizes (< 250 μm, 250-500 μm, > 500 μm) (105).	89
Figure 70. FTIR spectra of F310 in different particle sizes (< 250 μm, 250-500 μm, > 500 μm) (105)	90
Figure 71. FTIR spectra of CV290 in different particle sizes, (< 250 μm, 250-500 μm, > 500 μm) (105).....	91
Figure 72. FTIR spectra of the composites made with 2% (a) raw and (b) treated beech. The CO ₂ peak has been omitted for better visual clarity (105).....	92
Figure 73. FTIR spectra of the composites made with 5% of (a) raw, and (b) treated beech (105).....	93
Figure 74. FTIR spectra of the composites made with 2% of (a) raw, and (b) treated fir (105).....	94
Figure 75. FTIR spectra of the composites made with 5% of (a) raw, and (b) treated fir (105).....	95
Figure 76. FTIR spectra of the composites made with 2% of (a) raw, and (b) treated CV (105).....	96
Figure 77. FTIR spectra of the composites made with 5% of (a) raw, and (b) treated CV. The CO ₂ peak has been omitted for better visual clarity (105).....	97
Figure 78. (a) TGA and (b) DTG curves of the PU samples.	97
Figure 79. (a) TGA, and (b) DTG curves of the samples of PU, beech composites of both raw and treated wood at 2% at the NCO/OH ratio of 0.8.....	99
Figure 80. (a) TGA, and (b) DTG curves of the samples of PU, beech composites of both raw and treated wood at 2% at the NCO/OH ratio of 1.0.....	101
Figure 81. (a) TGA and (b) DTG curves of the PU samples, beech composites of both Raw and treated wood at 2 % at the NCO/OH ratio of 1.2.	102
Figure 82. (a) TGA and (b) DTG curves of the samples of PU, fir composites of both Raw and treated wood at 2 % at the NCO/OH ratio of 0.8.	104

Figure 83. (a) TGA and (b) DTG curves of the samples of PU, fir composites of both Raw and treated wood at 2 % at the NCO/OH ratio of 1.0.	106
Figure 84. (a) TGA and (b) DTG curves of the samples of PU, fir composites of both Raw and treated wood at 2 % at the NCO/OH ratio of 1.2.	108
Figure 85. (a) TGA and (b) DTG curves of the samples of PU, beech composites of both Raw and treated wood at 5% at the NCO/OH ratio of 0.8.	110
Figure 86. (a) TGA and (b) DTG (b) curves of the samples of PU, beech composites of both Raw and treated wood at 5% at the NCO/OH ratio of 1.0.	111
Figure 87. (a) TGA and (b) DTG curves of the samples of PU, beech composites of both Raw and treated wood at 5% at the NCO/OH ratio of 1.2.	112
Figure 88. (a) TGA and (b) DTG curves of the samples of PU, fir composites of both Raw and treated wood at 5% at the NCO/OH ratio of 0.8.	114
Figure 89. (a) TGA and (b) DTG curves of the samples of PU, fir composites of both Raw and treated wood at 5% at the NCO/OH ratio of 1.0.	115
Figure 90. (a) TGA and (b) DTG curves of the samples of PU, fir composites of both Raw and treated wood at 5% at the NCO/OH ratio of 1.2.	116
Figure 91. (a) TGA and (b) DTG (b) curves of the samples CV composites with both Raw and treated wood at 2% at the NCO/OH ratio of 0.8.	118
Figure 92. (a) TGA and (b) DTG curves of the samples CV composites with both Raw and treated wood at 2% at the NCO/OH ratio of 1.0.	119
Figure 93. (a) TGA and (b) DTG curves of the samples CV composites with both Raw and treated wood at 2% at the NCO/OH ratio of 1.2.	120
Figure 94. (a) TGA and (b) DTG curves of the samples CV composites with both Raw and treated wood at 5% at the NCO/OH ratio of 0.8.	121
Figure 95. (a) TGA and (b) DTG curves of the samples CV composites with both Raw and treated wood at 5% at the NCO/OH ratio of 1.0.	122
Figure 96. (a) TGA and (b) DTG curves of the samples CV composites with both Raw and treated wood at 5% at the NCO/OH ratio of 1.2.	123
Figure 97. Storage modulus and tan δ plotted as a function of temperature.	125
Figure 98. Diagram showing the T_{g1} and T_{g2}	125
Figure 99. DVS curves of the PU samples.	126
Figure 100. Types of absorption isotherms and hysteresis loops (120). Adapted figure.	127

Figure 101. DVS curves of the PU 0.8 and the beech composite samples at 2% and 0.8 NCO/OH ratio.	128
Figure 102. DVS curves of the PU 1.0 and the beech composite samples at 2% and 1.0 NCO/OH ratio.	129
Figure 103. DVS curves of the PU 1.2 and the Beech composite samples at 2% and 1.2 NCO/OH ratio.	130
Figure 104. DVS curves of the PU 0.8 and the fir composite samples at 2% and 0.8 NCO/OH ratio.	131
Figure 105. DVS curves of the PU 1.0 and the fir composite samples at 2% and 1.0 NCO/OH ratio.	131
Figure 106. DVS curves of the PU 1.2 and the fir composite samples at 2% and 1.2 NCO/OH ratio.	132
Figure 107. DVS curves of the PU 0.8 and the Comp B Raw 5% and 0.8 NCO/OH ratio.	133
Figure 108. DVS curves of the PU 1.0 and the Comp B Raw 5% and 1.0 NCO/OH ratio.	134
Figure 109. DVS curves of the PU 1.2 and the Comp B Raw 5% and 1.2 NCO/OH ratio.	135
Figure 110. DVS curves of the PU 0.8 and the Comp F Raw 5% and 0.8 NCO/OH ratio.	135
Figure 111. DVS curves of the PU 1.0 and the Comp F Raw 5% and 1.0 NCO/OH ratio.	136
Figure 112. DVS curves of the PU 1.2 and the Comp F Raw 5% and 1.2 NCO/OH ratio.	137
Figure 113. FTIR spectra obtained from the attempt to synthesize a polyol called Polyol P1 (105).	160
Figure 114. FTIR spectra obtained from the attempt to synthesize a polyol using zinc chloride as catalyst (105).	160

List of Tables

Table 1. Some examples of FA (42).	23
Table 2. Oil content for each part of the macauba fruit (9).	26
Table 3. Composition of kernel, pulp and peel from macauba oil (48,52).....	26
Table 4. Some properties of Glycerol at room temperature (67).	32
Table 5. Composition of glycerol obtained by different methods (67).....	34
Table 6. Biodegradability of some possible lubricant bases (74).....	41
Table 7. Quantity of reagents for MKO epoxidation.	53
Table 8. Density of the wood species.....	61
Table 9. Mass losses in the thermal treatment of the three wood species studied in this work.	62
Table 10. Properties of MKO.....	79
Table 11. List of bands used to interpret the FTIR spectra in Figure 62 (105,107).	81
Table 12. Bonds and chemical shifts relevant to the interpretation of the ¹ H NMR spectra seen in the Figure 63 (105,110,112).	83
Table 13. Quantities of reagent used for each NCO/OH ratio used in the synthesis of the PU samples.	84
Table 14. Quantity of wood used in each percentage for each NCO/OH ratio. Do note that the same quantities were used for all the three used species of wood.	87
Table 15. Thermal properties of the PU samples.	98
Table 16. Thermal properties of the samples of PU, beech composites of both raw and treated wood at 2% at the NCO/OH ratio of 0.8.....	100
Table 17. Thermal properties of the PU samples, beech composites of both raw and treated wood at 2% at the NCO/OH ratio of 1.0.	102
Table 18. Thermal properties of the beech samples at 2% and 1.2 NCO/OH ratio.	103
Table 19. Thermal properties of the fir samples at 2% and NCO/OH ratio of 0.8.	105
Table 20. Thermal properties of the fir samples at 2% and 1.0 NCO/OH ratio.	107
Table 21. Thermal properties of the fir samples at 2% and 1.2 NCO/OH ratio.	109

Table 22. Thermal properties of the beech samples at 5% and 0.8 NCO/OH ratio.	111
Table 23. Thermal properties of the beech samples at 5% and 1.0 NCO/OH ratio.	112
Table 24. Thermal properties of the beech samples at 5% and 1.2 NCO/OH ratio.	113
Table 25. Thermal properties of the fir samples at 5% and 0.8 NCO/OH ratio.	115
Table 26. Thermal properties of the fir samples at 5% and 1.0 NCO/OH ratio.	116
Table 27. Thermal properties of the fir samples at 5% and 1.2 NCO/OH ratio.	117
Table 28. Thermal properties of the CV samples at 2% and 0.8 NCO/OH ratio.	119
Table 29. Thermal properties of the CV samples at 2% and 1.0 NCO/OH ratio.	120
Table 30. Thermal properties of the CV samples at 2% and 1.2 NCO/OH ratio.	121
Table 31. Thermal properties of the CV samples at 5% and 0.8 NCO/OH ratio.	122
Table 32. Thermal properties of the CV samples at 5% and 1.0 NCO/OH ratio.	122
Table 33. Thermal properties of the CV samples at 5% and 1.2 NCO/OH ratio.	123
Table 34. DMA results of PU samples.....	125
Table 35. Maximum water uptakes of the composite samples with 2% of wood.	133
Table 36. Results of oxidative stability caused by the addition of α -tocopherol.	161

List of Acronyms

^1H NMR - Proton Nuclear Magnetic Resonance

ANP - Agência Nacional de Petróleo, gás natural e biocombustíveis

CAPES - Coordenação de Aperfeiçoamento de Pessoal de Nível Superior

CNPQ - Conselho Nacional de Desenvolvimento Científico e Tecnológico

CONAB - Companhia nacional de abastecimento

CV - Carvoeiro

DTG - Derivate Thermogravimetric analysis

DVS - Dynamic Vapor Sorption (DVS)

FA - Fatty acids

FTIR - Fourier Transform Infrared Spectroscopy

GlyMKO - Polyol made with MKO and glycerol

Hform - Formic acid

MDI - Methylene Diphenyl Diisocyanate

MKO - Macauba kernel oil

MPO - Macauba pulp oil

PU - Polyurethane

TGA - Thermogravimetric analysis

VF - Vegetable fibers

Chapter 1

Introduction

1.1 Introduction

The creation of plastics has brought countless benefits to many areas of life and different industries, such as transportation and medical industries, among several others. The increasing population and accelerated economic growth has caused the demand and, consequently, the production of plastics to experience a rapid increase, with the global yearly production of plastics reaching about 400 million metric tons of plastic, about 75% (1) of which is discarded after a being used a single time. As most plastics produced in the world are of petrochemical origin, this enormous amount of discarded plastic becomes a major cause of environmental issues, as petrochemical products are non-renewable and, often, toxic (1).

Plastics, however, are quite versatile, important materials, cheap and easy to produce, resulting in them having widespread applications in important industries like packaging, construction and textiles, where they are most used. With all the important applications they have, it is unreasonable to expect them to be suddenly fully replaced, despite the many known environmental problems caused by them (2).

Among plastics, the polyurethane (PU) is one of the most widely produced and consumed in the world. It can be made into films, soft foams, rigid foams, adhesives, and others, making it versatile and it is easy to produce polymer, as its basic components are polyol and an isocyanate. Even though PU is, as most polymers are petrochemical, the polyol used in its synthesis can be easily made from bio-based materials, such as vegetable oils (3). As PU are so popular, several different synthetic routes for the production of polyol from vegetable oils have been studied and developed, as presented by (4), each resulting in a different polyol leading to a different PU. The availability of bio-based material for polyol synthesis attracts a lot of attention to PU in the field of green chemistry (4).

Vegetable oils are seen as promising replacements for petrochemical materials for their variety, easiness in obtaining and processing, low toxicity and, specially, renewability (5,6) Vegetable oils also have a variety of reactive sites that can be used for other chemical modifications (7) which can be used to modify them to fit into a wide array of specific applications. They are usually used in

industries such as cosmetics, pharmacology and biofuels, and their usage increases constantly (8).

Macauba (*Acrocomia aculeata* (Jacq.) Lood. ex Mart) is a palm that is found, in Brazil, mostly in the states of Minas Gerais, Mato Grosso, Mato Grosso do Sul and Goiás, but it is also found in other countries in south America (9). Its fresh fruits show from 50% to 60% of oil content (10) and produce mainly 2 kinds of oils: the kernel oil and the pulp oil (MKO and MPO, respectively), which have found use in the feeding, cosmetics and pharmacy industries, among others. In MKO, the most significant fatty acid (FA) is saturated lauric acid, at about 40% of its fatty profile. The second most significant FA in MKO, and its only unsaturated FA, is oleic acid, at about 25%. MPO, on the other hand, is richer on unsaturated acids, and oleic acid makes up for about 50% of its composition, containing also other unsaturated acids, including even polyunsaturated acids (11).

A possible and interesting usage for PU is to produce polymeric composites. Composites are materials that are made up of two or more different materials. Composites expand the already wide range of applications for PU, as the addition of reinforcement materials to their polymeric matrix can further tailor their properties to be adequate to other specific applications (12). Zou *et al.* (2023), for example, used ceramic particles as reinforcement material in a PU composite, and their tests showed a good bonding between the matrix and their numerical simulations have shown it can a promising material for stress attenuation (12).

PU are particularly interesting in the production of composites because, as they are made mainly of polyol and isocyanate, they possess great affinity with any hydroxylated material, like vegetable fibers. Vegetable fibers are mostly made of lignocellulosic material, being, then, highly hydroxylated, thus, interesting for the usage as reinforcement materials in PU composites. Lopes *et al.* (2021) used castor oil based PU and waste bamboo fibers from a shish kebabs sticks production facility for the preparation of strand boards. The resulting boards not only fit the industry standards but also showed greater mechanical performance when compared to other commercial boards (13). This great compatibility between the PU polymeric matrix and vegetable fibers has led to a great number of researches in this area, with different fibers yielding different properties in the final material, such as improved sound absorption, compressive

strength, tensile strength, etc. as investigated by Kuranchie *et al.* (2021) in their review article (14).

As mentioned above, vegetable fibers are highly hydroxylated. That is due to them being mostly made up of cellulose, hemicelluloses and lignin (known together as lignocellulosic material). Except for the lignin, those biopolymers are rich in hydroxyl groups, granting them not only the vegetable's mechanical strength by hydrogen bonding between the biopolymer chains but also helps them in the transport and storage of water. In a vegetable fiber, hemicelluloses, short and branched chains made up of many different monomers work as a matrix in which the cellulose, strong, long, linear and often crystalline chains, are inserted. Lignin works as a glue, keeping the whole structure together by chemically bonding to the hemicelluloses chains (15).

Both cellulose and hemicelluloses are hydroxylated, but the cellulose has a greater mechanical strength than the hemicelluloses so, for the preparation of composites, the hemicelluloses can be removed by chemical means, such as the reaction with concentrated NaOH (16). That generates important foot print carbon and toxic wastes that need to be treated before being discarded. In this work tries to avoid the usage of concentrated base for the removal of hemicelluloses by degrading it via thermal treatment.

Thermal treatments by soft pyrolysis or torrefaction aim to modify the properties of wood by treating them at certain temperatures (250-300 °C) under different inert atmospheres. It is commonly used by wood industries to increase the longevity of wood logs, boards and outside use. In this works was made the thermally degrading the wood's hemicelluloses, the less thermally resistant of the wood's biopolymers, protecting the products from the attacks of fungi, improve his dimensional stability, decrease is moisture content, change the color (15).

Glycerol, is a tri-functional alcohol present in vegetable oils as the backbone of their triglyceride molecules, bonding the three FA molecules of the triglyceride (Triglyceride) together, being their main component. It is obtained a byproduct of the synthesis of biodiesel, which is one of the most important applications of vegetable oils nowadays. The rapid increase in demand for biofuels, caused by the rise in environmental awareness, created such a big surge in glycerol production that even all its usual applications, such as in cosmetics, animal feed, fermentation and food packaging, cannot keep up the

supply, giving rise to the glycerol valorization field of research. In 2021, about 2.8 billion liters of glycerol was produced as byproduct of biodiesel by only five of the biggest biodiesel producers in the world (17).

Ben *et al.* (2022) studied the usage of glycerol as a non-toxic plasticizer for food packaging. The hydroxyl groups present on the glycerol molecule interfered with the intermolecular interactions between the polymeric chains of the food packaging material, resulting in increased plasticity for the film (17).

Glycerol is hydroxylated, so it can be used to produce PU. Usually, glycerol is used to produce PU by inserting it into other molecules. Calderon *et al.* (18), synthesized polyglycerol polyester polyol and synthesized PU with it. The resulting products were thermoplastics that have shown acceptable results regarding their thermoplasticity.

While the integration of glycerol in polymers by itself is not new, to the best knowledge of the author, using glycerol as an epoxide ring opener, a simple and straightforward way to produce polyols that are used in this work, is still novel.

1.2 Justification

Despite the great advances brought to us by plastics, the overwhelming quantity in which they are produced, associated with their usual inherent non-renewability, has caused a great deal of environmental harm, that has created an ever-growing necessity for the research on environmentally friendly polymers.

Polyurethane is a quite popular kind of polymer that can be easily made from natural materials like vegetable oils. Vegetable oils are easy to produce and process, but they often are also a source of food for people and animals, so it is interesting to be responsible when using them. Macauba fruits have greater oil content than soy, for example but, despite not being a traditionally edible oil, the macauba kernel oil is poorly studied. A better understanding of the possible uses of macauba kernel oil could not only give rise to a new and possibly interesting raw material but also valorize the fruits, increasing the income of the families that make living from harvesting them.

Another source of environmental damage that green chemistry has been trying to address is the disparity between the supply and demand of glycerol, which lowers its value to the point that it is usually discarded as waste in great

quantities. The glycerol valorization research field tries to avoid this by developing new ways to use glycerol, which could be a cheap and widely available raw material that could be used in important applications.

Wood and vegetable fibers in general, despite being inherently green and renewable, often produce great quantities of waste such as sawdust and not so desirable fibers. Those wastes have potential to be used in many different applications, such as in the production of composites, as is the case in this work.

With an attempt to promote renewability using waste that is discarded, often without correct management and which is low cost, glycerol was used, the objective of which was to promote the opening of the epoxide ring, enabling the addition of more hydroxyl groups to the hydrocarbon chains of FA, thus promoting an increase in the hydroxyl index. This reaction method is innovative because water is an agent commonly used in this type of reaction. Saw dust is also a residue from the usage of wood that adds value to the final product and contributes to its renewable character.

1.3 General Objectives

This research was performed in two different universities (University of Brasília, in Brazil and Université de Lorraine, in France), each part of it having its own specific objective, but working towards a global objective for the research.

- University of Brasília: Synthesis and characterization of a polyol from MKO and glycerol. Using this polyol for the synthesis and characterization of PU foams using different NCO/OH ratio.

- Université de Lorraine: Thermal treatment of beech, fir and carvoeiro samples, followed by their characterization, to access the best operative conditions (time, temperature) to degrade the most hemicelluloses from the samples without degrading their cellulose.

- Common objective: Synthesis and characterization of PU composites using the different NCO/OH ratios for the PU and both raw and treated sawdust of three wood species studied in this work.

1.4 Specific Objectives

The specific objectives of this work are as follows:

- Characterization of the macauba kernel oil by spectroscopy techniques of Fourier-Transform Infrared (FTIR) and Proton Nuclear Magnetic Resonance (^1H NMR), Thermogravimetric Analysis (TGA) and Derivative Thermogravimetry (DTG);
- Synthesis of the macauba kernel oil epoxide (MKO) and its characterization by FTIR and ^1H NMR;
- Synthesis of the macauba kernel oil polyol with glycerol (GlyMKO) and its characterization by FTIR and ^1H NMR;
- Synthesis of the polyurethane foams using the synthesized polyol and MDI and its characterization by FTIR, TGA, DTG and Dynamic Vapor Sorption (DVS);
- Synthesis and characterization of PU composites;
- Thermal treatment of samples of beech, fir, carvoeiro (CV) for different temperatures (same time);
- Delignification gravimetry and characterization of the raw and treated wood samples by TGA, DTG and FTIR to infer right temperature/time to degrade their hemicellulose limiting the damage to their cellulose as much as possible.

Chapter 2
Bibliographic Review

2.1 Wood and vegetable fibers (VF)

Wood is a natural material made up of mostly carbon, hydrogen and oxygen at approximately 50%, 6% and 44%, respectively, containing also small quantities of other elements, including salts and natural extracts. Molecularly, a vegetable organ, such as wood, is made up mostly of three biopolymers: cellulose, hemicelluloses and lignin in quantities varying according to species, climate, conditions and others. Woods and vegetables in general also present varying quantities of natural extractives such as waxes, oils, gums, pigments and others (15).

Cellulose is present in all vegetable biomasses, being found even in some animals, like the tunicates. In a vegetable, it usually makes up from 20% to 45% of the biomass. It is a linear polymer made up from unities of glucose bound by β -(1-4) glucose bonds, forming a unit of cellobiose, the actual monomer of cellulose (15,19). Figure 1 shows the molecular structures of glucose, cellobiose and cellulose.

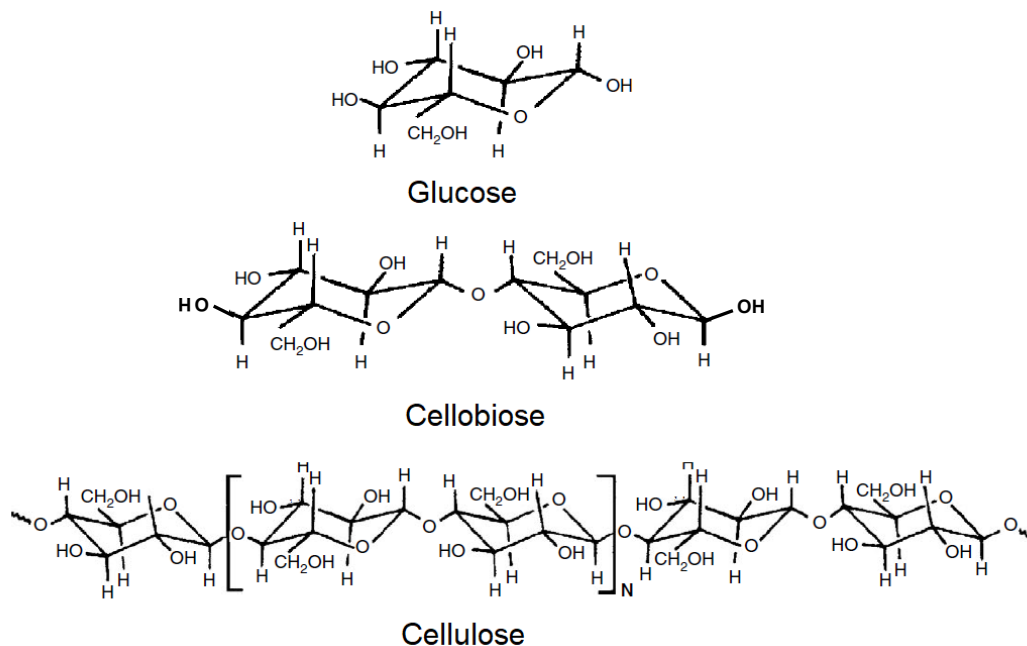


Figure 1. Molecular structures of glucose, cellobiose and cellulose (15).

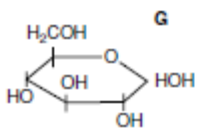
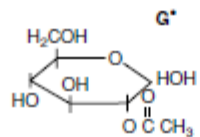
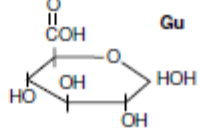
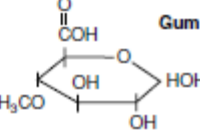
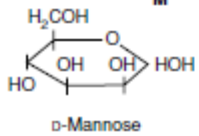
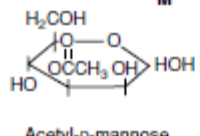
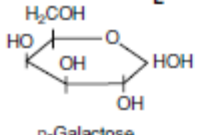
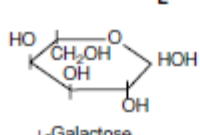
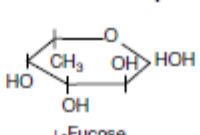
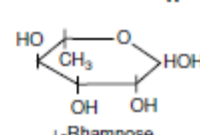
Each unity of glucose in the cellulose has free -HO groups, that used to hydrogen bond both to other cellulose chains and to hemicelluloses chains. Cellulose can be found as amorphous or crystalline, both can present a single cellulose chain, forming amorphous and crystalline domains. Their linear chains present high polymerization degree, reaching from 9.000 to 15.000 cellobiose

unities. The linearity and size of those chains make cellulose the strongest polymer present in vegetable fibers, being responsible for their mechanical strength and their high degree of hydroxylation also makes them greatly responsible for the storage and transport of water, two of the most important functions in a vegetable (15,19).

The most prominent usage for cellulose is the production of paper. For this, the wood is chipped, boiled to remove hemicelluloses and lignin, then treated with NaOH and Na₂SO₃ at high temperatures. This procedure is known as the Kraft process after the stronger (kraft meaning strength in German) pulp that can be obtained this way when compared to previous pulping processes (20).

Hemicelluloses are a family of various sugars, which make up 15% to 25% of a vegetable biomass. They are amorphous, branched and made up from many different monomers, classified as hexoses (six carbons monosaccharides) and pentoses (five carbons monosaccharides). They can be further classified as glucose, mannose and galactose (for the hexoses) and in xylose and arabinose (for the pentoses). Those monomers form well defined different kinds of hemicelluloses, that is why this biopolymer is treated in plural (21). The hemicelluloses' monomers are shown in Figure 2, and Figure 3 represents the fragment of a hemicellulose chain.

HEXOSES

Hexose	Acetylated hexoses	Hexose uronic acid	Methylated hexose uronic acid
 G D-Glucose (pyranose)	 G* Acetyl-D-glucose	 Gu D-Glucuronic acid	 Gum 4-O-Methyl-D-glucuronic acid
 M D-Mannose (pyranose)	 M* Acetyl-D-mannose	6-Deoxy sugar	
 L D-Galactose (pyranose)	 L' L-Galactose (pyranose)	 F L-Fucose (pyranose)	 R L-Rhamnose (pyranose)

PENTOSES

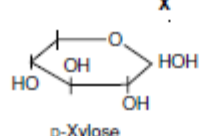
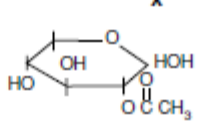
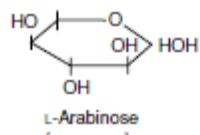
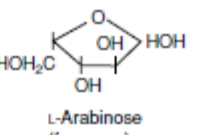
Pentose	Acetylated pentose
 X D-Xylose (pyranose)	 X* Acetyl-D-xylose
 Ap L-Arabinose (pyranose)	 Af L-Arabinose (furanose)

Figure 2. Hemicelluloses monomers, their symbols are show on the top right of the molecules (21).

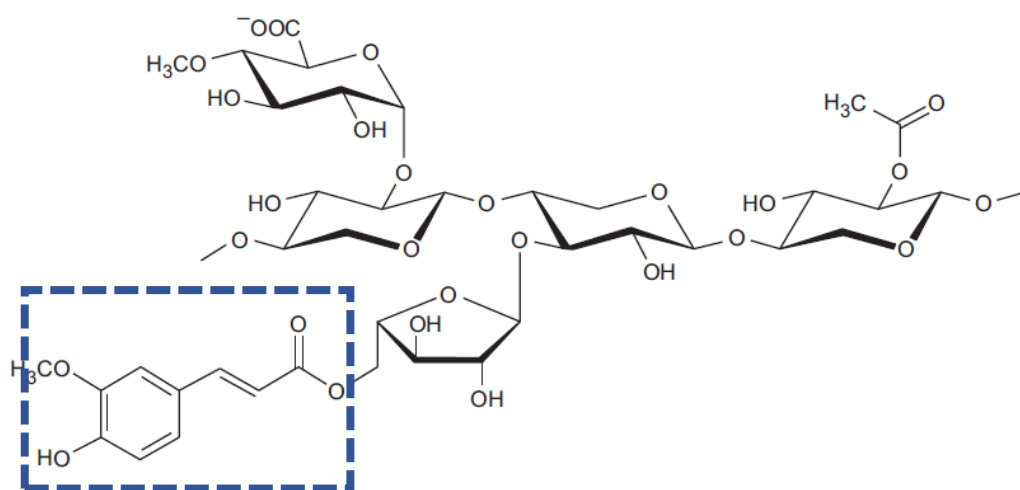


Figure 3. Fragment of a hemicellulose chain bonded to a lignin monomer (highlighted) (19).

In a vegetable tissue, the hemicelluloses work as a matrix in which the cellulose chains are inserted, they bond themselves and cellulose chains via hydrogen bond and to lignin via ester bond, as highlighted in the Figure 3. Being shorter, branched and amorphous chains, they are less mechanically and chemically resistant than cellulose, being the target of many xylophage threats like fungi and bacteria (15).

Cellulose and hemicelluloses, known together as holocellulose, are both highly hydroxylated biopolymers, thus they are highly hydrophilic. They are responsible by the absorption and transportation of water in the vegetables, among other functions(15).

Lignin is also an amorphous biopolymer made up of different monomers, like the hemicelluloses. Its repetitive unities are derived from phenylpropane, mainly *p*-coumaryl alcohol, coniferyl alcohol and sinapyl alcohol (15), shown in the Figure 4.

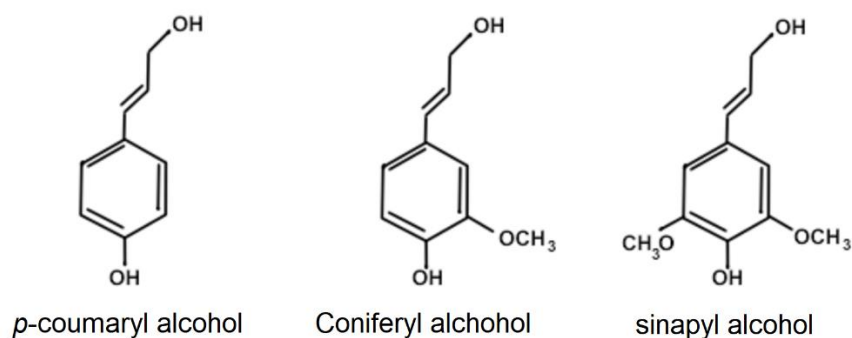


Figure 4. Lignin precursors (15).

Those precursors bound to one another by C-O-C and C-C bonds, forming random non-linear complex structures that present no upper polymerization or estimated molar mass (19). A proposed structure for a fragment of lignin is shown in the Figure 5. It is important to remember that, because of its high structural complexity, lignin cannot be extracted from the vegetable structure without being modified, making it hard to precise its structure (15).

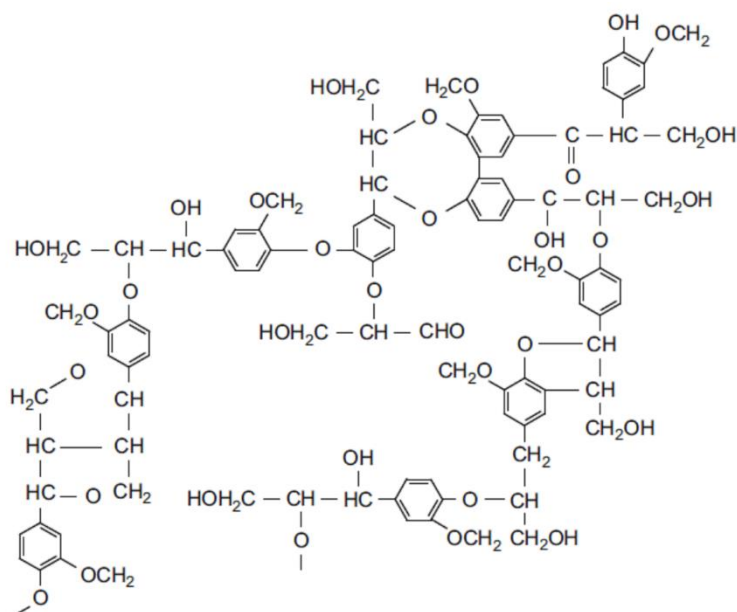


Figure 5. Proposed structure for a fragment of lignin (19).

Despite its precursors being hydroxylated, as seen in Figure 5, the lignin itself is not, as seen in Figure 5, they use their -OH groups to C-O-C bond to one another, making lignin a hydrophobic biopolymer. Its high complexity is hard to degrade by enzymes, giving vegetables some resistance to microorganisms, bugs, fungi and other threats, acting as a protection factor for the vegetable. Another role of lignin in a vegetable is to act as a glue, keeping the vegetable structure whole by ester bonding to hemicelluloses' chains, as seen in the Figure 6, being important for the mechanical rigidity of a vegetable (19). In a vegetable, those three biopolymers are organized as shown in Figure 6.

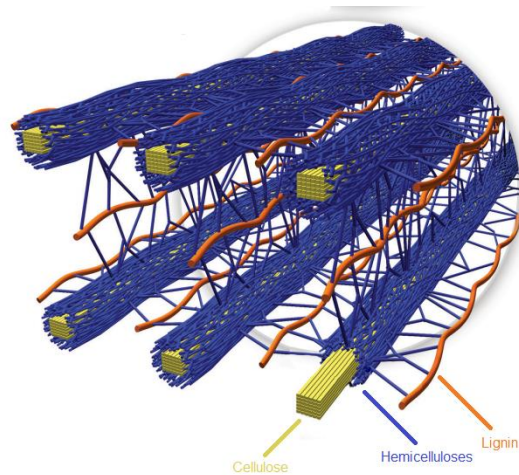


Figure 6. Organization of the biopolymers in a vegetable (22).

Figure 6 represents the organization of the biopolymers in vegetable fiber, from a piece of wood, for example. It is possible to see the linear highly organized cellulose chains, bond to each other by hydrogen bonding, wrapped up in chains of hemicelluloses. The hemicelluloses chains bond to each other by hydrogen bond and by ester bond to lignin, holding the whole structure together (15). Hydrogen bonds are not represented in Figure 6.

At a cellular level, vegetables are made up of vegetable cells: eucaryotic cells that differ from animal cells, among other differences, by the presence of lignocellulosic cell walls (15). The basic structure of a vegetable cell is shown in Figure 7.

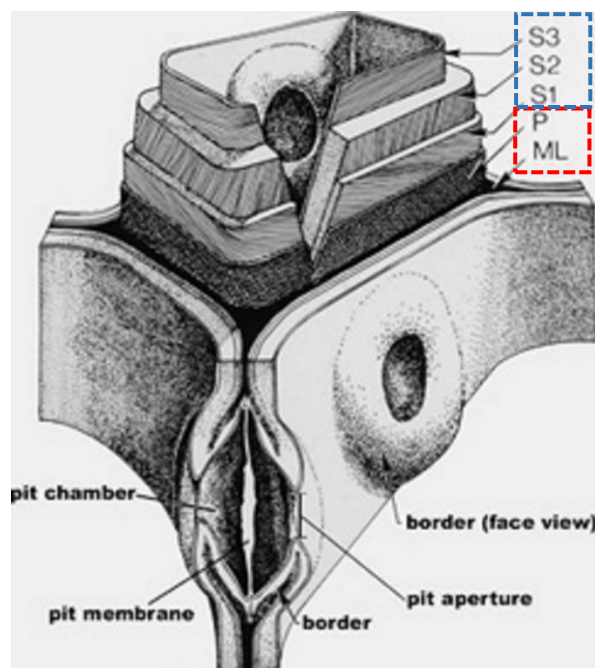


Figure 7. Structure of a vegetable cell wall (15).

The cell wall is composed of 3 main structures: the Middle lamella (ML), the primary wall (P) and the secondary wall, which itself is composed of three layers: S1, S2 and S3. The next few paragraphs will describe the structures shown in the Figure 7 (15).

- ML: a thin interfacial layer shared between cells. The ML causes the adhesion between the two or more cells that share it. As could be expected for an adhesion layer, it contains the highest relative lignin content of all layers of the cell wall;

- P: a thin layer composed of randomly oriented microfibrils. Being also a thin layer, it can be hard to tell it apart from the ML with certainty, so they are often named together as composed middle lamella;

- S1: a fine layer whose fibrils have well defined angles from 50° to 70°. Despite being thin, it is thicker than the ML and the P layers.

- S2: the thickest and most important layer in defining the wood's properties. Its fibrils present low angles (from 5° to 30°) and, even though it has a low relative amount of lignin, especially when compared to the ML, it has the biggest absolute value of this biopolymer due to its sheer thickness;

- S3: relatively thin, containing high angle microfibrils. It is the part of the cell within which the water is transported, thus it contains nearly no lignin, as its hydrophobicity would negatively impact the water transportation.

- Borders: interface between two cells, allowing changes of molecules to be done between them. Molecules like water, for example, that cross the borders need to pass through the membrane, slowing down the process of water transportation.

One of the most vital activities within a vegetable is the water transport from the root to the leaves. In softwoods, from a tree bark, for example, most of the cells present are long, rectangular and empty cells named tracheids. These are cells specialized in the transport of water. For that, the vegetable kills those cells, leaving only their cell wall delimiting an empty known as void, through which water freely cross, making up for a more efficient transportation mean than transporting it through living cells (15).

Woods can be broadly divided into two categories regarding the presence of more efficient water transport structures in them: softwoods (gymnosperms, conifers, evergreens) and hardwoods (angiosperms, deciduous). Despite the

names, the wood's softness or hardness cannot be always accurately estimated based on only this classification (15).

Softwood is composed mainly of tracheids, lacking in more specialized structures to transport water. These cells, however, are closed at both ends, forcing the water molecules to cross the membrane between two cells seen in Figure 7 to make their way through the vegetable, going in a zig-zag fashion as it goes up from the root to the leaves. Those characteristics make the water transportation slow and not as efficient as it could be wanted (15).

Hardwoods present water transporting structures named "vessels", they are like long tubes made by the stacking of special cells named "vessel elements". Those cells are shorter than the tracheids, but are much wider and are open, or at least semi open, at both top and bottom ends. As result, the water does not need zig zag through membranes to make its way up the vegetable, it can freely traverse the vessels through their openings, a much more efficient and faster way to transport water when compared to that of the softwoods (15). Figure 8 shows a comparison between a vessel element and a tracheid.

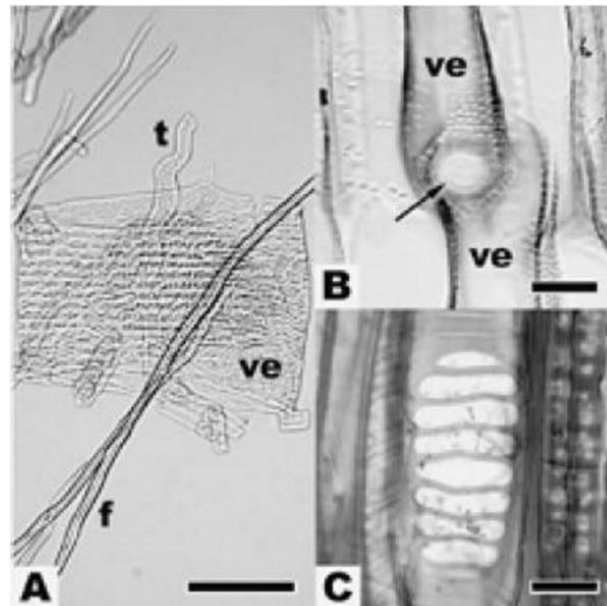


Figure 8. (A) A vessel element (ve), a tracheid (t) and a fiber (f), another structure present in hardwoods, (B) The stacking of two vessel elements and (C) the opening at an end of a vessel element (15).

Figure 9 shows the comparison between a soft and a hard wood, as well as the comparison of a microscopy of those kinds of wood.

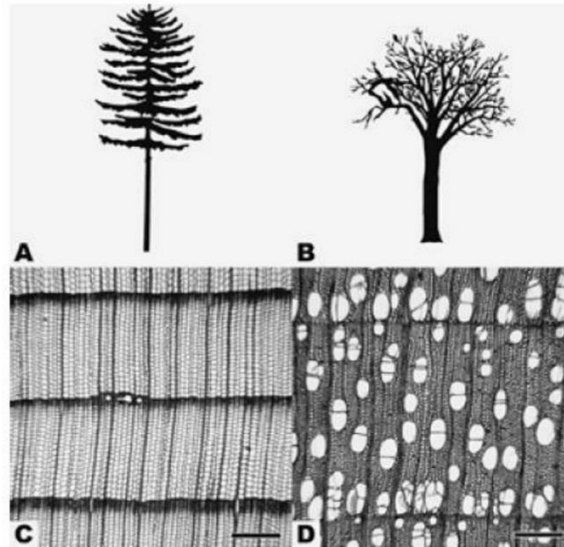


Figure 9. A softwood (A) and its microscopy (C); a hardwood (B) and its microscopy (D) (15).

Microscopy (D) In Figure 9, it can be noticed the morphology difference caused by the presence of vessels in hardwoods. As vessels assume the role of transporting water, the size of the tracheids in softwoods is smaller than the vessels in softwoods, giving these woods its namesake usual hardness. In Figure 9, the dark horizontal line seen in both (C) and (D) are the growth rings.

2.2 Thermal treatment

As already explained, woods are highly hygroscopic materials due to their lignocellulosic composition. The water sorption and desorption cycles negatively impact important properties of the wood, like dimensional stability, strength, energy density, longevity and others, limiting their possible usage, especially for outside applications and energy generation. Wood is also easily attacked by fungi, bacterial, bugs and other threats because of their lignocellulosic composition, compromising their structural integrity and longevity (23,24).

As wood is a quite important material in many areas of society, there is plenty of research on ways to overcome those listed drawbacks. One of these methods is the thermal treatment by soft pyrolysis or torrefaction, which has shown to greatly improve wood's resistance to fungi attack, lower its hygroscopicity, higher hydrophobicity, color changing, improvement of dimensional stability and increase its energy content (24,25).

In return, the wood is mechanically weakened after its transformation. This thermodegradation is realized under different inert atmospheres: vacuum, nitrogen, smoke, steam, oil, etc. To avoid the combustion phenomenon, it's important to work with an oxygen content lower than 5%. In this condition the thermodegradation is not oxidative. The intensity of the process depends on the temperature, but also on the treatment time. The heating rate is another parameter important for the final quality of the transformed wood, its value is close to $1^{\circ}\cdot\text{min}^{-1}$ and depends on the wood species, the water content, the thickness of the board, and the charge of wood in the oven. Generally, wood is transformed at a temperature between 200 and 220 °C for a duration between 30 min and 2 h, these values are purely indicative, the companies don't communicate on this sensitive subject.

Bellon *et al.* (2020) (26) treated 60 samples of eucalyptus, each species pine and teak by the industrial thermal treatment known as VAP HolzSysteme® to assert its influence on the wood resistance to the brown rot fungus (*Lentinula edodes*). Three different treatments were run on each wood species: room temperature (control), 140 °C and 160 °C. 20 samples were treated at 140 °C and another 20 samples at 160 °C. The thermal treatment showed decreased biodeterioration by the fungus in eucalyptus but lowered the fungi resistance in the pine samples while the teak samples suffered little modifications. It is important to note that pine teak itself is naturally resistant to the fungus, so the physical-chemical modifications caused by the treatment might have interfered with its natural protection. Their work has shown the possibility in the usage of thermal treatment to increase a wood's resistance to fungi, but that it is not a one size fits all solution, it is necessary to consider each type of wood and their properties carefully.

One of the most common usages for wood is burning it for energy generation, that is also negatively affected by the wood's affinity with water. Richa *et al.* (2024) (27) studied the effects on potassium catalyzed torrefaction of beech boards at 275 °C. Their studies found that potassium impregnation causes wood to burn more similarly to coal, producing smaller quantities of volatiles, making for a more environmentally friendly generation of burn wood.

In a thermal treatment, the first step, at 100 °C, is the loss of water (drying) present in the wood. As the temperature increases (from 170-180 °C) hydroxyl

groups and side chains in hemicelluloses are removed, eventually moving on to the decarboxylation, then the charring of the wood, producing char (28).

The pyrolysis of wood is a rather complicated process, due to the complexity of wood. Many different models have been proposed to explain it. A simplistic model for wood pyrolysis is to consider it a one-step reaction, where heat turns wood into gas and coal. This model did not gather much popularity because of its simplicity (29). Alternative methods have been proposed to explain the pyrolysis in more details, like the model proposed by (30) who proposed a one-step model in which heat would lead to concurrent simultaneous reactions to produce gas, tar and char. Figure 10 shows a comparison of older one-step models and the Shafizadeh and Chin's model.

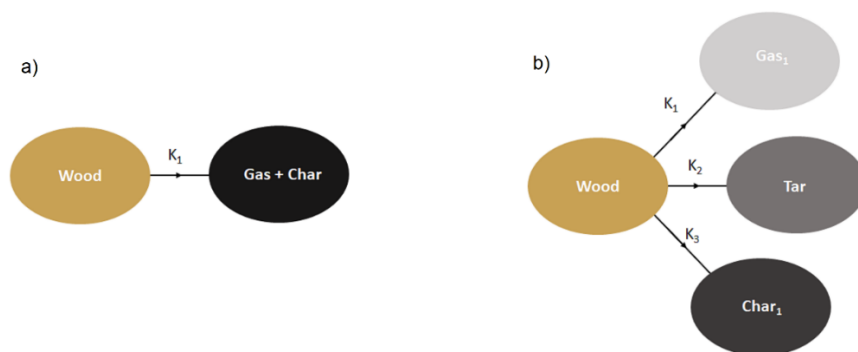


Figure 10. (a) Old one-step pyrolysis model, and (b) the model proposed by Shafizadeh (31), Adapted figure.

Despite still being a one-step reaction, it became more popular than previous and more simplistic models, as it could more accurately explain the observed experimental values and results of wood pyrolysis. Further models were developed based on Shafizadeh and Chin's model, like Prakash and Karananihi (2008) (32), who proposed that the tar could be further decomposed into gas and char, also in simultaneous concurrent reactions.

A current way to look at a wood pyrolysis is to see it as a series of steps, each of them resulting in a solid component (SC) and a mass loss by volatilization, creating a gaseous component (GC). The solid and gas phases are known as pseudo-components, as seen in Figure 11. The number of steps varies according to the complexity of the pyrolysis (33).

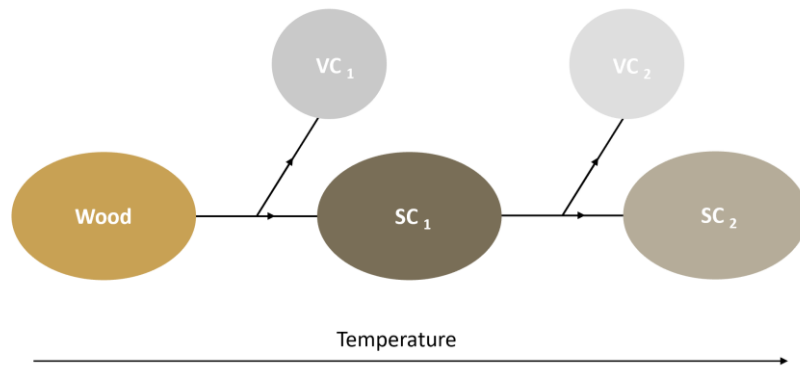


Figure 11. Multiple steps pyrolysis of wood (33).

It is important to remember that even though those models show wood as a single thing for simplicity, an actual pyrolysis is the sum of the pyrolysis of its main components, namely: hemicelluloses, cellulose and lignin, each producing their own solid and gas components (29).

The first biopolymer to be degraded in a thermal treatment are the hemicelluloses, followed by cellulose and, finally, lignin. Figure 12 shows the deconvolution of a rubberwood DTG made by Lin *et al.* (2021) (34), representing each the experimental and calculated TGA and DTG curves, including also the deconvoluted peaks for the individual biopolymers.

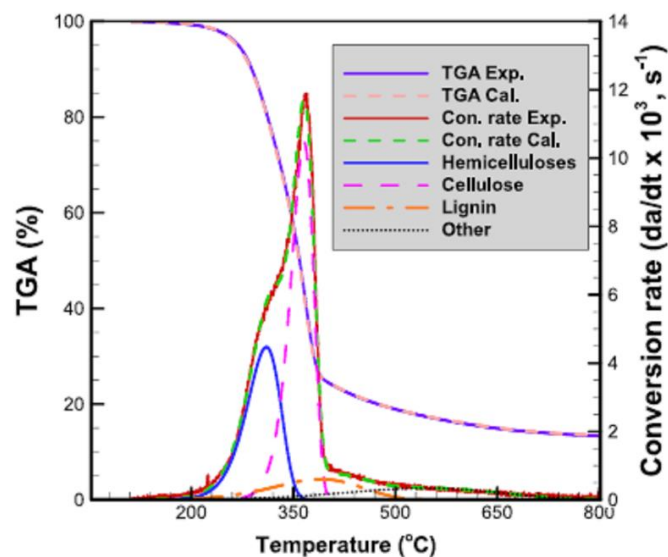


Figure 12. Experimental and calculated thermal degradation profile of a rubberwood sample, showing also the deconvolution for each individual biopolymer (34).

Figure 12 represents a typical wood DTG, beginning with a “shoulder”, which the deconvolution shows to be caused by the hemicelluloses peak,

followed by a sharp cellulose peak, then a lignin “tail”. Notice that despite the hemicelluloses and cellulose being degraded first, in this order, the lignin thermal degradation happens in a wider temperature range when compared to the other biopolymers, beginning during the temperature of hemicelluloses degradation. That can be explained by the randomized nature of the lignin structures, creating many segments with different thermal resistances, opposed to the well-defined properties of hemicelluloses and, specially, cellulose. The degradation, however, is low in all the temperatures.

There exists interest in the study of TGA to study wood’s biopolymers as it is a simple and cheap way to investigate their behaviors. Carrier *et al.* (2011) (35) analyzed the different kinds of vegetables by DTG, comparing area of the deconvoluted peaks and their quantities affected by wet chemistry methods. The study showed great correlation between the peaks’ areas and the actual quantities of hemicelluloses and cellulose, but showed poor correlation with lignin, likely due to its more complex nature and wider degradation temperature range.

2.3 Biocomposites

2.3.1 Vegetable oils

Chemically, vegetable oils are classified as lipids. They are hydrophobic and less dense than water and are made up mostly from triglyceride (Triglyceride), molecules composed of three FA chains bound together by a glycerol molecule, containing also minor quantities of dyes, hydrocarbons, tocopherols, steroids and fatty alcohols. They are usually found in grains and seeds, but can also be found on pulps and peels of fruits, from where they can be usually extracted by mechanical pressing and/or solvent extraction (36). Figure 13 shows the basic structure of a triglyceride.

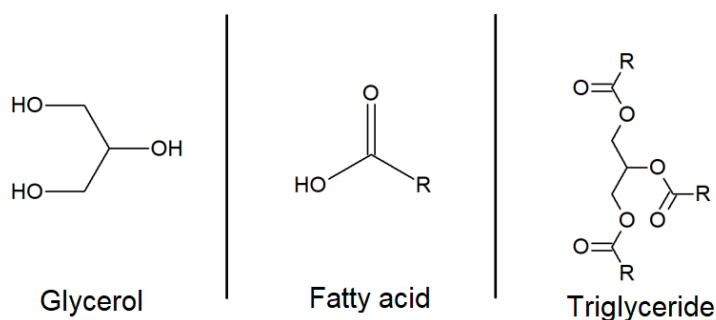


Figure 13. Glycerol, FA and triglyceride. R represents the rest of the FA molecules in a triglyceride and are not all necessarily the same (36).

FA are monocarboxylic aliphatic acids, found in their esterified form in oils, fats and waxes, both in animals and vegetables (International Union of Pure and Applied Chemistry, IUPAC) (37). They can be either saturated, with no double bonds, or unsaturated, with at least one double bond. In nature, nearly all of the FA are found as their *cis* isomers, but there are some *trans* FA found in nature, like brassic acid, naturally found in rapeseed (38). Figure 14 represents a saturated, an unsaturated *cis* and an unsaturated *trans* FA.

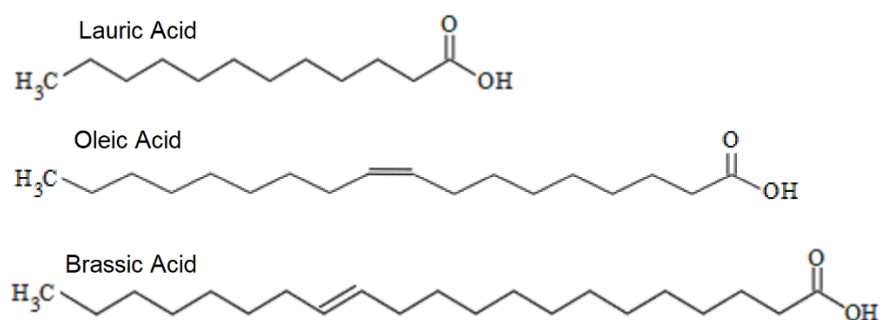


Figure 14. Lauric acid, saturated; oleic acid, a *cis* unsaturated FA and brassic acid, a *trans* unsaturated FA (39).

Many reactive sites can be found in FA molecules, like the ester group, the unsaturations and the carbon neighboring the unsaturations. These reactive sites can be used for chemical modifications to adapt the triglyceride and oils to achieve specific properties (40,41). Figure 15 shows the reactive sites present in a triglyceride.

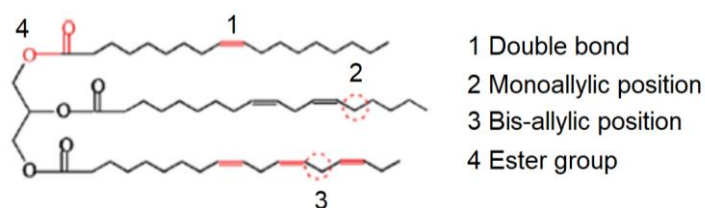


Figure 15. Reactive sites found in a triglyceride (40).

Due to the variety of reactive sites found in triglycerides, a variety of chemical modifications can be done on them, granting them the huge versatility that has attracted the interest of researchers in many fields to research on the modification vegetable oils (7). Figure 16 shows some examples of reactions that can be done on vegetable oils. Despite the versatility of this variety of reactive sites present in vegetable oils, one drawback caused by it is the low oxidative

stability caused mostly by the presence of unsaturations on the FA molecules, decreasing their longevity and the shelf life of products made with them.

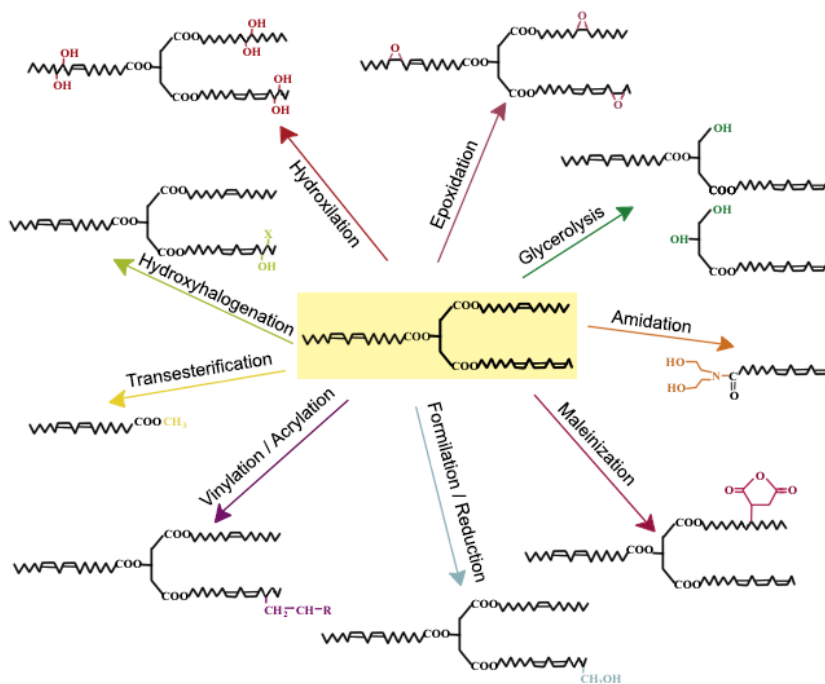


Figure 16. Example of possible reactions with vegetable oils (7).

FAs can vary mainly in both number of carbons and number of unsaturations, both bearing great influence in the FA's physical, chemical and biological properties and, naturally, the properties of the triglyceride these FA make up (42). Table 1 shows a list of common FA.

Table 1. Some examples of FA (42).

Symbol	Name	Structural formula	T _{fusion} (°C)
Saturated FA			
12:0	Lauric	CH ₃ (CH ₂) ₁₀ COOH	44,2
14:0	Myristic	CH ₃ (CH ₂) ₁₂ COOH	52,0
16:0	Palmitic	CH ₃ (CH ₂) ₁₄ COOH	63,1
18:0	Stearic	CH ₃ (CH ₂) ₁₆ COOH	69,1
22:0	Behenic	CH ₃ (CH ₂) ₂₀ COOH	
24:0	Lignoceric	CH ₃ (CH ₂) ₂₂ COOH	81,0 84,2
Unsaturated FA			
16:1	Palmitoleic	CH ₃ (CH ₂) ₅ CH=CH(CH ₂) ₇ COOH	-0,5
18:1	Oleic	CH ₃ (CH ₂) ₇ CH=CH(CH ₂) ₇ COOH	13,2
18:2	Linoleic	CH ₃ (CH ₃) ₄ CH=CHCH ₂ CH=CH(CH ₂) ₇ COOH	-9,0
18:3	α-Linolenic	CH ₃ (CH ₂)(CH=CHCH ₂) ₃ (CH ₂) ₆ COOH	-17,0
20:4	Arachidonic	CH ₃ (CH ₂) ₄ (CH=CHCH ₂) ₄ (CH ₂) ₂ COOH	-49,5
24:5	Nervonic	CH ₃ (CH ₂) ₇ CH=CH(CH ₂) ₁₃ COOH	39,0

FA, as represented in Table 1, are identified by their number of carbons, the number before the colon, and unsaturations, the number after the colon.

2.3.2 Macauba and its oils

Macauba is a tropical palm found mostly in Brazil but, as it is highly adaptable, has spread to central and even some parts of North America, with Brazil remaining as its biggest producer (43,44).

Its tall palms can reach up to 16 m, yielding about 25.000 kg·ha⁻¹ each year. Its fruits have high oil content, reaching 50% to 75% of oil content, amounting to about 6.2 tons per hectare each year (44,45), being even more productive than soy, the most produced oil seed in Brazil, which averaged 4.111 Kg·ha⁻¹ in 2022, according to National Supply Company (*Companhia Nacional de Abastecimento, CONAB*) (46), that being one of the key factors that have attracted attention from researchers to those fruits.

The macauba fruits are drupes (the pulp and the seed are bound to one another, like in a mango) that grow in bunches containing from 300 to 600 fruits that are composed of peel, or epicarp, (23,0% in mass); pulp, or mesocarp, (46,7%); endocarp (23,0%) and kernel (6,3%). Those fruits present mainly 2 different oils: the macauba kernel oil (MKO) and the macauba pulp oil (MPO). There is also oil in the peel, but the peel is not as rich in oil as the other parts of the fruit and the oil itself is not as well studied as the other oils from the fruit. MKO is rich in saturated acids, especially oleic acid, its main FA. Macauba pulp oil on the other hand, is rich in unsaturated acids like oleic acid, its most important FA (47-49). Figure 17 shows the macauba fruits.



Figure 17. Intact macauba fruits (left) (48), and a cut fruit (right) (49). Adapted figure.

Other than the oil production of the macauba fruits being considerably high, another interesting part of the oil production is that the production's byproducts also present commercial value that can help the funding of the oil production itself. The kernel and the pulp's cake (the solid residue left after the mechanical pressing for the oil extraction), which are nutritious, possessing 9% and 23%, respectively in proteins, that can be used in both animal and human feed. The endocarp, can be used to produce high energy coal, that can be sold for the steel industry, for example, or even used to power up the oil extraction itself (50-52). Figure 18 shows the main usage of each part of the macauba fruits.

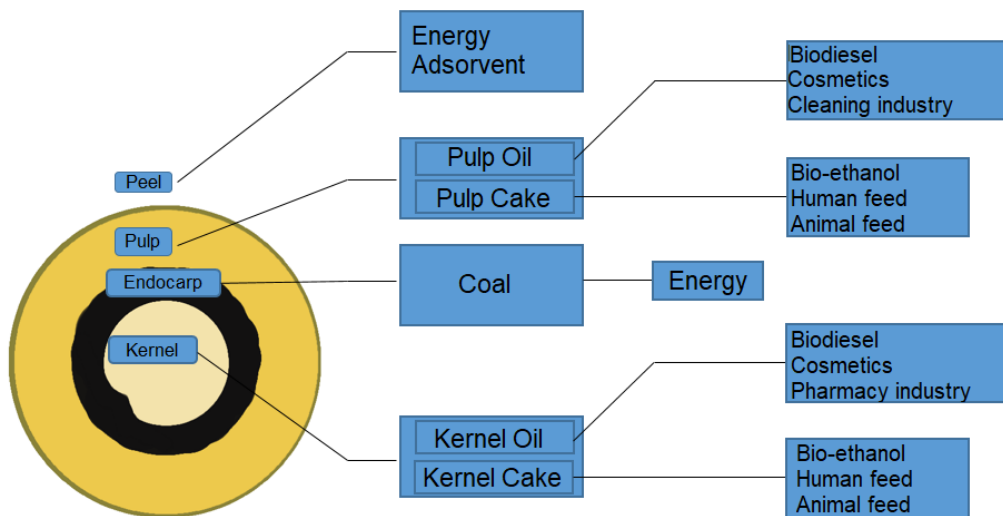


Figure 18. Parts of the macauba fruit and their main commercial usages (50). Adapted figure.

Macauba also presents an interesting potential for the production of biodiesel, as was shown by Santos *et al.* (2020) (49), who have produced biodiesel by transesterification of MPO with homogeneous catalysis, with 4h and 24h of reaction time. Their results showed that both reaction times yielded acceptable products, according to the tests and standards of the National Agency of Oil, Natural Gas and Biofuel (*Agência Nacional de Petróleo, Gás Natural e Biocombustíveis, ANP*), though a higher transesterification index was reached with the longer reaction time.

Macauba crops were also studied by Moreira *et al.* (2020) (50) as a mean for carbon sequestration. They tested different aged macauba palms and quantified their biomasses, concluding that 9-year-old macauba could sequester 221.17 tons of CO₂ per hectare every year, generating 761.01 euros

in carbon credit per hectare. Moreira *et al.* (2018) (51) have also studied the effect of intercropping coffee and macauba to reduce the climate changing effect of the coffee crops. The intercropping resulted in reducing the air temperature on the crops and has increased the amount of available radiation for photosynthesis.

Amaral *et al.* (2007) (9) calculated the oil content of each part of the macauba fruit, the results are shown in the Table 2.

Table 2. Oil content for each part of the macauba fruit (9).

Part	Oil content
Peel	6.5
Pulp	59.8
Endocarp	---
Kernel	55.6

As mentioned above, MKO and MPO have different compositions. The average composition of the kernel, pulp and peel oil is listed in Table 3.

Table 3. Composition of kernel, pulp and peel from macauba oil (48,52).

FA structural formula	Percentage (%)		
	Pulp	Kernel	Peel
Oleic acid 	53.0	23.0	51.5
Palmitic acid 	22.0	17.5	24.6
Lauric acid 	2.9	39.0	---
Miristic acid 	2.0	11.0	---
Estearic acid 	6.0	4.5	5.1
Capric acid 	---	4.0	---
Caprilic acid 	---	2.0	---
Palmitoleic acid 	5.5	---	6.2
Linoleic acid 	5.0	---	11.3
Margaric acid 	4.5	---	---
Linolenic acid 	---	---	1.3

The content of the main FA in each oil has been highlighted.

The MKO, being low in unsaturated acids, has a low iodine index, meaning it is less susceptible to oxidation, while the higher iodine index in MPO, while it makes it more oxidizable makes it more easily to chemically modify it, making both oils interesting for different fields of research (53), but their most prominent line of it the synthesis of biofuels.

Silva *et al.* (2016) (54) used transesterification of MKO using methanol, ethanol, isopropanol and isobutanol for the usage as biodiesel and jet fuel. Better conversion results were observed for the reaction with ethanol and methanol, and their tests showed that while acceptable results for the usage as biodiesel were achieved, the preliminary results for jet fuel, especially at low temperatures, were not adequate.

Despite the rising interest in macauba, its production is still rather primitive. Fruits are usually picked from the ground after falling from the palms, damaging and possibly infecting, there isn't as much study on optimal planting and harvesting conditions as there are for other oil seeds, like soy and corn, as a consequence, properties and results involving macauba tend to not be as reproducible as it would be ideal (48,55,56).

Despite the relatively low knowledge about the crop, it is an important source of income for the family farmers that make a living from it. The research on the fruits and their applications might increase their value, increasing the income for those families, giving research these researches a social appeal. For better valorization, it is interesting to add value to all the parts of the fruits. MPO is more well studied than the MKO, probably for the higher modifiability and being easier to obtain. The valorization of MKO is also important, as it can not only make the fruits more valuable for those who depend on it to live but it can also generate knowledge on a whole new variety of possibly interesting molecules for all kinds of usage.

2.3.3 Polyurethanes

Polyurethanes (PU) are a versatile and widely used class of polymers, made by the reaction of a polyol (an alcohol with at least two -OH groups) and an isocyanate with at least two -NCO groups (while needing two or more -NCO is

not implied by the name, it is necessary for its reaction with the polyol to result in a polymer, not in an urethane monomer) (57).

The notable variety of both polyols and isocyanates, as well as possible additives and reaction conditions creates a virtually infinite number of possible PU to be synthesized. They can be made as soft foams, rigid foams, elastomers, thermoplastics and many others. Its versatility has given the PU a position as one of the most consumed plastics in the world, making up about 8% of all the polymers consumed in the world. It is estimated that, by 2025, the world demand for PU might go up to about 24,2 million tons (60,61).

As most of the polymers also are, PU are majorly produced as a petrochemical polymer all around the world. However, the ever growing concern about depletion of petroleum, as well as the rise in environmental awareness in both industries, governing bodies and the general public has led to the search of renewable ways to produce such an important material (58).

Natural polyols do exist, like hemicelluloses and cellulose, the main biopolymers of wood and vegetable fibers in general. Ricinoleic acid, for example, the main FA present in castor oil, is a natural polyol. It has been studied by (15,62). Zhang *et al.* (2023) (59) who used castor oil based bio oil, in different proportions (5, 10 and 15%) as asphalt binder. The final products were shown to have good low temperature performance, thermal stability and resistance to moisture damage, but the high temperature performances were less than ideal, leaving space for further research on the subject.

Despite the availability in nature, being able to prepare different polyols with specific physical-chemical properties to prepare PU and other products is rather interesting, as it gives us finer control on their properties. In the past few decades, the synthesis of polyols has been intensely researched, leading to the discovery of several ways to prepare a variety of polyols (15,62). Figure 19 presents some examples of possible polyol synthesis.

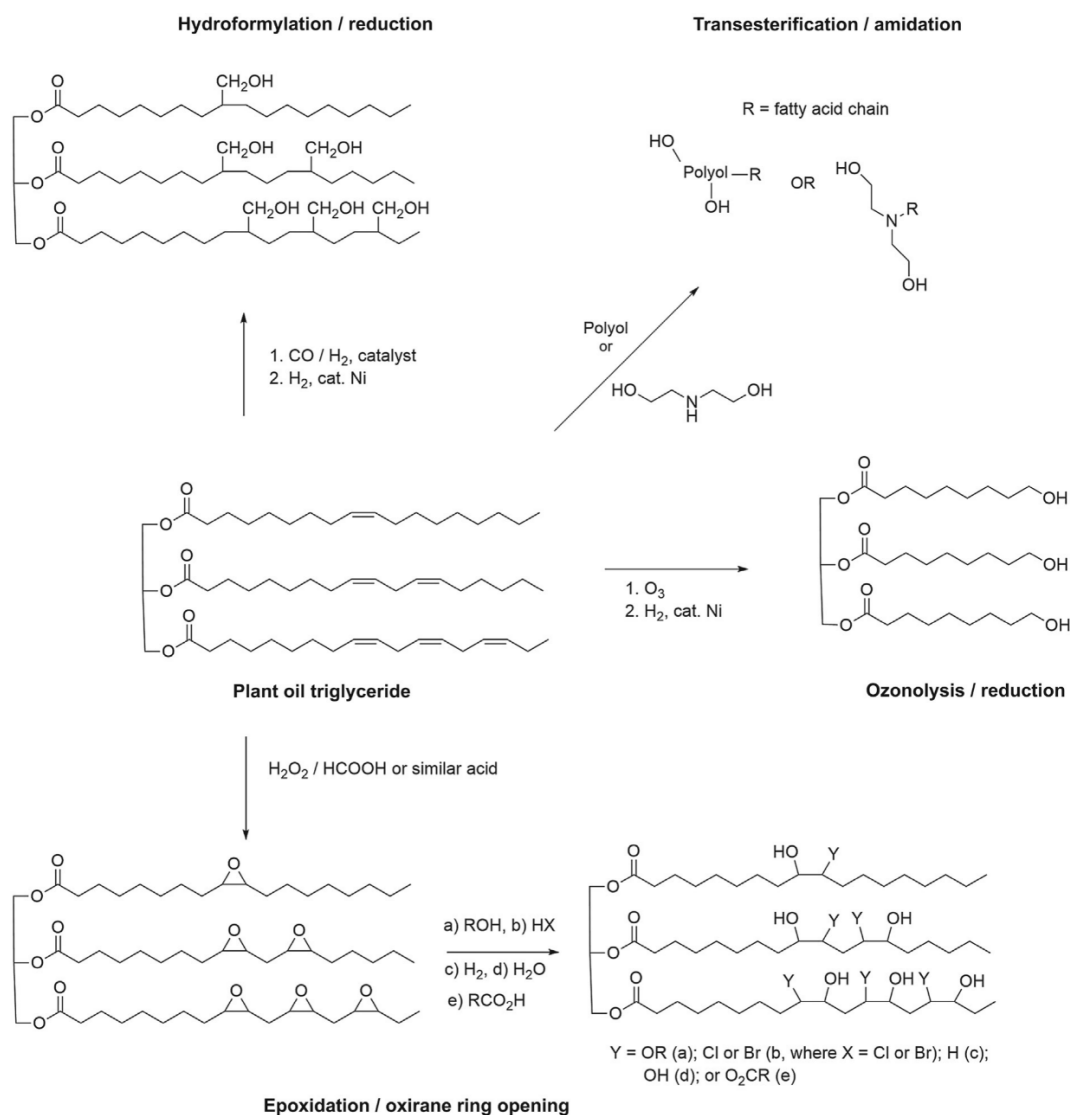


Figure 19. Example of possible ways to form polyols (4).

Borowicz *et al.* (2020) (58) used epoxidized mustard seed oil (whose main FA is the polyunsaturated linoleic acid) (60), to produce polyol by epoxide ring opening with diethylene glycol to open the ring. The obtained polyol was used to prepare PU foams that showed good mechanical properties, aging resistance and better biodegradability than the tested petrochemical PU.

Paraskar *et al.* (2020) (61) prepared PU coatings for metals made from different vegetable oils: Linseed oil, castor oil and orange oil. They reacted with diethanolamine to make fatty diethanolamine, then with itaconic acid to make polyesteramides, which were then reacted with HDI, an isocyanate. The resulting PU coatings have shown correlation between the number of -OH groups in the

polyol and the crosslinking between the layers of polymers, yielding better thermic, mechanic and anti-corrosion properties.

For this work, the chosen way to produce polyols was the epoxidation followed by the epoxide (oxirane) ring opening reaction. The epoxide is opened using $\text{BF}_3(\text{Et}_2\text{O})$ (which will be only referred to as BF_3 , from now on) as catalyst and glycerol is used as the hydroxylated compound (ROH in Figure 20).

The other reagent for the synthesis of polyol is the isocyanate. Just like the polyol, isocyanates are also quite diverse, making up numerous possible combinations between polyol and isocyanate. Figure 20 shows some kinds of isocyanates.

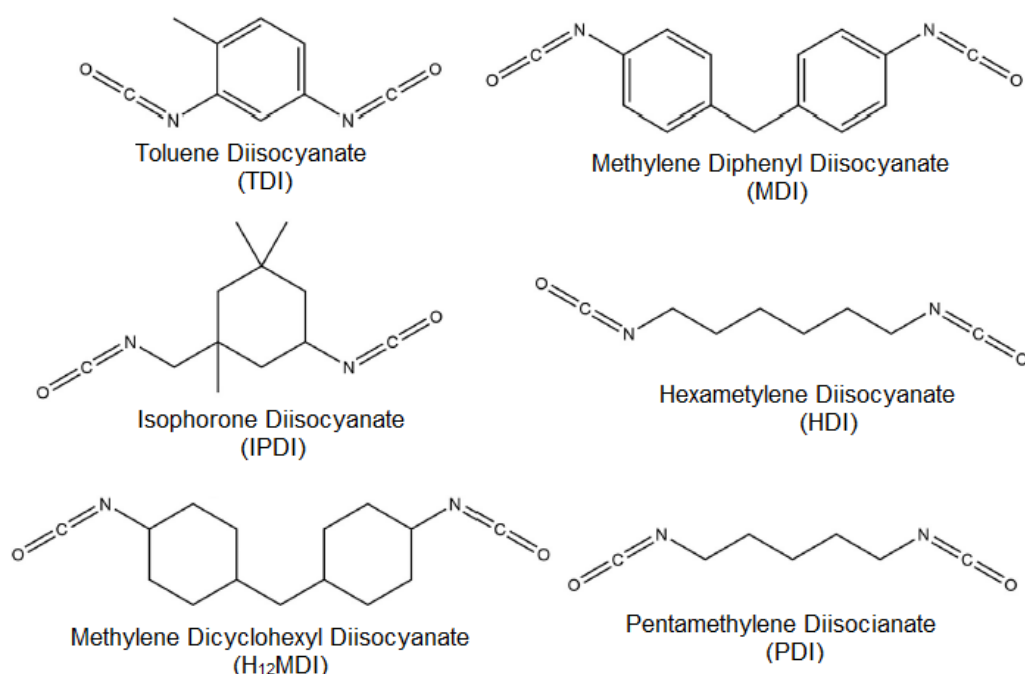


Figure 20. Some commercially available kinds of isocyanates (4).

For this work, the chosen isocyanate was Methylene Diphenyl Diisocyanate (MDI).

PU differ from conventional polymers in that there is no urethane monomer. The name of the polymer, instead, refers to the -NHCOO (urethane) groups formed during the polymerization reaction between the polyol and the isocyanate (62). Figure 21 shows the formation of a urethane group.

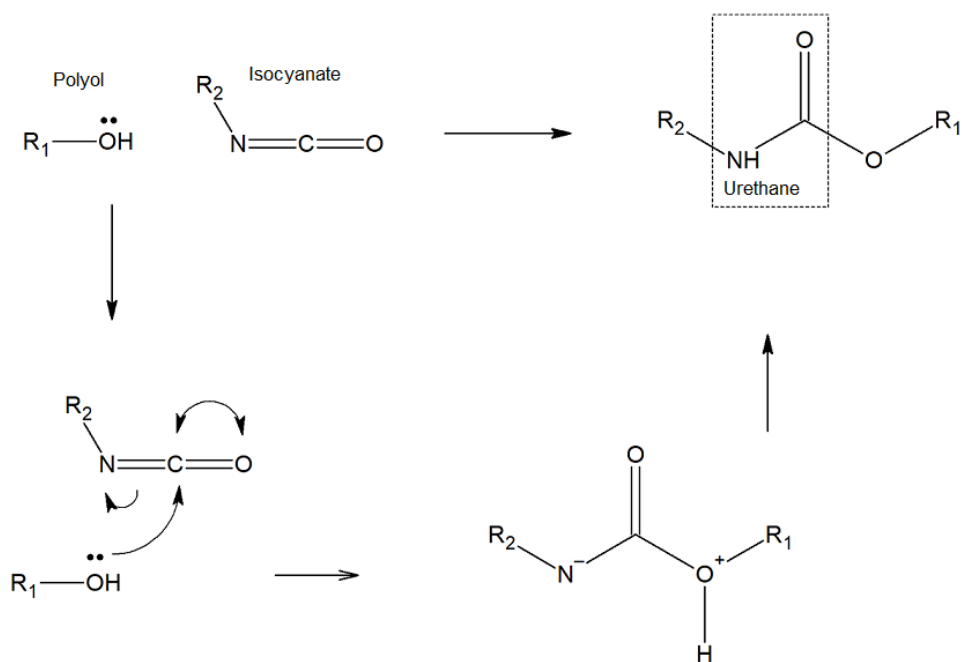


Figure 21. Formation of an urethane group (63). The rest of the polyol and isocyanate have been omitted for better visual clarity.

In the PU synthesis, the polyol and the isocyanate form different regions, or segments in the final product, as shown in Figure 22. Polyols, higher mobility, longer molecules, form soft segments, responsible for the softness and flexibility of the final product. The isocyanate, on the other hand, form the rigid segments, as they are shorter and more crystallizable molecules. The combination of soft and rigid segments is responsible for the final properties of the PU (64).

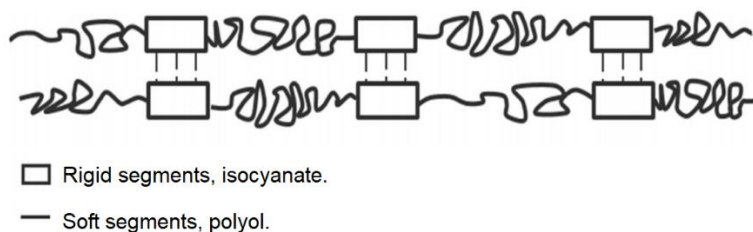


Figure 22. Rigid and soft segments in a PU (64).

2.3.4 Glycerol

Glycerol is a trifunctional alcohol, most usually found in Triglyceride, where it is the backbone that binds its three FA molecules together (17). It can be produced petrochemically, by the chlorination/hydroxylation of propylene, for example (65), having historically been produced from oils and fats. It is believed

that its molecule was discovered in 1779 by K. W. Scheele, a Swiss pharmacist after heating up a mixture of olive oil and litharge (lead oxide) (66).

Glycerol is a sweet tasting, oily, colorless, odorless and viscous liquid. It presents three hydroxy groups (as seen in previously Figure 13), rendering it highly hygroscopic and soluble in water. The hydrogen bonding abled by its -OH groups also lower its volatility and vapor pressure, as usually happens with alcohols, remaining nearly constant from 0 °C to 70 °C (67).

Technically, the name glycerol itself is only applicable for the pure 1,2,3 propanotriol (its IUPAC name) compound. Solutions of glycerol, usually in water, with 95% or higher purity should be called glycerin. This work, however, mostly uses the term glycerol, as it refers to the molecule, not a solution. It is widely used in pharmaceutical and selfcare industries for its hydrating, mild antimicrobial and antiviral properties, being also used in the food industry as sweetener. It is also possible to burn it for energy, as it as a higher caloric value when compared to fossil fuels (70,71). Table 4 lists some of the glycerol properties.

Table 4. Some properties of Glycerol at room temperature (67).

Property	
Chemical formula	C ₃ H ₈ O ₃
Molar mass (g·mol ⁻¹)	92.094
Appearance	Colorless hygroscopic liquid
Odor	Odorless
Density (g·cm ⁻³)	1.261
Melting point (°C)	17.8
Boiling point	290
Solubility in water	Miscible
Lower heating value (MJ·Kg ⁻¹)	24
Refraction Index (η _D)	1.4746
Viscosity (pas·S)	1.412

Glycerol production dates back to centuries ago, being produced as a byproduct of Triglyceride hydrolysis for the production of soap, with the first industrial application of this process dating back to 1860's (65). Nowadays, glycerol is mostly produced as a byproduct of Triglyceride transesterification, a process first conducted in 1864 and is now mostly used to produce biofuel (65).

In the early 20th century, glycerol was mostly produced as a byproduct saponification of fats and was used to produce nitroglycerine, creating a high demand for the product during the 1st world war. Early in the 1990's, about 75%

of the consumed was obtained from saponification, the other 25% being made petrochemically (67).

With the rapid increase of biofuel production all over the world, global production of glycerol has risen dramatically (17), it is estimated that each 100kg of biofuel yields about 10kg of 50% to 55% purity (65). Over 2.8 billion liters of glycerol being produced only by the five largest biofuel producers as byproduct in the world in 2021. (Ben *et al.*, 2017) (65) Figure 23 shows the transesterification of a triglyceride molecule with methanol.

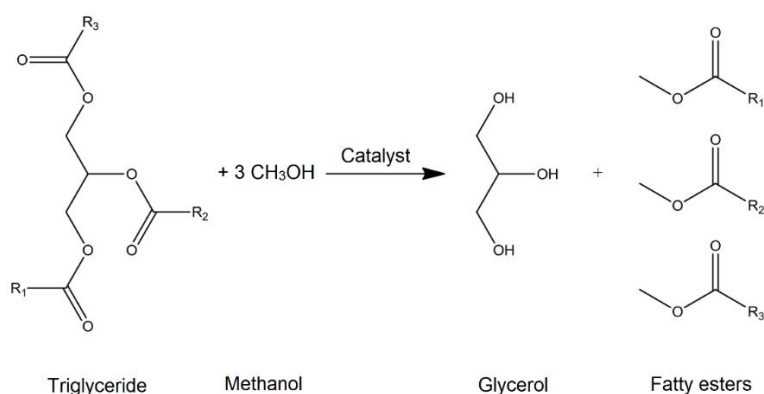


Figure 23. Transesterification of a Triglyceride (65). The fatty ester molecules represent the biofuel produced by the transesterification.

With the increasing demand for biofuels, debates on the ethicality of using human and animal food to produce fuel began taking place. The use of waste products (used cooking oil, for example) and non-edible oils gives the industry a chance to diversify its raw materials and increase production, as it creates an unforeseen variety of materials that can be used for biofuels and, as the biofuel production increases, so does the glycerol production (66,67). Figure 24 shows the growth of biofuel and, consequently, glycerol since the year 2000.

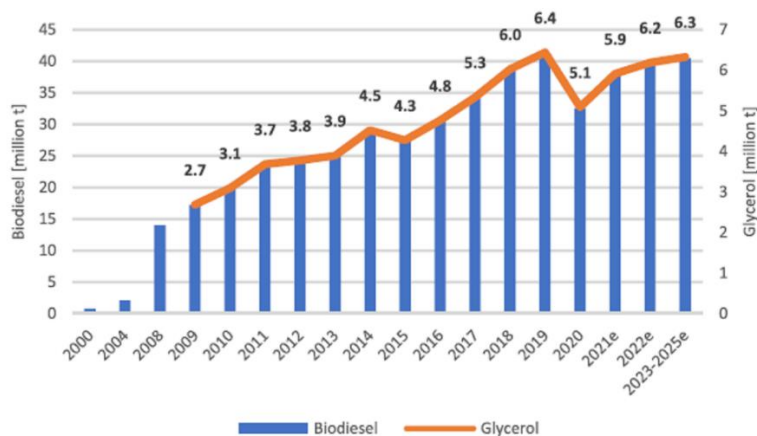


Figure 24. Growth in the world production of biodiesel and glycerol (67).

The growth in biodiesel (and glycerol) production seen in the Figure 24 is partially due the effort of governing bodied to insert it into the market, like the Brazilian program PROBIODIESEL, created in 2004 by the Brazilian Federal Government to gradually replace the use of petrochemical diesel with biodiesel, which ruled that biodiesel should be mixed with diesel in steadily increasing proportions, starting at 3% in 2008 and aiming to reach 20% in 2030 (70,72).

As good as the increasing, popularization and acceptance of biofuel in the market and by the population is for the environment, it brought with it massive surges in glycerol production, with the percentage of glycerol provided by the biofuel industry going from 9% in 1999 to 63% in 2003 (67). Glycerol, however, can be divided into different grades regarding its purity, with its most common usages, the pharma/health care and food industries needing at least 96% and 99.5% purity, respectively. This becomes a new environmental problem considering that the glycerol obtained from the transesterification in the biofuel industry is, as shown in the Table 5, not high in purity enough for its most important applications (67).

Table 5. Composition of glycerol obtained by different methods (67).

Component	Transesterification (%)	Saponification (%)	Hydrolysis (%)
Glycerol	30-60	83-84	88-90
Ash	10-19	8.5-9.5	0.7-10
Water	≤10	6-7	8-9
MONG*	≤40	3-4	0.7-1.0

* Matter organic non glycerol

From Table 5 the biggest part of all glycerol produced in the world, glycerol from transesterification, has considerably low purity. Figure 25 indicates the most important applications of glycerol in the world.

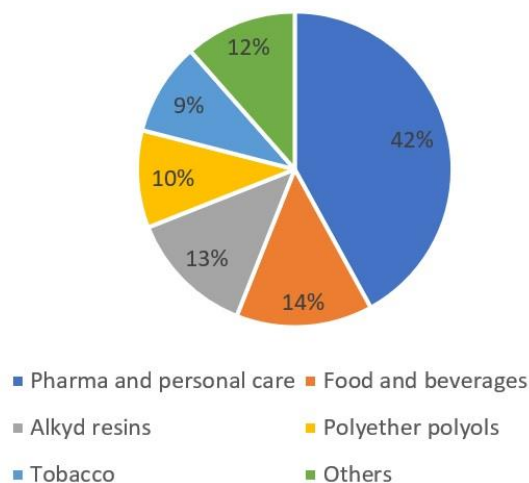


Figure 25. Main usages of glycerol in 2019 (67).

The chart in Figure 25 indicates that the main application of glycerol, pharma/personal care and food/beverage industries, making up together about 56% of all the glycerol consumption in the world. As already said, those two applications require high purity glycerol, that not obtainable by transesterification unless it undergoes intense purification processes (67).

The excessive supply of glycerol, a whole new environmental problem in one of itself, has brought researchers all over the world together to find new ways to valorize and use it. Ben *et al.* (2022) (17), for example, reviewed the pros and cons of using glycerol as a plasticizer in starch films for food packaging, noting how the hydrophilic nature of the molecules interrupts hydrogen bonds between starch molecules, working as a lubricant between them, increasing its overall plasticity. Calderon *et al.* (2023) (18) prepared a polyglycerols polyester polyol with coconut oil and glycerol from biodiesel synthesis to prepare thermoplastic PU, managing to produce thermoplastic PU that could still properly melt and remelt even after three heating cycles, which is up to industrial standards, proving that to be one possible way to valorize glycerol.

The global market value for glycerol is about US\$ 3,3 million dollars, and it has dramatically grown in the last 30 years since its introduction, though it has decreased in 2020 due to the Covid-19 pandemics. It is estimated that about 4.04 million tons of glycerol will be produced from feedstock by 2025, making up for 63% of all the glycerol produced in the world, but its purity will make it hard to be applied in its most usual ways. The expected demand of glycerol for 2025 is about 4 million tons. This obviously drastic difference between supply and demand causes its market prices to drop, and the loss of interest by the market results in much of the world's glycerol to be simply discarded as waste (67).

This work tried to valorize glycerol by using it in vegetable oil modification for the preparation of PU and composites. While the usage of glycerol, a polyol, for the synthesis of PU and other polymers, is not new, as shown by the works of Calderon *et al.* (18), using it as an epoxide ring opener is, to the best of the author's knowledge, a novelty.

2.3.5 Composites

By definition, a composite is a material made from two or more different materials/products with different properties and distinct boundaries. Combining

materials to create new materials for new applications is not a new idea, it has been used by humanity for millennia. Currently, most of new materials created can be considered composites (68).

Composites can be broadly classified in two categories:

- Filled materials. Materials whose polymeric matrix's properties are improved by particles used as reinforcement material, or fillers. The matrix usually makes up more than 50% of the materials and bear more weight in their main properties. The reinforcement material's properties are usually treated as homogenous and isotropic in the composite. The composites made in this work are considered filled materials (68).

- Reinforced materials. Also known as advanced composites, the matrix in these materials is usually less than 50% of the composite. The reinforcement materials are usually long thin fibers of high strength and stiffness and govern the main properties of the material. Glass fiber is an popular example of reinforced material (68).

Currently, natural fibers, like vegetable fibers are seen as promising materials to be used as reinforcement materials. They are diverse, readily available in large quantities, being often seen as waste and discarded by many industries and. VF are also usually lighter than synthetic fibers, like glass fiber, being already extensively used to produce lightweight materials for packaging, furniture, automotive interior linings and others (69).

One usual application of composites is made with vegetable fibers insulation. Good insulation can reduce the energy consumed with heating, which attracts the interest of green chemistry research. Azzouzi *et al.* (70) created insulating materials from plaster and dried ground pea pod in different proportions. Their materials present lower density than pure plaster and reached 27% less thermal conductivity with the addition of 25% of pes pod in mass to the plaster. Their results showed the possibility of creating composites with VF that not only are more insulated but are also lighter than some commercially available products.

Lopes *et al.* (2021) (13) produced composites from castor oil based PU and residue of bamboo fibers to produces strand boards, using 20% and 40% of the volume in continuous and aligned baboo fibers. The composites presented better moisture absorption, mechanical strength, flexural strength and met commercial standards expected for strand boards, showing the possibility of

obtaining materials that not only match but surpass the quality of commercially available materials with composites made with VF.

As already discussed, VF are made mostly of hemicelluloses, cellulose and lignin, hemicelluloses and cellulose being hygroscopic. Most of the commonly used polymers, however, are hydrophobic and might not have good interactions with those hygroscopic fibers (69). PU, on the other hand, are greatly compatible with them, as their polymerization itself happens by the reaction of isocyanate and -OH groups, forming actual chemical bonds with the reinforcement materials, as their biopolymers can act as the polyol in the polymerization. The following Figure 26 represents an isocyanate bonding directly to a chain of hemicellulose via its -OH groups.

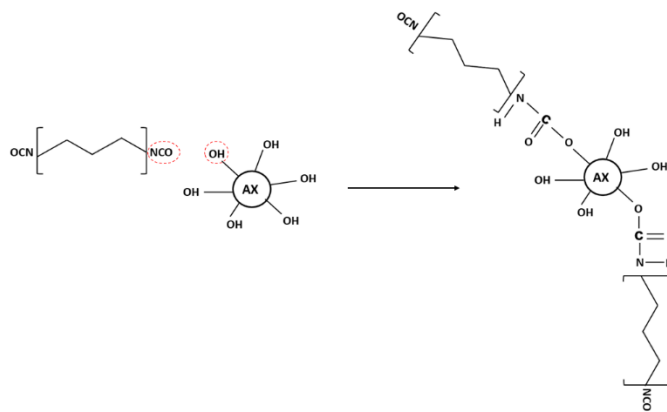


Figure 26. Bonding between an isocyanate and a chain of hemicellulose in the synthesis of a polyurethane composite. (71) Adapted figure.

Despite the good interaction between isocyanate and hemicellulose, shown above, often it is interesting to chemically pre-treat the fibers to decrease or reduce the number of hemicelluloses in the fibers, as will be explained further ahead. There are many kinds of well-studied and documented pretreatments available, like silane pretreatment, peroxide pretreatment and alkaline pretreatment, whom usually aim to promote better interfacial bonding between the matrix and the filler (69).

Among the treatments mentioned above, alkaline pretreatment is particularly interesting when working with VF. The fibers are treated with concentrated solutions of strong bases like NaOH to partially or completely remove the hemicelluloses from the samples. This exposes the cellulose's -OH groups. That is seen as more advantageous as not only is cellulose a stronger

polymer, but it also breaks some bonds between the chains of cellulose, increasing the fiber's roughness and, consequently, the surface area available for reactions with the polymeric matrix. Figure 27 shows the effect of NaOH in the bonding between two cellulose chains (16,69).

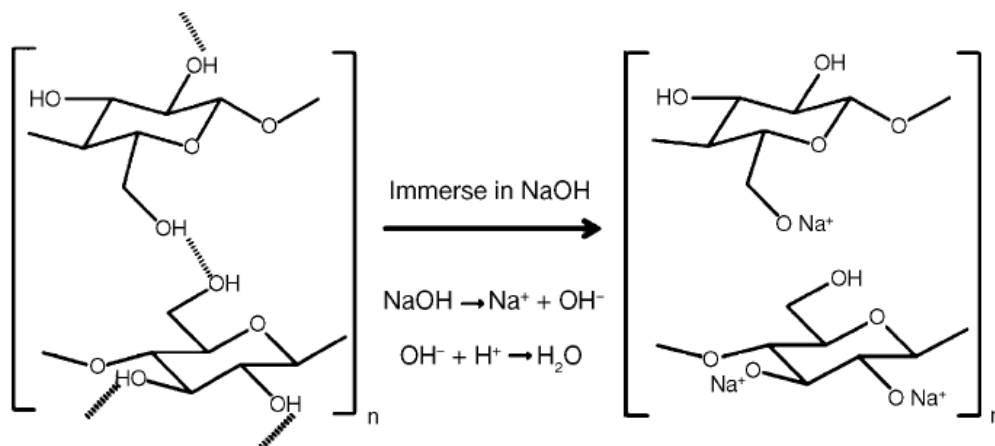


Figure 27. Effects of alkaline treatment on the cellulose chains (16).

As can be seen in Figure 27, the alkaline treatment separates cellulose chains, creating more reactive surface for the reaction with the isocyanate, increasing the compatibility between the two and the adhesion of fibers to the polymeric matrix.

2.3.6 Additional work

The initial thesis work focuses on the valorization of vegetable oils from Brazilian plant species. When establishing joint supervision between UnB and UL, we went further by testing these new products in the development of 100% biosourced biomaterials. Here, I present additional parts on the valorization of macauba fruit, for lubricants, bio-degradable lubricants and stability of vegetable oils. The results of these works will be shown in Annex 1.

2.3.6.1 Lubricants

Lubricants are materials that form film between two or more surfaces, minimizing the contact between them and, as a consequence, the friction between them (72) (Figure 28).

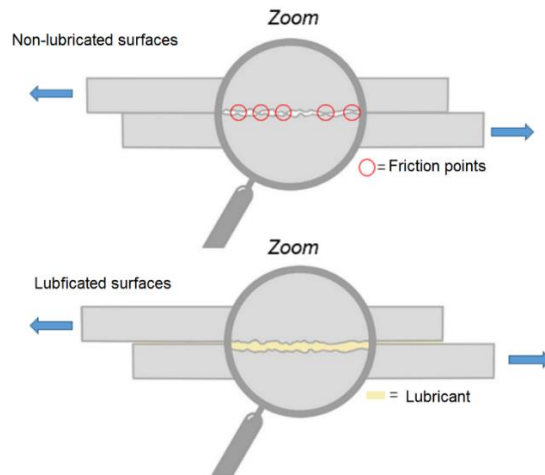


Figure 28. Zoom in a region between two non-lubricated surfaces (up) and two lubricated surfaces (down). Adapted figure (73).

Other than reducing friction damage between surfaces, lubricants also have the functions of cooling down, protecting against corrosion and cleaning the surfaces they are on. All of those are critical functions for the good and last useful life of a mechanism or machine (72).

One of the most important properties of a lubricant is its viscosity. Viscosity is the result of friction between the lubricant infinitesimal layers. Creating a flow resistance (74). Figure 29 shows the shearing between layers of lubricant between two moving surfaces.

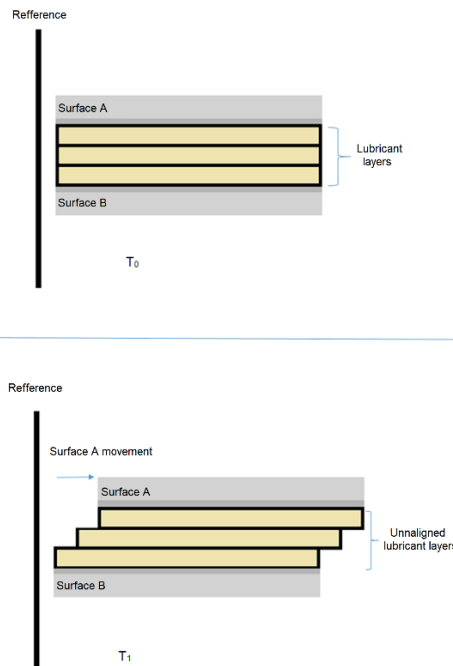


Figure 29. Shearing of lubricant layers (74).

In Figure 29, at time T_0 , surfaces A and B are stationary. On T_1 , however, surface A is PU head to the right. The friction between the lubricant layers causes a resistance in the flow of the layers (represented by the middle lubricant layer not moving as much as the top layer that) is proportional to the intermolecular interactions between the lubricant molecules. These interactions are influenced by factors such as polarity, weight, and molecules size (74).

Another interesting property of lubricants is the viscosity index. This property measures how stable a lubricant's viscosity is with increasing temperature, the higher the index is, the less the viscosity varies with the temperature. A high viscosity index is ideal, as it makes the lubricant's properties more stable and predictable.

It is also favorable for lubricants to have low pour point and high oxidative stability, as well as high flash point and good corrosion resistance (75).

It is estimated that about 50% of the lubricant produced in the world is wasted, ending in the environment by leakage, evaporation, human mistake or for loss of function. As over 90% of the world produced lubricants are petrochemical, it has become a major source of environmental damage. Considering how important and widely used lubricants are, the development of environmentally friendly lubricants is rather important (76,77).

Knowing the number of petrochemical lubricants out there that end up being improperly discarded, some researchers investigate ways to purify them into a usable state again. Chen *et al.* (2018) (78), studied filtering as a technique to purify used automobile lubricant, using natural and chemically modified sawdust as adsorbent. The modified sawdust showed better results regarding absorption of organics, inorganics, and insoluble resins from the used lubricant when compared to natural sawdust and the traditional filtering with filter papers. The results show potential for this technique to increase the longevity of lubricants.

Vegetable and animal's oils and fats were always traditionally used as lubricants, but the rise in the petroleum industry in the 19th century greatly reduced the price of petrochemical materials, which ended up replacing all other forms of traditionally used lubricants in most cases (79).

2.3.6.2 Biolubricants

There are inconsistencies in the usage of the term “biolubricant” (BioLub). In this work, a BioLub will be referred to as a biodegradable lubricant that is also made from biodegradable raw materials.

Table 6 shows the average biodegradability of some products typically used as lubricant (74).

Table 6. Biodegradability of some possible lubricant bases (74).

Product	Biodegradability (%)
Mineral oil	20-30
Vegetable oil	95-98
Ester	75-100
Polyol	75-100

According to Table 6, vegetable oils are about 20 times more biodegradable than mineral oils, the most usual base oil for lubricants. Implying they could be a promising green replacement for mineral oils, especially considering the easiness in obtaining, handling and discarding them (63,80).

A BioLub made from a vegetable oil is composed mostly from Triglyceride, while mineral oils are mostly from hydrocarbons (79). Figure 30 shows the comparison between a Triglyceride and some hydrocarbons present in mineral oils.

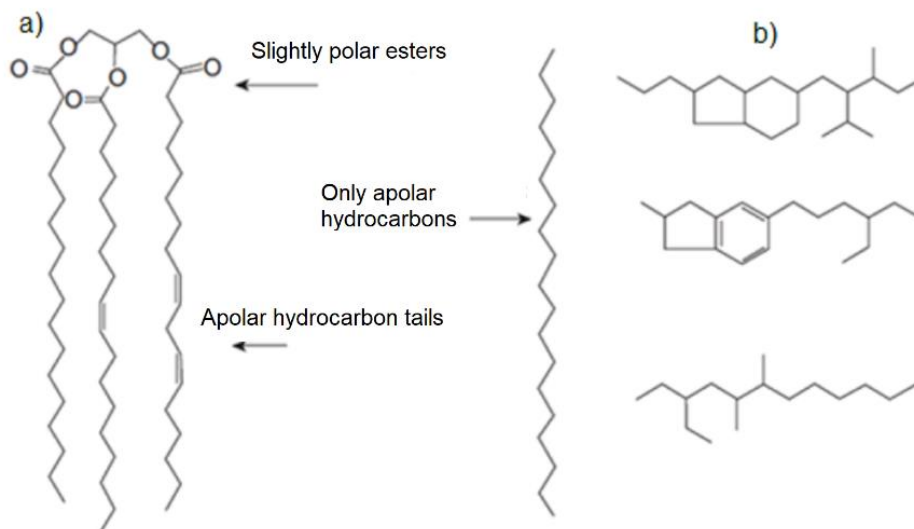


Figure 30. Comparison between (a) a Triglyceride and (b) hydrocarbons (74).

As seen in Figure 30, triglycerides are bigger and heavier molecules, rendering them better at lubricity, higher viscosity and lower volatility than the hydrocarbons. The presence of polar groups also increases the viscosity and lower the volatility, increases the flashpoint and favors the formation of a more consistent film on the surfaces it will be on, giving it better anti-wear properties when comparing with mineral oils, especially on metallic surfaces (79). Figure 31 presents the formation of a lubricant film on a metallic surface (79).

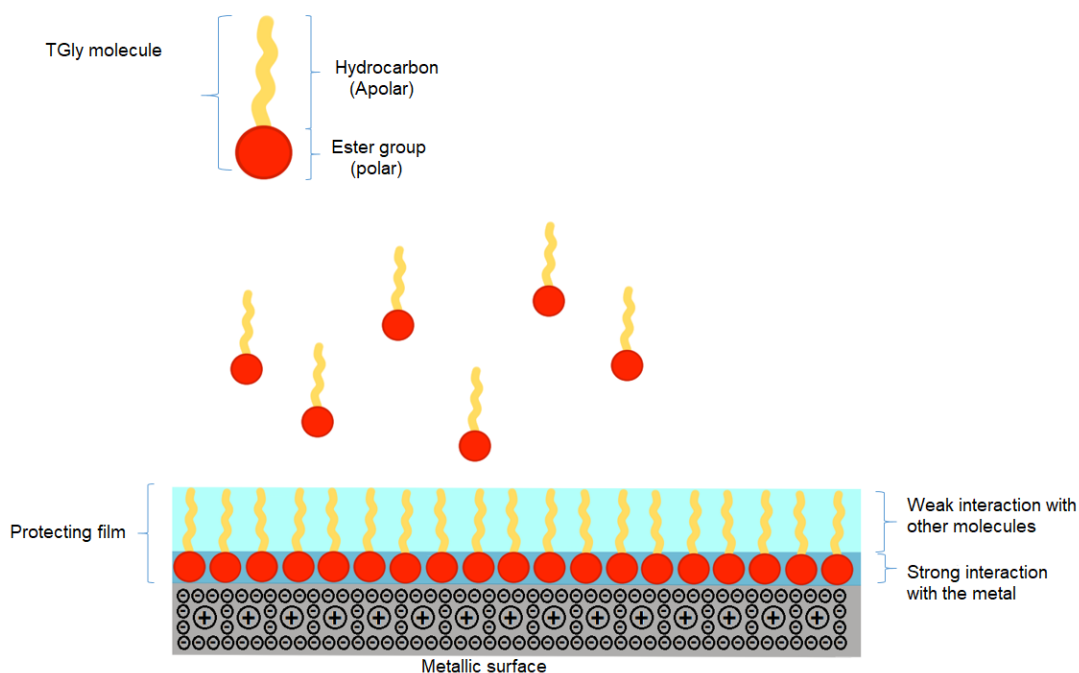


Figure 31. Formation of a protecting lubricant film of Triglyceride over a metallic surface (79).

Despite the many apparent advantages in using vegetable oils as lubricants, they suffer from low oxidative stability, caused mostly by the presence of unsaturations, and bad low temperature properties, caused mostly by their mass and polarity (77). If BioLubs are to be accepted in the lubricant's market, they need to overcome those drawbacks at similar prices, being still non-toxic and renewable.

The usage of BioLubs is indicated for applications with inherent big losses in lubricant, like in chainsaws, and also application that happen in food production and near bodies of water (79,81).

In the search for renewable lubricants, Rios *et al.* (2020) (82) tested different modifications on castor oil's FA. First esterification with 2-ethyl butanol, followed by epoxidation of these esters' unsaturation with two different

nucleophiles (water and 1-butanol). These modifications affected the physical chemical properties of the products, such as density, viscosity, viscosity index, thermal stability and flow point, all properties being satisfactory to the Society of Automotive Engineers (SAE), indicating that castor oil could be an interesting alternative for the preparation of automotive lubricants, especially in Brazil, where castor seeds are abundant.

2.3.6.3 Vitamin E

Unsaturation lowers the oxidative stability of vegetable oils, as already stated. One way to overcome this drawback is by using appropriate additives. Vitamin E is a family of 8 compounds, known as tocopherols, characterized by a chromanol ring and an apolar poliprenil tail. They can be classified as tocopherols, in case the poliprenil tail is completely saturated, or tocotrienol, in case they are unsaturated. Tocopherols are, still, differentiated, by the methylation of its chromanol rings (83,84). Figure 32 presents the molecular structure of 8 tocopherols.

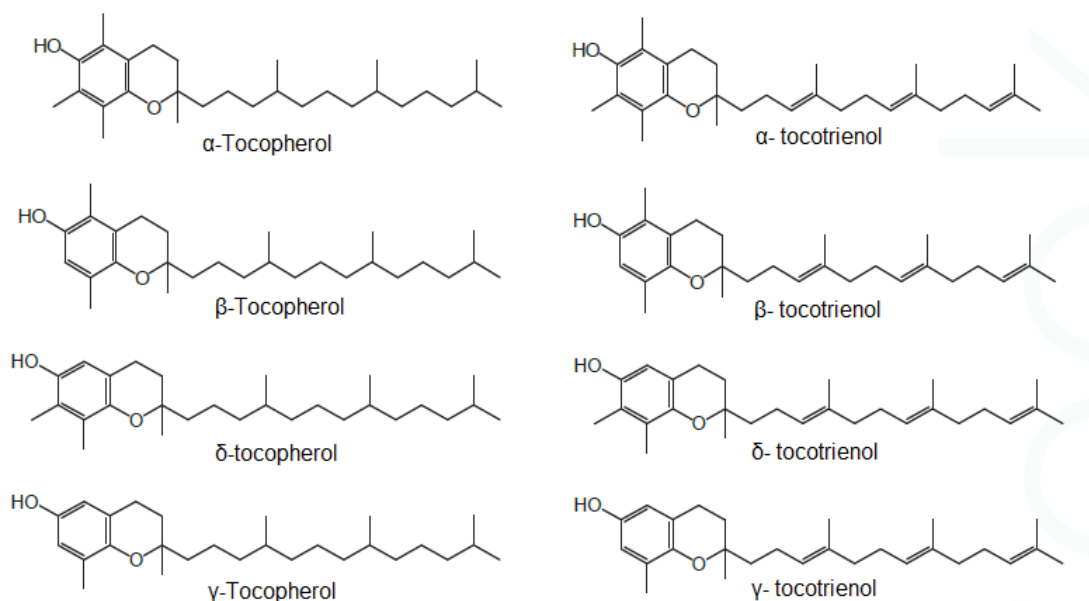


Figure 32. Molecular structures of some tocopherols (85).

Vitamin E is a liposoluble vitamin that is essential in animals, but that it is not synthesized by them. It needs to be ingested from feeding, being usually in vegetable oils sources, like seeds, grains, nuts and others. Despite being produced in almost its totality by photosynthesizer, as algae, vegetables and

cyanobacteria, some studies have also found it in *Plasmodium falciparum*, the parasite that causes malaria (83,86).

The main function of Vitamin E in living beings is to protect the unsaturated lipids in cell membranes against oxidation by free radicals, being the most important liposoluble anti-oxidant present in cells, specially α -tocopherol (87). The tocopherol reaction mechanism is radical scavenging, in which the tocopherol donates a hydrogen radical, from its hydroxyl in its chromanol group, to neutralize radicals, as reactive oxygen species (ROOS), free radicals, peroxides, lipids and others (85). The proposed radical scavenging mechanism for α -tocopherol is shown in Figure 33.

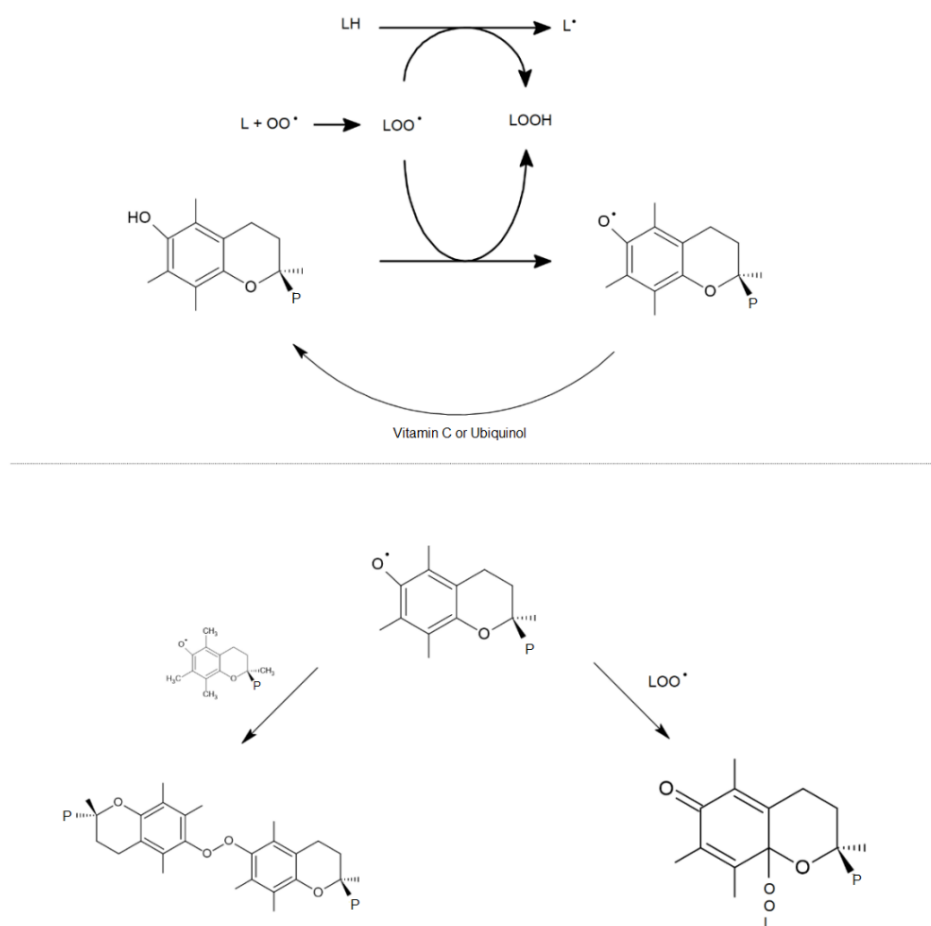


Figure 33. Antioxidant action of α -tocopherol, where P means phytyl and L means lipid.

The importance of liposoluble vitamins, like α -tocopherol, other tocopherols and other vitamins for the oxidative stability of a vegetable oil was shown by Nagy *et al.* (2016) (83). They studied the oxidative stability of many vegetable oils by multiple linear regression based on the fatty profile of each oil

and comparing with it with the oxidative stability value obtained by the OSI method at 120 °C and by the sum of oxidation products obtained, like hydroperoxides, aldehydes and others. After that, multiple linear regressions were calculated taking into consideration the quantity of vitamins present in the starting products. The addition of liposoluble vitamins increased the oxidative stability of the products, indicating a relation between them and the vegetable oil's oxidative stability.

2.3.6.4 α -tocopherol acetate

The α -tocopherol acetate is, as is the α -tocopherol itself, and antioxidant. It is less reactive than α -tocopherol, and it can be used as a replacement for vitamin D in some cases, since its lower activity also means it can remain active for longer. It is often used in cosmetics and as conservant for foods. α -tocopherol acetate was chosen in this work for its lower price and easiness to obtain.

As a potential replacement for α -tocopherol, α -tocopherol acetate has been studied in the food industry, in the works of Maiorano *et al.* (2016) (84), for example. Their research consisted in injecting α -tocopherol acetate in lambs to study its effect on their meat, which presented better oxidative properties than the control group meat.

Chapter 3

Materials and methods

3.1 Materials

The MKO was bought from the Mundo dos óleos ®, from Brazil. Hydrogen peroxide 30% was obtained by Merk® (Germany). Formic acid (Hform) 85% was acquired from Vetec® (Brazil). The samples of beech (*Populus nigra*) and fir (*Albies alba*) was provided by Vosges Promoboiss ® (France). The samples of CV (*Tachigali vulgaris*) were given by Professor Adail, from the forestry engineering department from University of Brasília and Água Limpa, the university's farm, in Brazil. Bi-distilled glycerin was purchased from Synth. A-tocopherol acetate was purchased from Engenharia das Essências Comercial LTDA. The Thermal treatments were performed in a Shimadzu GC-14A convection oven with a reactor under nitrogen flow. The wood samples, both raw and treated, were ground in a Retsch SM 100 grinder. The TGA and DTG analyses had to be done in two different equipments, due to time and place constraints. Most of the TGA/DTGs were performed in a NETZSCH STA 449F3 using an alumina crucible, but the composites with treated CV had to be performed in a Shimadzu DTG-60H, on platinum crucibles,

The ground wood was sieved by particle size with VWR 250 µm and 500 µm sieves.

Sodium chlorite 80% was obtained from Thermo Scientific©. Acetic acid was obtained from Merk © and sodium peroxide was obtained from VWR©.

The MDI used for the PU reactions was already available in the laboratory BFE was purchased from Sigma Aldrich.

DVS analysis was run on a DVS Intrinsic plus.

3.2 Methods

3.2.1 Wood samples and vegetable oils.

The wood species and vegetable oil chosen for this work were beech (*Fagus sylvatica*), fir (*Albies alba*) and carvoeiro (*Tachigali vulgaris*). The vegetable oil chosen for this work is the macauba kernel oil, for reasons already discussed.

3.2.2 Sampling

The wood samples were cut into boards, then cut into 2 cm x 14 cm x 6 cm samples, as shown in Figure 34.

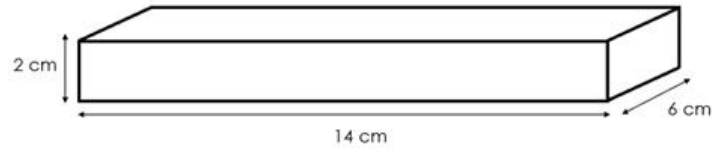


Figure 34. Dimensions of the wood samples used in this work (up), and a piece of wood sample (down).

3.3 Pretreatment

All the wood samples used in this work, after being cut into shape, are left to dry at 103 °C until mass stabilization, to determine the anhydrous mass, being weighed after the thermal pre-treatment to measure the loss of water. Before weighing the water, loss and going for the thermal treatment were left to cool down to room temperature in the desiccator.

3.4 Wood density

To measure the specific gravity of the three wood species of studied in this work, samples in the dimensions described above were left to dry in an oven at 103 °C, then left to cool down to room temperature in desiccator. After that the samples were immediately weighed and had their sides measured with a caliber. 3 samples of each species of wood were used to calculate density.

3.5 Thermal treatment

The samples of wood were put inside the reactor and conditioned at room temperature for 2 min under 25 mL·min⁻¹ N₂ flow to eliminate the air from the reactor. The nitrogen flow was maintained throughout the treatment. All treatments consisted of a 2 °C·min⁻¹ heating rate until a set temperature, followed by a 30 min isothermal. Figure 35 illustrates a schematic view of the reactor used for thermal treatments.

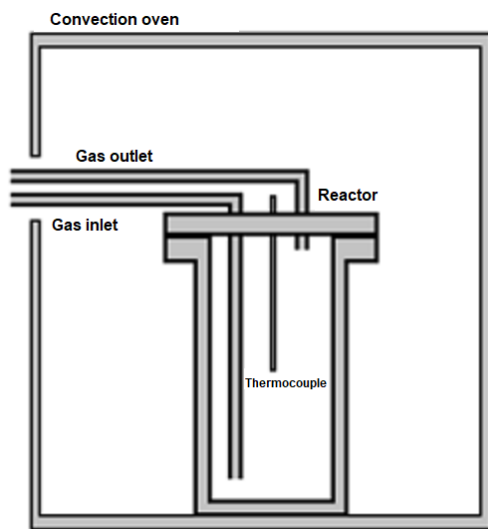


Figure 35. Representation of the reaction used in the thermal treatment of the wood samples.

The thermal profile of the thermal treatment done on the samples follow the profile shown in Figure 36.

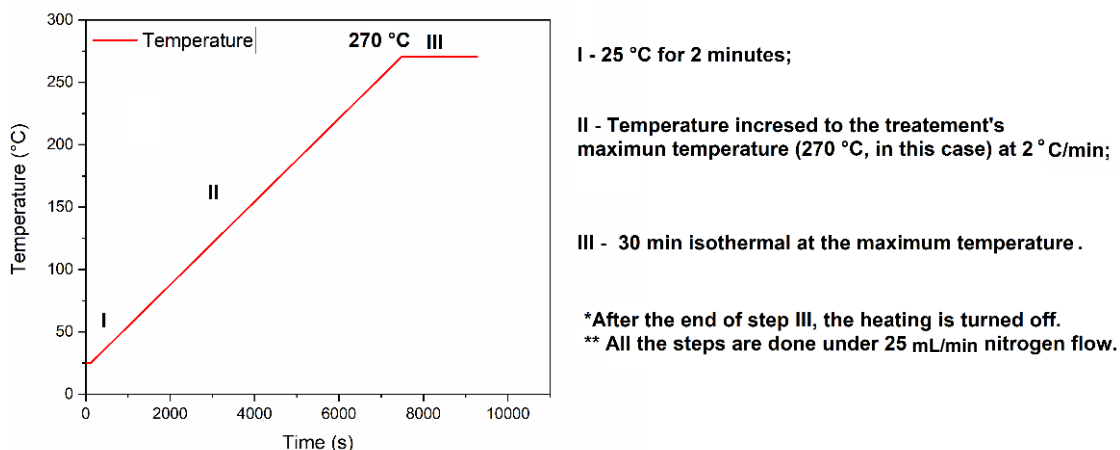


Figure 36. Thermal profile of the thermal treatments done on the wood samples.

After the treatment, the samples, loaded two at a time in the reactor, are left to cool down to room temperature on dissectors, then weighed to measure the mass loss caused by the thermal degradation. After weighing, the samples are put again in the oven at 103 °C.

3.6 Grinding

After the treatment, the wood samples are then cut into small blocks, ground on the Retsch SM100 grinder using a 1mm grid, then the ground wood is put on the 103 °C oven for further analysis. Samples of raw wood had to be first ground using a 5mm grid due to their mechanical hardness, then ground again in using the 1mm grid. After each grinding, the equipment was cleaned by a vacuum cleaner and with a brush to remove as much dust from the previous samples as possible.

3.7 Thermogravimetric analysis/Derived thermogravimetry analysis (TGA/DTG)

Two types of DTG were done in this work: for the DTG deconvolution of wood samples and for studying the thermal stability of PU and composites. Both will be explained in the following paragraphs.

The TG analysis used for the deconvolution of the wood was based on the method described by Carrier *et al.* (2011) (35). 5 mg to 10 mg of ground wood were loaded into alumina crucibles and the temperature increased from 25 °C to 700 °C, followed by a 700 °C isothermal for 30 min and then equipment was cooled down at 50 °C·min⁻¹. Although TG analyses on the Carrier were performed under an Argon atmosphere, this work used Nitrogen for its availability. The equipment used was a Mettler Toledo TGA 2 Star System NETZSCH STA 449F3.

The other TG/DTG analyses, used to study the thermal properties of the PU and composites, were done following the thermal profile shown in Figure 37, run on a NETZSCH STA 449F3. The conditions were the same, but with synthetic air atmosphere.

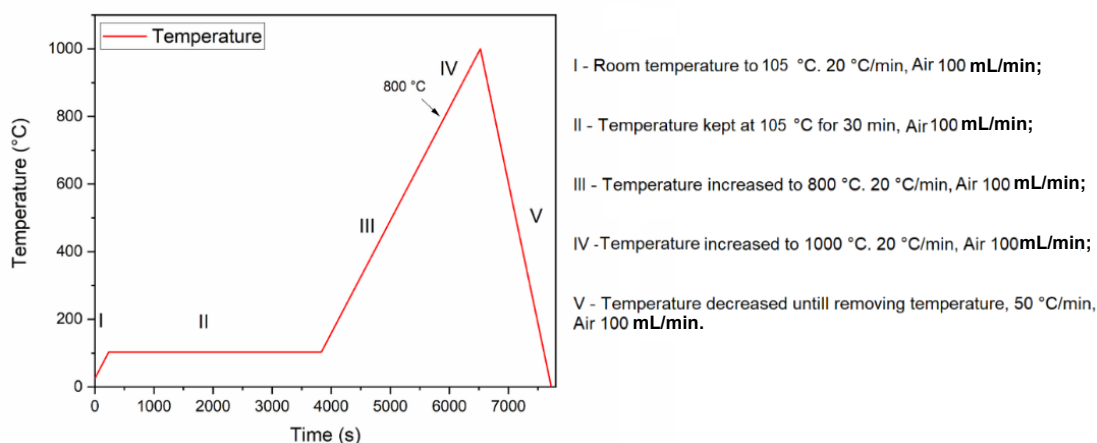


Figure 37. Temperature profile used in the TG/DTG analyses done in this work.

3.7.1 DTG Deconvolutions

For the deconvolution of the sample's DTG, a few changes were made to achieve better fittings than Carrier *et al.* (2011) (35). Carrier used gaussian curves for the deconvolutions, while this work used bigaussian curves, as their asymmetrical nature better represent the thermal degradation behavior of the biopolymers. The DTG deconvolutions were calculated on origin, and the DTG is broken down in five peaks: water, hemicelluloses, cellulose, lignin and others, while carrier used only three (hemicelluloses, cellulose and lignin). Those changes have allowed us to achieve better fittings than the obtained by a Carrier *et al.* (2011) (35), as shown in Figure 38.

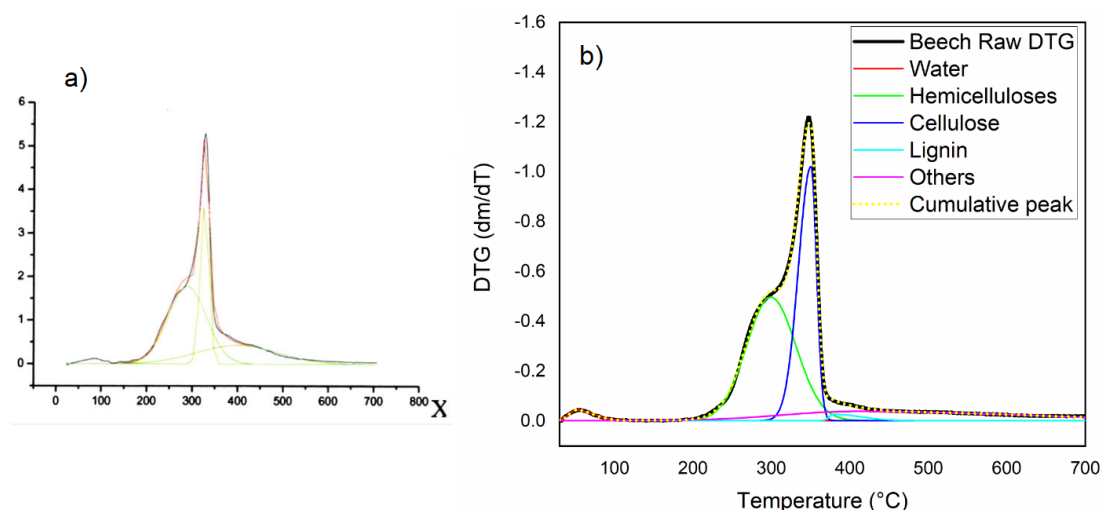


Figure 38. Comparison between (a) the deconvolution made by Carrier *et al.* (2011) (35), and (b) this work.

To quantify the number of biopolymers left after the thermal treatment, the deconvoluted peaks were integrated, also on Origin.

As the thermal treatment progresses, the hemicelluloses' peak decreases, while the cellulose's peak remains mostly stable. At some point, the thermal treatment starts decreasing the cellulose peak, which means it is the maximum temperature we can go for the objective of this work. To quantify the best temperature to eliminate the most hemicelluloses with as little effect as possible on the cellulose, the integrated peaks are used to calculate the ratio between cellulose and hemicellulose (Cel/Hemi ratio). As the temperature of increases in the thermal treatment, the hemicelluloses integrate will decrease, increasing the ratio until it reaches a critical point when the cellulose peak decreases, causing a decrease in the ratio. Past this point, the software could not accurately calculate the deconvolution with the five usual peaks used in this work, indicating that either the hemicelluloses peak is completely gone, or it is so small that it cannot be quantified. As we do not calculate the Cel/Hemi ratio up to this point, there is no risk of an infinite ratio as there will be no division by zero.

3.8 Wood Fractioning

- Delignification gravimetry

- About 4 g of ground wood is added into an Erlenmeyer flask with 160 mL of room temperature distilled water;
- 0.4 g·g⁻¹ of wool of sodium chlorite and 0.4 mL·g⁻¹ of wood were added into the erlenmeyer flask;
- The mixture is put in a water thermal bath with magnetic agitation, heated up to 70 °C, then is kept between 70 °C and 75 °C for 8 h. In each 2 h of reaction, for the first six hours, acetic acid and sodium chlorite are added to the mixture in the same quantities as before. The product is then transferred to a water trump vacuum, washed and filtered until neutralizing the pH. The holocellulose is carefully scrapped from the filter paper, dried for at least 24h AT 103 °C, then weighed after reaching room temperature in a desiccator.

-α-Cellulose gravimetry

About 1.5 g of dried and ground holocellulose is reacted with 10 mL of a 17.5% (m/v) solution of NaOH in water at room temperature under magnetic

stirring for 30 min. The product is transferred to a water trap vacuum filter, washed twice with 200 mL of water, then 15 mL of a 10% acetic acid solution and, finally, with 500 mL of hot water. The final content is filtered, dried for at least 24 h and then weighed. Both methods are based on the work described by Kumar *et al.* (2013) (86).

3.9 Epoxide synthesis

The quantification of molar mass and unsaturations per mole in the oil follows the method described by Miyake *et al.* (1998) (88). This method uses a quantitative ^1H NMR spectrum of oil and integrating key ^1H NMR signals and applying the values to the equation described in their work.

From the oil properties calculated as described above, the reagents quantities used for the epoxidation of MKO are listed in Table 7, they are empirical, but based both on the works of (88) and in previous work by the author (3,89).

Table 7. Quantity of reagents for MKO epoxidation.

	MKO	Hform	H₂O₂
Quantity	55.554 g	53.572 mL	200.197 mL

The first step for the reaction is the addition of MKO and Hform together in a round bottle flask under mechanical stirring of at least 500 rpm (90). Still under stirring, H₂O₂ was slowly dripped into the mixture. After the end of the dripping, the mixture was heated up to 60 °C in a glycerin thermal bath and the temperature was kept between 60 °C and 65 °C for two hours. Past those two hours, the product was then transferred to a separation funnel and two organic extractions were made with saturated NaCl solution, the first being immediately after transferring the mixture to the funnel to remove the excessive peracid still in the solution. Further extractions were left decanting overnight before changing the saline solution. After the extractions, the product was neutralized with a Na₂CO₃ m.v⁻¹ solution, left decanting overnight, filtered, rotatory evaporated then filtered again. The apparatus for the epoxidation reaction is illustrated in Figure 39.



Figure 39. Apparatus used in the MKO epoxidation.

The epoxidation mechanism has been suggested and are shown in the Figure 40 (91).

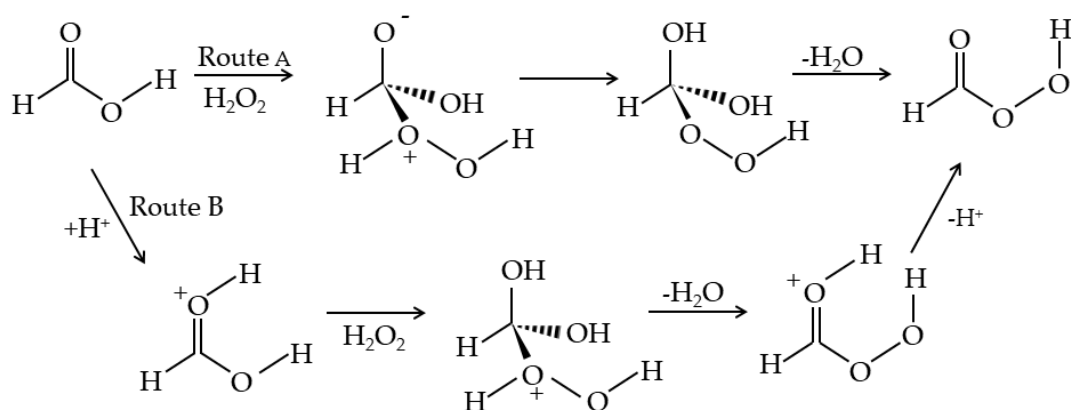


Figure 40. Suggested mechanism for the formation of peracid (91).

The first step for the epoxide synthesis is the formation of an epoxidation agent, which is performic acid, in this case. Two synthetic routes have been suggested for the peracid formation, one catalytic (Route B) and one non-catalytic route (Route A):

Route A - The peroxide attacks the non-activated carbonyl carbon, forming an intermediate with a positive and a negatively charged oxygen. The negative oxygen attacks the hydrogen in the positive oxygen, neutralizing both and eventually forming the peracid by an intramolecular water elimination (91).

Route B - The carbonyl oxygen is first activated by a proton in the solution. The carbonyl carbon then suffers a nucleophilic attack by the peroxide oxygen, forming a positively charged oxygen, which is neutralized by OH^- in the solution, resulting in water elimination. The result is a peracid with an activated carbonyl, which eliminates proton, forming the peracid (91).

After the peracid is formed, the epoxide itself can be formed by the proposed mechanism in the Figure 41 (92).

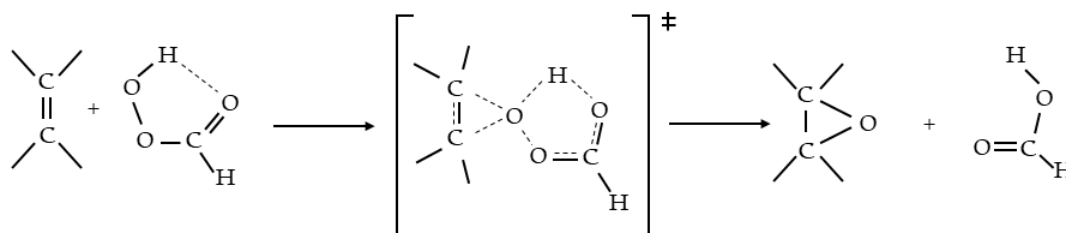


Figure 41. Epoxide formation (92).

As seen in Figure 41, the peracid is activated by an intramolecular hydrogen bond, which allows it to be attacked by a double bond from a vegetable oil, for example, resulting in a transition state that breaks down into an epoxide and an organic acid, that can once again react into a peracid by the mechanism shown in Figure 40.

3.10 Polyol synthesis

In the early stages of this work, different strategies to synthesis polyol from MKO were attempted. Those will be discussed later, for now the focus will be on successful synthesis, as it is the one that was used for the rest of the research.

The polyol (GlyMKO) synthesis begins with the 1:1 volume addition of glycerin and EPMKO in a double necked flask under magnetic stirring. A water reflux condenser is attached to the top of the flask. $\text{BF}_3(\text{Et}_2\text{O})$ is slowly dripped with a syringe through the side opening of the flask in the proportion of 10% v/v the of EPMKO. After the $\text{BF}_3(\text{Et}_2\text{O})$ injection, the side opening is sealed and the reaction keeps on under mechanical stirring at room temperature for 30 min, ethyl ether is added in the proportion of 2:1 in volume of EPMKO and the stirring is adjusted until a vortex form in the mixture, then the reaction keeps going for 5h:30min. After the end of the reaction, the mixture is transferred into a separation

funnel and left overnight. The next morning, saturated salt solution is added to the mixture to decrease the viscosity of the aqueous phase (glycerin) and the product is neutralized with 0.5 M KOH solution, then it is extracted twice with saturated salt solution, leaving the mixture separate overnight between each extraction. After that, the solution is rotatory evaporated, dissolved with ethylic ether, filtered then evaporated again. Figure 42 shows the apparatus used for polyol synthesis.



Figure 42. Apparatus used for GLMKO synthesis.

The proposed mechanism for the epoxide ring opening by the glycerol is given in Figure 43.

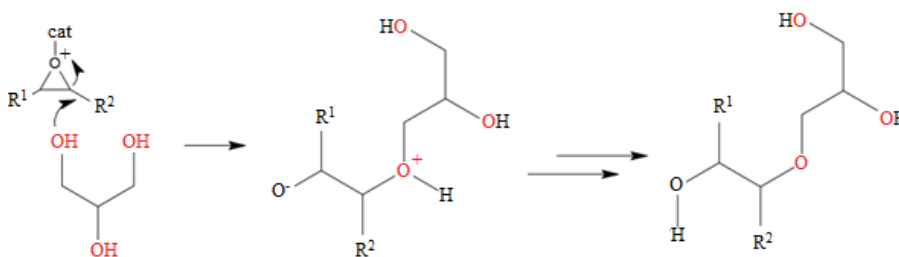


Figure 43. Proposed mechanism for the epoxide ring opening and formation of polyol. Cat represents catalyst, R¹ and R² represent the rest of the Triglyceride molecule.

In this mechanism, the epoxide ring is first activated by the catalyst $\text{BF}_3(\text{Et}_2\text{O})$, then the one of the carbons in the epoxide ring suffers a nucleophilic attack by one of the glycerol's OH, breaking the C-O bond of the ring and forming a polyol with three OH after hydrogen exchange.

3.11 OH index

The OH index for the GLMKO was calculated using the ASTM Standard D1193 norm (93). The method consists in the acetylation of the polyol followed by a titration with KOH.

3.12 Polyurethane/composites synthesis

The PU synthesis followed the previous works from the author (3). It was done by adding the appropriate quantity of polyol into a Teflon® beaker, then adding the isocyanate and immediately stirring it mechanically for one minute. The mixture is then transferred to Teflon® molds and it is left to cure in a pre-heated oven at 65 °C for 24 h, after which it is removed, left to cool down to room temperature then stored for characterization.

The composite synthesis followed a similar route, but after the initial 1 min mechanical stirring, the wood was added, and the mixture was stirred for one more minute. The rest followed the same procedure of the PU synthesis.

3.13 Fourier transform infrared spectroscopy (FTIR)

The FTIR of the samples was obtained in a Varian 640 by the Attenuated Total Reflectance (ATR) method, using 4000 cm^{-1} to 600 cm^{-1} , using 16 scans and 4 cm^{-1} resolution. The analyses were run at the Chemistry Institute Analytical Central (CAIQ), UnB.

ATR-FTIR was also used to determine the best particle size for the sawdust used in the formation of composites by comparing the -OH peaks on the different particle sizes normalized spectra.

3.14 Dynamic vapor sorption (DVS)

The DVS analysis was run in a DVS Intrinsic Plus. In this equipment, a sample is added to the plate of a scale inside a humidity chamber, which is then

sealed shut. The humidity of the chamber is then increased at a pre-programmed rate and the increase in the sample mass is used to measure the interaction of the material with water. In this work About 5 mg of sample was added into the scale of the equipment's chamber, which then had its water partial pressure (humidity) increased 5% by 5% (waiting for the stabilization of each value before moving on to the next) to a maximum humidity of 95%, with a scale continuously measuring the water uptake in the sample. After that, the partial pressure was reduced every 5% until reaching 0%.

3.15 Dynamic mechanical analysis (DMA)

Dynamic mechanical analysis (DMA) tests were performed using a Q800 DMA Instrument manufactured by TA Instruments in New Castle, DE, USA. The experiments used a three-point bend fixture. Samples labeled as PU 0.8, PU 1.0, and PU 1.2 were prepared by cutting specimens with dimensions approximately 5.0 mm × 9.0 mm × 5.0 mm (length × width × thickness). Each specimen was initially cooled down to 0 °C, then heated to 150 °C at a heating rate of 3 °C·min⁻¹ under an iso-strain mode, 1 Hz frequency and 14 μm of amplitude were employed. Two replicates of each sample were cut out. Each replicate was tested individually, and the results represent the average of the trials.

3.16 Additional work

3.16.1 Other attempts at polyol synthesis

- Polyol T1

The first polyol synthesis attempted, labelled Polyol T1 was similar to the epoxide synthesis and based on previous works of the author (3) with different oils. The reaction goes similarly to the epoxide synthesis previously described but lasts 5 h after the end of the H₂O₂ dripping. After that the product was transferred into a separation funnel, extracted twice with saturated salt solution, being the first extraction immediately after the transference. The product was then neutralized with 10% m/v sodium carbonate solution, filtered and evaporated, then taken to FTIR (3).

- Polyol using zinc as a catalyst

Two syntheses like polyol T1 were attempted, but with different quantities of ZnCl_2 added as a Lewis acid to the solution to catalyze the epoxide ring opening. In the first reaction, 25 g of EPMKO were added into a 3 necked flask with 22 mL of Hform. H_2O_2 was then slowly dripped into the mixture under mechanical stirring, after which the mixture was heated up to 60 °C and kept between 60 °C and 65 °C for 2 h (which is the know time to obtain the epoxide, according to epoxidation done for this work). After that, 0.01 mol and 0.005 mol of aqueous ZnCl_2 were added to the mixtures (being then labelled after the quantity added of ZnCl_2) and the reaction proceeded for 3 more hours. After which the products were extracted, neutralized and purified as done with Polyol T1. The product made with 0,01 g of ZnCl_2 was a pasty product labeled POZn 0.01 and the other was a biphasic product named PO Zn 0.005.

3.16.2 α -tocopherol acetate additivation

As an attempt to increase the MKO's oxidative stability, different quantities of α -tocopherol acetate (5%, 10%, 15% and 20%) v/v were added to MKO samples and compared to the EPMKO sample. The addition was done at room temperature under mechanical stirring until the mixture was homogeneous. The quantities were added in v/v proportions and were named according to the percentual of α -tocopherol acetate added. As an example, TCMKO10 represents a sample of MKO with 10% of α -tocopherol acetate. The samples were tested regarding their oxidative stability

The oxidative stability tests were run following the ISO 6886 norm. The sample is loaded into the equipment and synthetic air flow at 700 KPa is applied in the sample to oxidate it. The process releases gases that are dragged by the air into a demineralized water flask with electrodes to measure its conductivity. The oxidative stability of a sample is considered the point in which there is a surge in conductivity in the water flask caused by the oxidation gases using the accelerated oxidation tests for animals and vegetable fats and oils norm (94).

The test was run at ANP, in a Metrohm Rancimat 743, at 110 °C, 10 L·h⁻¹ with electrodes for readings from 0 $\mu\text{S}\cdot\text{cm}^{-1}$ to 300 $\mu\text{S}\cdot\text{cm}^{-1}$. For the test, 3 g of sample and 50 mL of demineralized water were used.

Chapter 4
***Production of modified wood fibers
by thermal treatment***

4.1 Wood's density

Before dealing with the results of the wood's thermal treatment, it is interesting to know the density of the three wood species to know how much they differ. Table 8 shows the result of density for the three wood species used in this work.

Table 8. Density of the wood species.

Wood species	Density (kg·m⁻³)
Fir	519.21
Beech	673.92
Carvoeiro (CV)	782.84

The density results show that, as usual, the European hardwood beech has a higher density than the softwood fir. The Brazilian wood, CV showed the highest density of all the three wood species, being even higher than the beech samples. As we are going to see, despite a density closer to that of beech, some of the CV results will be more closely related to fir. This higher density might be caused by denser biocomposites such as hemicelluloses and cellulose.

4.2.1 Thermal treatments

Table 9 shows the results of mass loss caused by thermal treatment of beech, fir and CV samples. Each treatment was made with two samples of wood at a time inside the reactor and the values shown represent the average of both mass losses.

For this point forward, the samples will be identified by the wood species (B for beech, F for fir and CV for carvoeiro), the treatment temperature (all listed on Table 9). For example, B275 is a sample of beech treated at 275 °C, while F310 means fir treated at 310 °C.

As for composites, the same name conventions for wood will apply, but with the prefix Comp, to indicate it is a composite rather than a sample of wood. The percentage of wood in the composite and the NCO/OH ratio of the polymeric matrix will also be listed. For example, Comp B275 2% 1.2 means the composite made with 2% of B275 in a polymeric matrix with a 1.2 NCO/OH ratio.

Table 9. Mass losses in the thermal treatment of the three wood species studied in this work.

Treatment temperature (°C)	Mass loss (%)		
	Beech	Fir	CV
240	5.039	---	3.619
255	12.766	4.804	8.6184
260	17.906	---	10.56
265	20.039	---	12.287
270	21.648	11.875	12.839
275	24.409	11.521	14.853
280	27.092	13.882	17.061
285	30.376	14.777	17.027
290	33.172	18.209	20.119
295	39.020	17.985	23.321
300	46.025	23.601	29.109
305	---	25.133	---
310	---	38.932	---
315	---	46.150	46.178

Table 9 shows that not all the temperatures tested were applied to all the three wood species. This was done to better study the thermal decomposition of hemicelluloses in all of the woods, as hardwoods are naturally richer in hemicelluloses than softwoods (95), they usually lose more mass at lower temperatures when compared to softwoods. The specific composition of the hemicelluloses is also important, hardwoods, for example, have larger amounts of acetylated hemicelluloses (95). During the thermal decomposition, the acetylated hemicelluloses releases acetic acid, which acts as a catalyst for the further degradation of the hemicellulose itself, causing the their hemicelluloses to be more easily degraded at lower temperatures (95,96). Because of that, the beech, a hardwood, was treated at lower temperatures (240 °C, 260 °C, and 265 °C) while the fir, a softwood, was treated at higher temperatures (305 °C, 310 °C, and 315 °C). The CV treatment was done with a bigger range of temperatures because, despite showing characteristics of hardwoods, the mass loss values were closer to that of the softwood fir, as will be explained in more details later in this work.

For beech, the works of Ruxanda *et al.* (2008) (97) and Mária *et al.* (2013) (98), found hemicelluloses content ranging from 21.35% to 26.59%, respectively, indicating that the best treatment temperature for their removal would be between 270 °C and 280 °C , according to the mass loss shown in the Table 9. Applying the same thought for fir, based on the works of Kučerová *et al.* (2019) (99) and Senila *et al.* (2019) (100), which found the content of hemicelluloses to be 20% and 27%, respectively, the ideal treatment temperature range was established to

be between 300 °C and 310 °C. While this alone does not constitute enough evidence to declare this the best temperature for thermal treatment, it is already indicating a possible range of temperatures to be selected.

Unfortunately, CV is not as well studied as beech and fir. One of its main usages is to be burned for coal (101) (carvoeiro meaning, in Portuguese, something that can be used to make coal) so their contents in hemicelluloses have not been as well explored and established to make this kind of inference. However, according to the work of Silva-Neto *et al.* (2020) (102), they exhibit characteristics of hardwood, such as vessels and fibers, but values of mass loss for CV, however, are closer to the values of mass loss for fir, a softwood, in all of the tested temperatures. The lower mass loss is most likely because the coming from the Cerrado, a Brazilian biome that is not only dry and warm but catches fires on yearly basis as part of its life cycles, the woods need to be better prepared to resist high temperature than typical European woods. Due to CV presenting hardwood characteristics but being more resistant to higher temperatures than beech the other hardwood studied in this work, it was treated at both lower temperatures, as a hardwood, and at higher temperatures as a softwood.

Figure 44 represents the plot of mass loss due to thermal treatment as a function of treatment temperature.

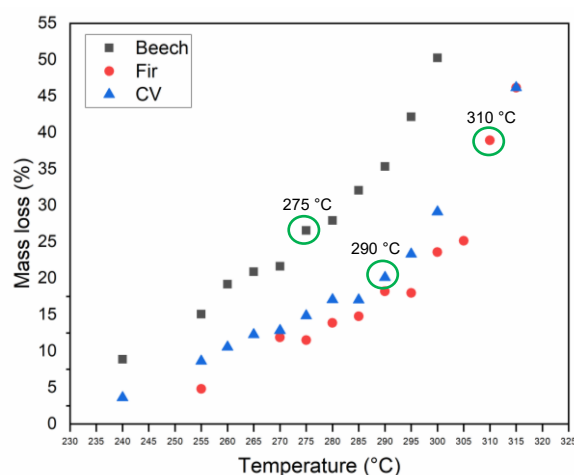


Figure 44. Mass loss as a function of treatment temperature. All samples were treated for 30 min (not counting the time needed to reach each target temperature). The best treatment temperature for each wood is highlighted with the green circle.

Figure 44 shows that, despite the hardwood characteristics, CV's mass loss behavior is much closer to that of fir, both presenting lower mass loss values

in all temperatures. Another observation that can be made from the picture, is that, at certain points, the increase in mass loss increase is relatively higher than that of the previous temperatures. That can be clearly seen for the beech from B270 to B275. This can possibly indicate that at some point between those two temperatures, the hemicelluloses got completely degraded and the degradation of cellulose begins, increasing the total amount of mass loss. While that by itself is also not sufficient evidence to decide this is the best temperature for this work, the results are in accordance to the values for beech hemicelluloses found by of Ruxanda *et al.* (2008) (97) and Mária *et al.* (2013) (98). Using the same line of thought, the point in which the mass loss spikes up for fir is at 310 °C, again in accordance to literature data regarding the quantity of hemicelluloses present in fir shown by Kučerová *et al.* (2019) (99) and Senila *et al.* (2019) (100). As the in-depth knowledge on CV's hemicelluloses is lacking, the same kind estimate based on literature cannot be made but, observing the point where the mass loss spikes up in the CV plot, we can infer that the best temperature for the degradation of hemicelluloses would be at 290 °C.

A possible reason for the lower mass loss of fir compared to the mass losses of beech is that the kinds of hemicelluloses found in hardwoods and softwoods are different. In hardwoods there is a bigger abundance of acetylated hemicelluloses, like glucuronoxylan, while softwoods are richer in non-acetylated hemicelluloses, like galactoglucomannan (96,97). The structure of both is shown in Figure 45.

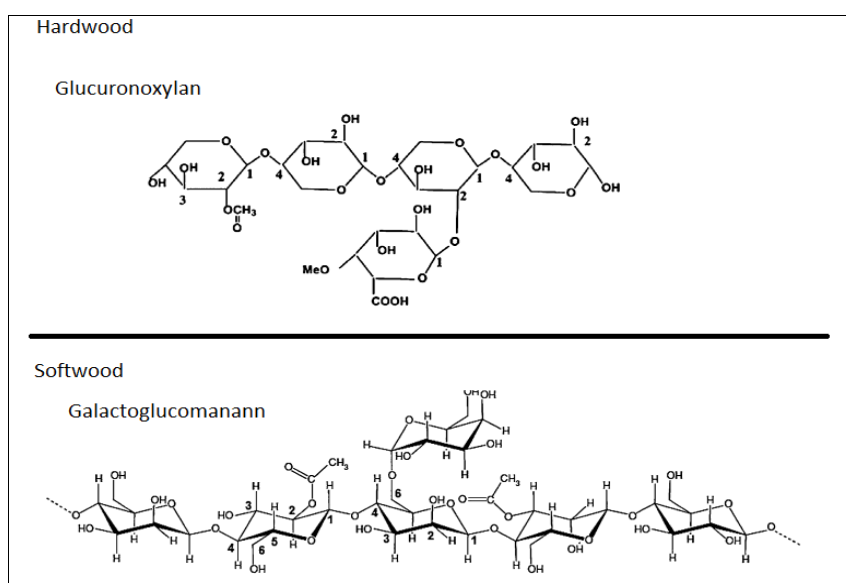


Figure 45. Common kinds of hemicelluloses found in hardwoods and softwoods (96).

This difference in hemicelluloses is important in the thermal degradation of wood as the acetylated groups present in the hardwood hemicelluloses release acetic acid during the treatment, which acts as a catalyst for the further degradation of hemicelluloses (95,96).

4.2.2 Deconvolutions DTG

Another way to estimate the optimal temperatures for intended thermal treatments of the woods is the integration of their deconvoluted DTG peaks, which was based on what was done by Carrier *et al.* (2011) (35). Figure 46 presents the decreasing of the hemicellulose peak as the temperature treatment increases for a sample of beech.

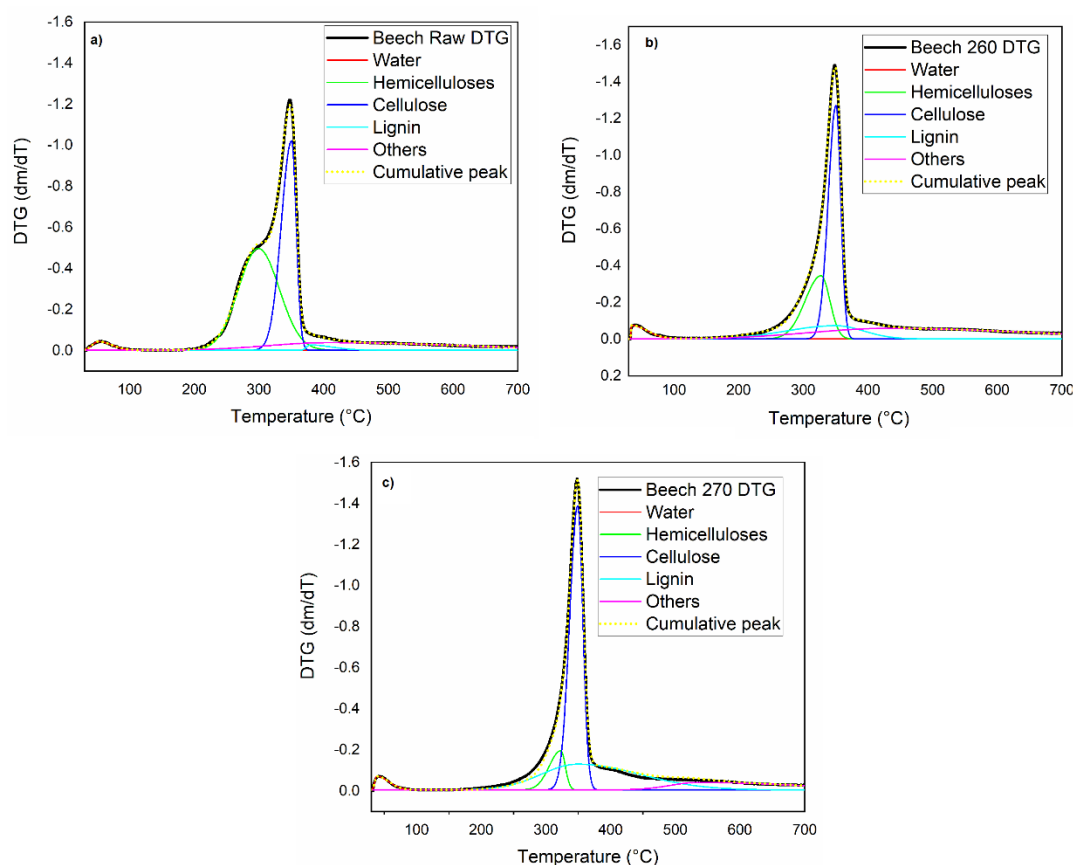


Figure 46. Deconvolution DTG curves of the (a) raw beech sample, and of the beech samples treated at (b) 260 °C, and (c) 270 °C.

Figure 46 represents the changes deconvolution DTG curves of three beech samples treated at increasing temperatures. It can be seen in the three DTG curves that the hemicelluloses peak (bright green) is shorter and wider than the cellulose peak. That is because, as previously explained, hemicelluloses are a family of biopolymers, having higher thermal sensitivity. Those peaks are also

the first ones to decrease as the treatment temperature increases. This allows us to try and degrade hemicelluloses with some selectivity, which is the aim of this part of the work. The cellulose peak (thin and dark blue) doesn't show any clearly noticeable trend, but it will be shown later by integration that it presents small fluctuations, usually increasing in size, since the degradation of hemicelluloses increases the resulting relative content of cellulose on the wood.

The lignin and other peaks are not in the scope of this analysis, as stated in carrier's work, but it can be clearly seen that they both increase with the treatment temperature. What happens is similar to the cellulose peak, as hemicelluloses decreases, lignin and other's relative quantity increase in the wood. Also, the degradation both of hemicelluloses themselves and what little lignin is degraded at those temperatures generates other products such as char, tar and others, which fall under the "others" category.

Based on the deconvolution DTG curves, the Cel/Hemi ratio of the three wood samples studied in this work were calculated on Origin by the integration of cellulose and hemicellulose peaks on Origin software. Figure 47 represents this ratio for the samples of beech.

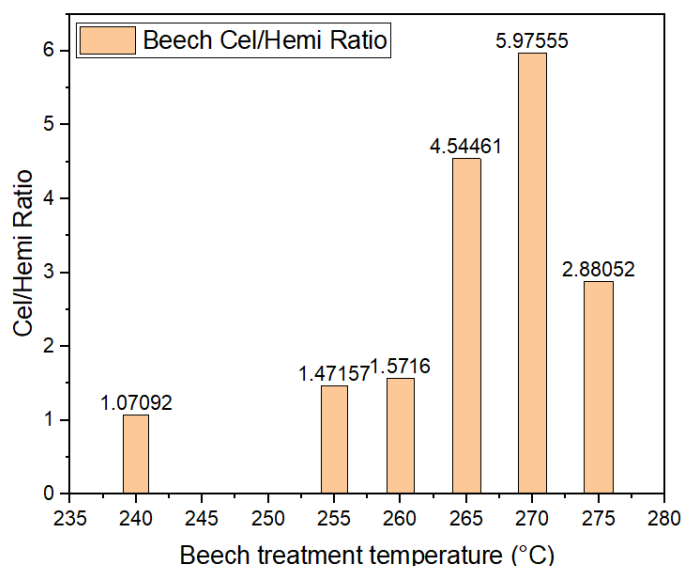


Figure 47. Cel/Hemi ratio for samples of beech treated at different temperatures.

Figure 47 shows the Cel/Hemi ratio stays relatively stable from 240 °C to 260 °C, with only small increases in value, showing that little degradation to hemicelluloses happened during this temperature, in accordance to the mass loss table, that showed a mass loss of only 17.9063% for B260, Past this point, at

265 °C, the ratio spikes up, indicating a sharp decline in the quantity of hemicelluloses, indicating the temperature in which it begins to degrade. The ratio increases again in B270 then decreases in B275, indicating that cellulose has started degrading. The deconvolution DTG curves (Figure 46) shows an overlap between the hemicelluloses and cellulose peak, meaning it is not possible to remove all a wood sample's hemicellulose without degrading some cellulose. The point where the thermal treatment reaches this overlap zone can be seen at 275 °C, where the Cel/Hemi ratio decreases. Past this point, the Origin software cannot keep deconvolution DTG curves with five peaks as it did before this point, meaning the hemicelluloses either no longer exist or is so small that the software cannot compute it using all the same parameters. 275 °C is also in accordance with the literature data for hemicelluloses content for beech and the point of increasing mass loss seen in the plot of mass loss, being one more indication that this temperature is adequate for this work. Figure 48 shows the Cel/Hemi ratio for the fir samples.

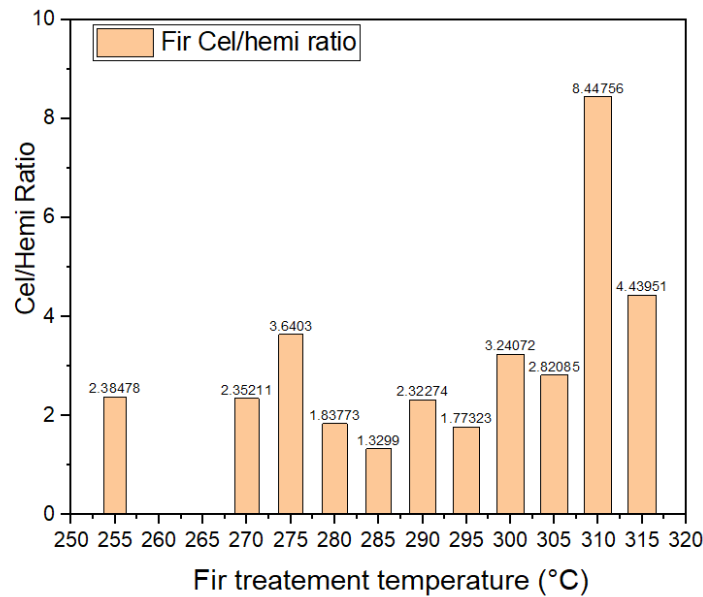


Figure 48. Cel/Hemi ratio for samples of fir treated at different temperatures.

Fir, a softwood, behaves differently than beech, a hardwood. The increments in Cel/Hemi ratio were not linear as with beech. This can probably be explained by the already mentioned fact that hardwoods are richer in acetylated hemicelluloses that, during heating catalyzes the degradation of hemicelluloses (95). In the case of the fir, a soft wood, this lack of catalyst causes each type of hemicellulose present in the wood to degrade at its own temperatures, causing

fluctuations in the proportion up to F305, observed after a large increase in the Cel/Hemi proportion. Softwoods are also known to contain less hemicelluloses than hardwood (95) making less biomass available for degradation at lower temperatures. Different from beech, the temperature chosen for the fir based on this deconvolution is 310 °C, the temperature before the drop in the Cel/Hemi ratio. That is done because that point is within the range of hemicelluloses percentage seen in literature and matches the temperature point in which the mass loss rapidly increases in Figure 44. The difference between the deconvolution DTG curves of hard and softwoods, explained ahead, is another reason why the temperature in which the ratio decreased, 315 °C was not chosen.

The deconvolution DTG curves profile of softwoods is also different, as shown in Figure 49 the deconvolution DTG curves of the raw fir.

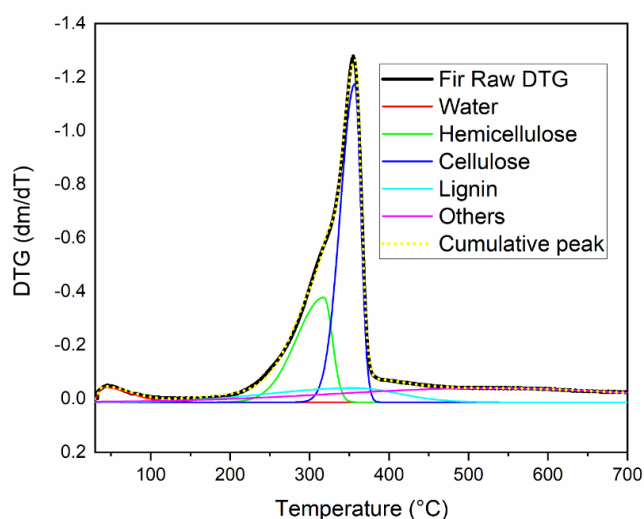


Figure 49. Deconvolution DTG curves of the raw fir.

The Figure 49 shows that, in fir, the softwood, the hemicelluloses “shoulder” is more subtle when compared to the hardwoods, meaning there is a bigger overlap between the temperatures for the degradation of hemicellulose and cellulose, so using the 315 °C would cause greater damage for the cellulose itself, which is not desirable. Considering that and the other reasons listed above as to why 310 °C is an adequate temperature, F310 was chosen for this work.

CV wood, despite having shown mass loss like that of the softwood fir, showed a Cel/hemi profile much closer to that of beech, as is shown in Figure 50.

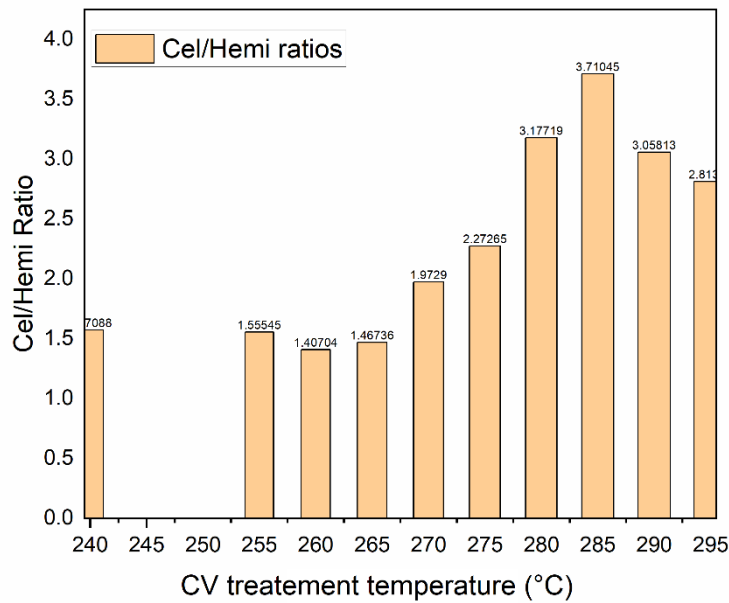


Figure 50. Cel/Hemi ratio for samples of CV treated at different temperatures.

Figure 50 shows that, in fact, the CV thermal degradation behaves more similar to that of the beech, as far as deconvolutions DTG curves go, with a stable beginning showing only small fluctuations that might as well be caused by experimental errors. The ratio continues stable up to sample CV270, when it begins increasing, showing the beginning of the hemicellulose's degradation. Different from beech, though, the ratio increases slowly, indicating a wider temperature range for its hemicelluloses' thermal stability, which can be, as explained before, an evolutive adaptation to the seasonal fires of the Cerrado. The ratio increases up to 285 °C, after which it decreases. This marks the point where the hemicelluloses can be degraded the most with as little cellulose degradation as possible. The 290 °C temperature also corresponds to the point in Figure 44 and has a relatively higher increase than for the previous temperatures. The Cel/Hemi ratio has matched the other experimental results obtained for the two other species of wood. This information was not found for CV, unfortunately, but the experimental data gathered will be used to infer the 290 °C to be the ideal for the objectives of this work. Deconvolution DTG curves of the raw CV samples in Figure 51.

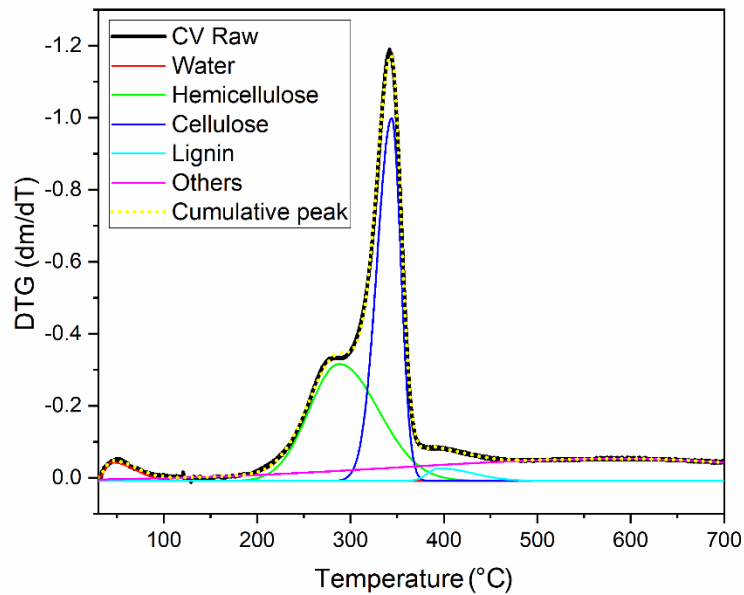


Figure 51. Deconvolutions DTG curves of the raw CV.

Figure 51 shows that the CV deconvolution DTG curves present a more noticeable shoulder of hemicelluloses than raw beech (and then the raw fir, consequently). This explains why the CV Cel/Hemi ratio presented in Figure 50 showed a longer range of temperature where the values were stable when compared to the beech Cel/Hemi plot.

4.3 Wood fractioning

4.3.1 Delignification

One more attempt to indirectly quantify the hemicelluloses degradation was by gravimetry of the sample's delignification. By using the delignification method described in the materials and methods section then weighing the dried product, it is possible to estimate the quantity of lignin that was left in each sample. As the treatment temperature rises, first the hemicelluloses, then, ideally, a little cellulose as possible is degraded, increasing the relative amount of lignin left in the samples, as shown in the wood deconvolution figures. The point at which the mass loss due to delignification peaks up should indicate the point where the cellulose is first degraded, the temperature this work aims for.

The delignification of the samples usually produces a white-out pulp, whose color darkens with the increasing temperature. Figure 52 represents the still to be dried pulp of the F270 sample.

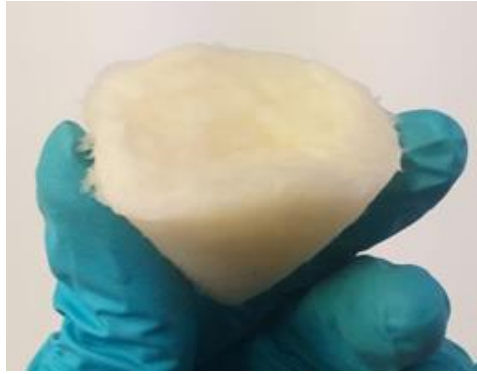


Figure 52. Wet pulp resulting from the delignification of the F270 sample.

Figure 52 shows that the delignification of thermally treated wood produces a pulp like paper. Figure 53 presents the dried pulp of delignified fir treated at different temperatures.

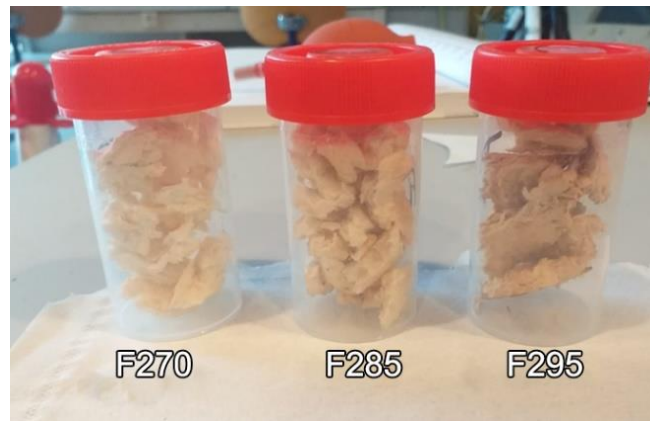


Figure 53. Dried delignified samples of fir treated at different temperatures.

Figure 53 shows the result of the delignification of different samples of fir. While all samples form pulps, the pulp gets progressively darker as the treatment temperature increases. That can be caused by the degradation of hemicelluloses by the treatment creating dark byproducts that are not removed either by the Soxhlet extraction or by the delignification.

Figure 54 represents the delignification gravimetry for the samples of fir in the different thermal treatment temperatures.

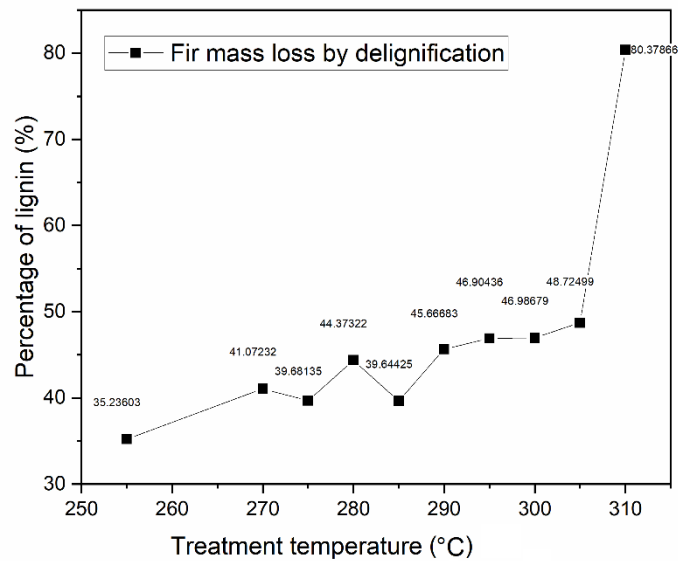


Figure 54. Delignification gravimetry of the fir samples.

Figure 54 shows a sharp increase in lignin percent at 310 °C, where the sample was about 80% lignin. While the temperature chosen based on the other experimental data previously presented in the work, the high amount of lignin indicated that it is possible that the actual best temperature was some non-tested temperature between 305 °C and 310 °C, which can be tested in further works. Still, the plot gives one more reason not to use the F315, by that point, the overlap between the degradation of hemicelluloses and cellulose in softwoods, shown in the deconvolution plot of fir, indicates that this temperature would have degraded also a great quantity of cellulose, rendering the sample not appropriate for the intended usage. Also, the F310 was so degraded the delignification of F315 was not attempted. Figure 55 presents the difference between the dried delignified F305 and F310 samples.

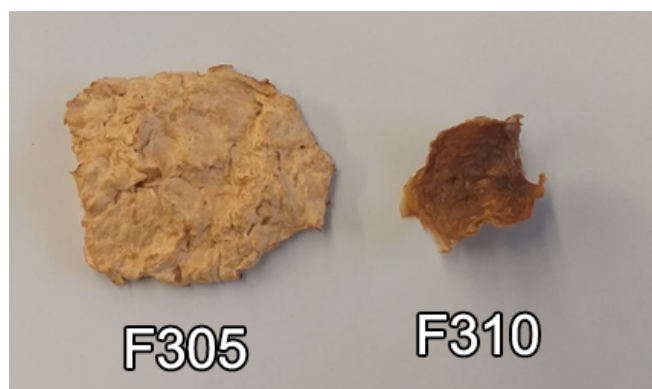


Figure 55. F305 and F310 after delignification.

As can be seen in Figure 55, the advanced state of degradation of F310 indicates that little other than lignin would remain in F315, the sample in which the Cel/Hemi ratio drops, making F310 the sample chosen to be used in this work.

Figure 56 indicates the percentage mass loss by delignification of the CV samples.

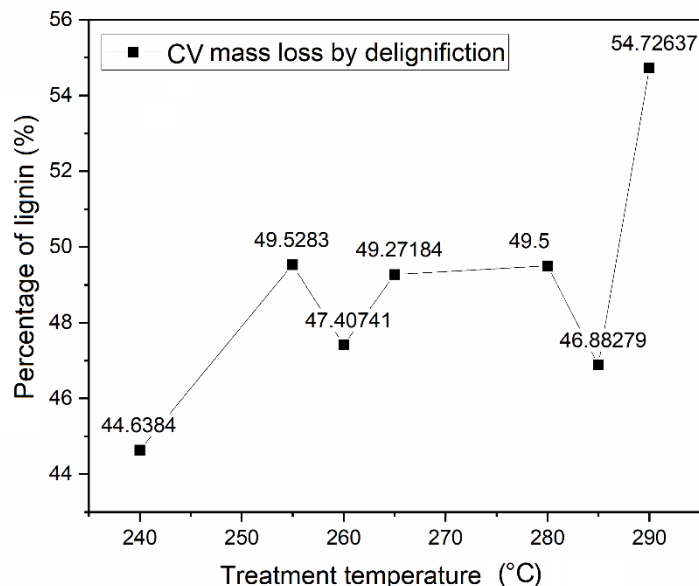


Figure 56. Delignification gravimetry of the CV samples.

The point of sharp increase in mass loss by delignification in the CV samples happens in the sample CV290, matching with the previous inferences made. Also, past 290 °C, the delignification of CV becomes quite harder, instead of forming a fibrous pulp similar to wet paper, as shown in the Figure 52, it forms a jam like substance that does not filter with a water trump vacuum and filter paper as it was done for the all the other samples. Figure 57 shows the attempt to filter the delignified CV295.



Figure 57. "Jam" resulting from the delignification of the CV 295 sample.

The unusual and hard to work with aspect of the delignified CV295, combining with the previously presented experimental data led the sample CV290 to be chosen as the CV sample for this work.

Figure 58 presents the mass loss caused by the delignification of the beech samples.

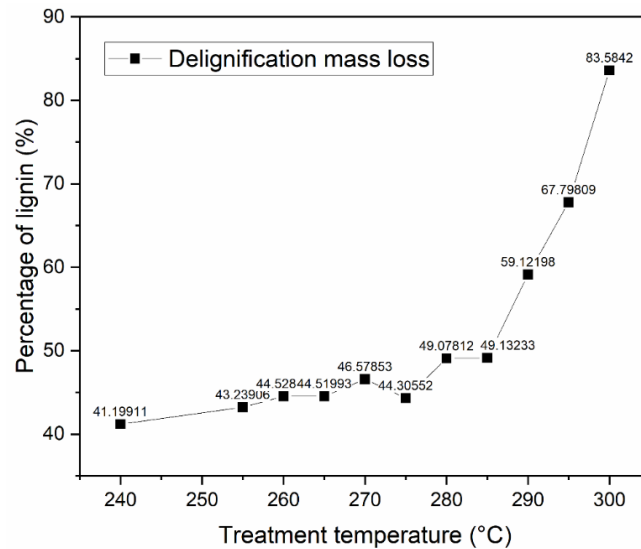


Figure 58. Delignification gravimetry of the beech samples.

In this case, the beech was shown last due to its abnormal behavior. The plot in Figure 58 shows quite different behavior when compared to the other 2 wood species. First, different from CV, it was possible to delignify all the samples of this wood, secondly, different from both other woods, the temperature that had been indicated by all the other experiments done so far, 275 °C, is not the point in which the mass loss due to delignification sharply increases, that happened at 290 °C. This could be explained in two different, but not exclusive ways: first, there is a better separation between the degradation temperature of hemicelluloses and cellulose in beech than in the other samples (especially when comparing with fir), so, despite the Cel/Hemi ratio for beech dropping at 275 °C, it is possible that the cellulose degradation at that point is minor, with the following temperatures, causing a much greater cellulose degradation, resulting into a higher relative lignin content. Another possible explanation is that the actual exact temperature for the hemicellulose degradation could be between 275 °C and 285 °C, as it was discussed with fir. None of those explanations change the fact that the other tests done on the beech indicate the 275 °C temperature, making B275 the sample of beech chosen for this work.

As a whole, while the delignification gravimetry has shown a good correlation with the other results, due to the complexity of lignin itself, it cannot be used alone for this kind of objective, working more as a supporting result to an already established tendency, like what we have seen in the previous results.

4.3.2 α -Cellulose gravimetry

One more attempt to indirectly determine the degradation of hemicelluloses was the α -Cellulose gravimetry. The reaction with NaOH was supposed to remove all the hemicelluloses of the samples, so the resulting mass should it steadily decrease until it flatlined at the point where the hemicellulose had all been degraded. Figure 59 shows the cellulose crystals obtained by the α -Cellulose gravimetry method.



Figure 59. α -Cellulose obtained.

The wet α -Cellulose crystals in the picture have the appearance of semi-transparent crystals that get swollen immediately with the addition of water. The α -Cellulose gravimetry, but did not work as intended, as shown in Figure 60.

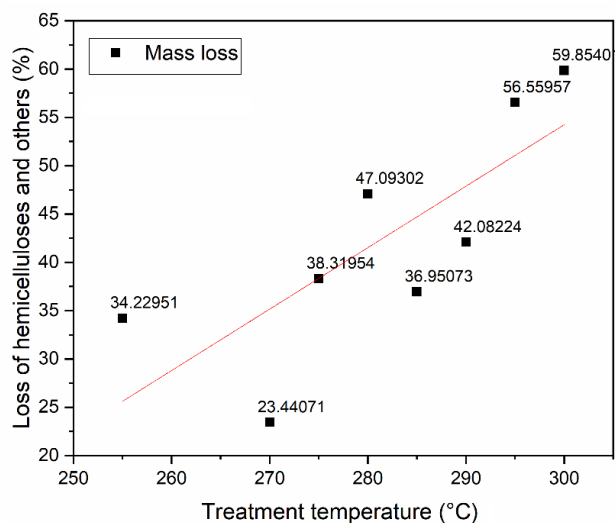


Figure 60. Mass loss by α -Cellulose gravimetry in samples of fir treated at different temperatures.

As can be seen in Figure 60, the results are not what was expected. The mass loss by α -Cellulose gravimetry only increased, showing the quantity of dissolvable mass by NaOH only increases with the treatment temperature. This can probably be explained by the work of Mathews *et al.* (2012) (103), who showed that high temperatures can change α -Cellulose's conformation into β -Cellulose, which, like hemicelluloses, is not resistant to NaOH, as shown in the works of Shaikh *et al.* (2021) (104). As a result, this method was discarded. Further techniques to chemically remove only hemicelluloses can be attempted in future works.

4.4. Conclusion

While we lacked methods to objectively determine the hemicelluloses degradation in the woods, the literature data found for beech and fir have shown a good correlation with the Figure 44 results. Not only that, but the deconvolution DTG curves data, validated by Carrier *et al.* (2011) (35), has indicated the same temperatures for as the literature data for hemicelluloses content for beech and fir. The three different and unrelated data pointing us to the same temperature gave us enough confidence to choose the treatment temperature they indicated to be used in this work. While this complete analysis was not possible for the CV wood, due to the lack of in-depth studies in this wood, the same methods were used as they had shown satisfactory results in for the other wood species, which led us to choose the treatment temperatures of 275 °C, for beech, 310 °C, for fir, and 290 °C, for CV.

Other techniques were also attempted to infer the best treatment temperature for this work, like delignification gravimetry. While it has shown reasonable results, the sheer complexity of lignin made the data not as precise and reliable as the other techniques used. Still, even though it cannot be used as a certain way to infer the desired temperatures, it can be used as an indicator, as long as there are other ways to validate the results.

α -Cellulose gravimetry did not work as intended, since the alkaline treatment, as shown in the literature, does not remove only hemicellulose, but also β -cellulose, which was converted from alpha cellulose during the thermal treatment.

Other than helping to determine the desired treatment temperature for this work, the deconvolution data helped to follow the hemicelluloses degradation behavior in the three wood species. It showed a rapid increase in degradation for beech, likely caused by the degradation catalyzation caused by the release of acetic acid during the treatment a slow degradation for fir which, as it does not self-catalyze the degradation of its own hemicelluloses, presented several stable peaks, probably showing each kind of hemicellulose degrading at its own temperature, until the point when the cellulose degradation begins, showing a big increase in the Cel/Hemi ratio.

The CV delignification was somewhat an intermediate between fir and beech, showing many small increments in the Cel/Hemi ratio until the point of cellulose degradation, which is likely caused by the wood naturally having more resistant to higher temperatures due to the biome it inhabits.

The CV, overall, despite showing hardwood structures like vessels, as seen in the literature, behaved closer to the softwood fir, showing that this division between hard and softwood might not have the impact in tropical woods as it has in European woods.

Chapter 5

Production of polyurethane foams and bio composite with thermally modified wood fibers

5.1 ^1H NMR spectrum of the MKO

To synthesize the polyol necessary to produce PU, the first step is to quantify the molar mass and amount of unsaturation per mole (unsaturation index) of the MKO. This was made by method described by (88), which is based on the integration of a quantitative ^1H NMR spectrum of the oil. Figure 61 represents the ^1H NMR spectrum of MKO. More details on the important peaks will be given further ahead.

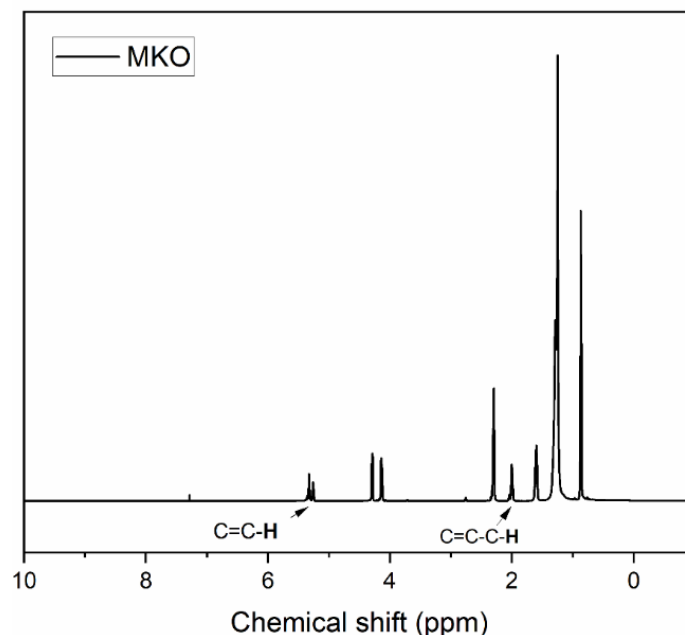


Figure 61. ^1H NMR spectrum for MKO (105).

Figure 61 shows the ^1H NMR spectrum for the MKO used in this work. While it only highlights the peaks representing unsaturation, which are what will be eliminated as the synthesis to polyol proceeds, a detailed list of peaks used has already been given in the methods section, described by Miyake *et al.* (1998) (88) and Monteavaro *et al.* (2005) (106), more details will be given when the spectrum is compared to that of EPMKO and GlyMKO. The calculated properties of MKO of given in Table 10.

Table 10. Properties of MKO.

	Molar mass	Unsaturation index
MKO	660.03 g·mol ⁻¹	0.85 unsaturations/molecule

The results show a relatively small molar mass for a vegetable oil, as well as a low unsaturation index. There are few literatures information about these

properties of this oil, as the pulp oil is more well studied, but the results are in accordance with previous characterizations of other samples of MKO made by the author, which have shown molar masses of $608.35 \text{ g}\cdot\text{mol}^{-1}$ and 0.7 unsaturation index. Both the low mass and unsaturation index can be explained by the most significant FA in the MKO being lauric acid, a small (12 carbons) and unsaturated FA, which makes up about 40% of the oil's composition. The only saturated acid present in MKO is oleic acid, a monosaturated acid that makes up for about 23% of the oil composition, as shown in the table showing the main FA of the oil. This results, together with previous empirical works done by the author, led to the quantities of reagents for epoxidation shown in the method section.

5.2 MKO, EPMKO and GlyMKO, synthesis and FTIR spectra

Figure 62 represents the normalized FTIR spectra of the MKO, EPMO and GlyMKO.

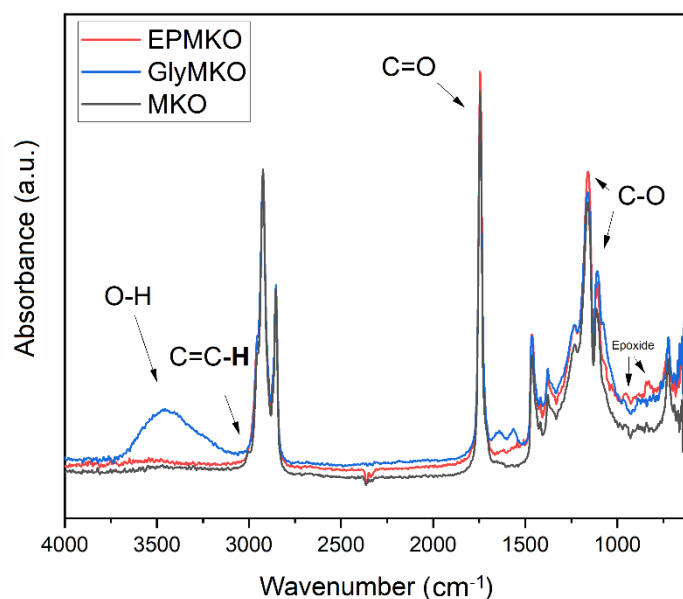


Figure 62. FTIR spectra of the MKO, EPMKO and GlyMKO samples (105,107).

The spectra show that, indeed, the unsaturation index of MKO is low, being hard to spot a small $\text{sp}^2 \text{CH}_2$ “shoulder” at around 2800 cm^{-1} . This small shoulder is no longer present in the EPMKO and GlyMKO spectra, showing that the double bonds breaking indeed happened as expected for the synthesis of MKO. The $\text{sp}^2 \text{CH}_2$ peaks, however, are much easier to spot on the ^1H NMR spectrum provided on Figure 61 and in Figure 63 presented further.

Another evidence of the successful epoxidation is the appearance of two small peaks at around 750 cm⁻¹ and 960 cm⁻¹, as described by Arjunan *et al.* (2017) (108), which represent the epoxide ring, it is also possible to notice a small increase in the C-O peaks in around 1090 cm⁻¹ and 1200 cm⁻¹, as described by Sideridou *et al.* (2016) (109), who also described the 2 epoxide bands previously mentioned.

In the GlyMKO spectrum, it is easy to notice the appearance of a wide OH band at around 3400 cm⁻¹ (105), indicating that the hydroxylation indeed happened. That is also supported by the decreasing in the two previously mentioned epoxide bands in the GlyMKO spectrum, indicating that the epoxide rings were opened to form hydroxyl groups. Table 11 lists the necessary bands to interpret the three spectra shown above.

Table 11. List of bands used to interpret the FTIR spectra in Figure 62 (105,107).

Wavenumber (cm ⁻¹)	Attribution
1700	C=O stretching
1200	C-O stretching
1090	C-O stretching
3000	CH ₂ sp ² stretching
1660	<i>Cis</i> C=C stretching
3400	O-H stretching
960	Asymmetric epoxide stretching
750	Epoxide stretching

5.3 MKO, EPMKO and GLyMKO ¹H NMR spectra

To confirm the successful synthesis of GlyMKO, ¹H NMR analyses of MKO, EPMKO and GlyMKO were performed under the conditions explained in the method section. Figure 63 shows the ¹H NMR spectra of those 3 samples.

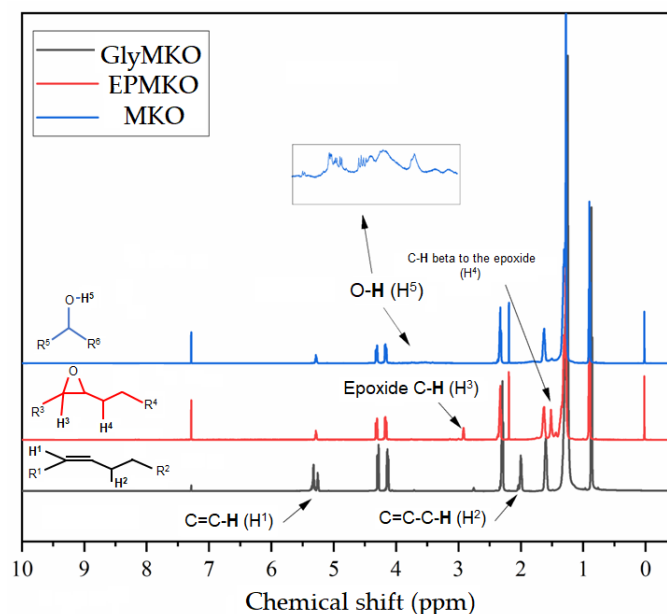


Figure 63. ^1H NMR spectra of the MKO, EPMKO and GlyMKO (105).

Although the Figure 63 shows many of the same signs, all the samples being made from Triglyceride, and the only modifications done are on the unsaturations, it is possible to see key differences between them. The MKO spectrum shows two signals representing unsaturations, one at 2.00 ppm, C=C-C-H, and another one at 5.3 ppm, for C=C-H. Both those signals are easier to spot than the unsaturation band on the FTIR of the oil, making it easier to confirm the oil does in fact present unsaturations to be chemically modified. One difference between the ^1H NMR spectra of MKO and EPMKO is the absence of those unsaturations signals, showing that they have been broken by the epoxidation reaction. What is the spectrum, instead, are two signals representing epoxide, one at about 3.0 ppm, representing epoxide C-H, and another at about 1.5 ppm, representing C-H beta to the epoxide itself, indicating that the epoxide formation did happen, that being the reason for the disappearance of the unsaturation signals. The ^1H NMR spectra of the MKO and EPMKO represent the signals expected by the works of Popescu *et al.* (2015) (110) and Ebran *et al.* (2008) (111), respectively.

The ^1H NMR spectrum GlyMKO is harder to analyze. The first thing that can be noticed is the absence of both unsaturations and epoxide signals, this shows that the epoxide rings were opened during the polyol reaction, and the unsaturations had not been reformed. However, the -OH signal that would confirm the sample as a polyol is difficult to appear. The hydrogen from hydroxyl groups,

are difficult to be seen in an ^1H NMR spectrum, with its chemical shift varying from anywhere to 1 ppm to 5 ppm and, being low in intensity (105). In the GlyMKO ^1H NMR spectrum, a real small signal at about 3.50 ppm, which can be seen in the zoom added to the figure could represent the O-H, as it is in an appropriate chemical shift. Despite the near absence of any hydroxyl signal, the easily noticeable hydroxyl band in the FTIR spectrum of the sample confirms that this sample was hydroxylated. Table 12 lists the important signals for the interpretation of the ^1H NMR spectra, together with their chemical shift.

Table 12. Bonds and chemical shifts relevant to the interpretation of the ^1H NMR spectra seen in the Figure 63 (105,110,112).

Chemical shift (ppm)	Bond
1.50	C-H beta to the epoxide
2.00	C=C-C-H
2.30	C-H bond to the ester carbonyl
2.76	C-H from epoxide
3.50*	O-H
4.25	CH ₂ from glycerol
5.25	CH from glycerol
5.35	C=C-H

*The identity of hydroxyl could not be confirmed, but it is likely it indeed represents hydroxyl.

5.4 OH Index

The first step for the synthesis of PU is to determine the OH, which was done following the ASTM Standard D1193 norm. The analysis was done in duplicate, and the average result was 85.57 mg KOH/g. A relatively low value when comparing with, for example, castor oil, a natural polyol, whose technical properties were analyzed in 2023 by Traquisa ® (113) [04\02\2024], which found an hydroxyl value of 150 mg MKO/g to 160 mg MKO/g. The low hydroxyl value is likely due to, despite glycerol adding reasonably three hydroxyls into the Triglyceride molecule, the oil itself not unsaturated enough to allow an inclusion of a large amount of glycerol in the polyol as a whole. It is also possible that the hydroxylation reaction was not complete.

5.5 Free NCO ratio

The Free NCO content of the MDI available in the lab had already been previously calculated by the ASTM D 5155-96 (114), and the value was found to be 0.3082%.

5.6 Synthesis of PU foam

Having both the Hydroxyl value of the GlyMKO and free NCO content of the available MDI, it is possible to synthesize PU samples with different NCO/OH ratios to study how this ratio can affect the final product properties. The NCO/OH ratios chosen to produce PU samples were 0.8, 1.0 and 1.2. The reagents quantities used for the synthesis of PU are given in Table 13.

Table 13. Quantities of reagent used for each NCO/OH ratio used in the synthesis of the PU samples.

NCO/OH ratio	Polyol (g)	MDI (g)
0.8	10	1.71
1.0	10	2.14
1.2	10	2.57

Figure 64 shows the digital images of the three PU foam samples produced in this work, labelled according to their NCO/OH ratio.



Figure 64. Digital images of the three produced samples of PU. Do notice they have stains from markers from the first attempt to label them.

To confirm whether or not PU synthesis occurred as expected, FTIR spectra of the samples were taken. The results are shown in Figure 65.

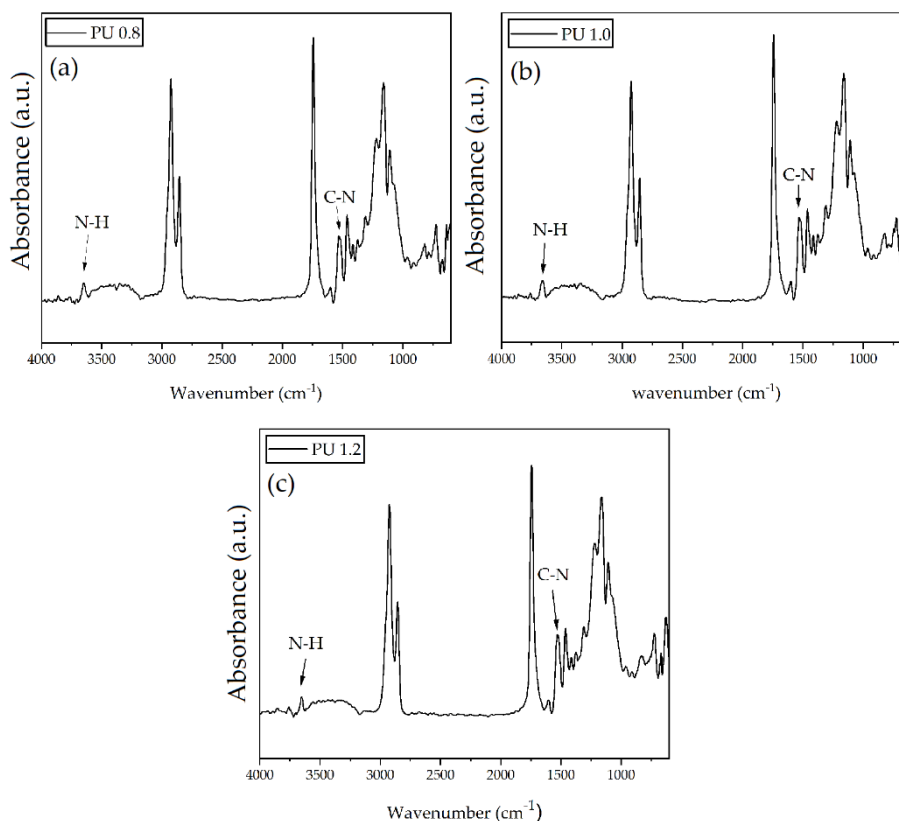


Figure 65. FTIR spectra of the three produced PU samples (105,107). The CO₂ peaks have been omitted for better visual clarity.

Most of the peaks seen in the FTIR spectra (Figure 65) are common to Triglyceride, of which they are made, so the analysis will focus on the peaks that are relevant to the PU synthesis. The Figure shows both the N-H peaks (although hard to notice), at about 3700 cm⁻¹, and the C-N peaks, at about 1500 cm⁻¹, in all spectra, showing that all the three NCO/OH ratios managed to produce PU (105).

It can also be seen that all three spectra are quite similar to each other, specially the FTIR spectra of the PU 1.0 and PU 1.2, which have nearly identical spectra. To analyze their similarity, the C-N peak of the spectra was integrated on Origin, resulting in 21.305, 27.995 and 26.891 for PU 0.8, PU 1.0 and PU 1.2, respectively. PU 1.0 and PU1.2 have shown nearly identical values, with the little difference seen being able to be attributed to experimental errors. Showing that the extra NCO added at ratios above 1.0 might simply remain as excess, which was discussed by Breves *et al.* (2024) (89).

FTIR spectrum of the PU 0.8 is also similar to the other two, but shows a slightly smaller C-N peak (105), indicating a lower formation of polyurethane during the reaction, as there is less isocyanate to react with the polyol.

FTIR spectrum of the PU 1.2, the one thought could be the same as the PU 1.0 but with an excess of NCO, different from the other samples, presented a few small orange crystals that are mechanically harder than the rest of the sample throughout the bottom side of the product. At first, the author assumed those crystals simply be to be remaining NCO. Figure 66 shows both the PU 1.2 sample, highlighting the crystals and their FTIR spectrum.

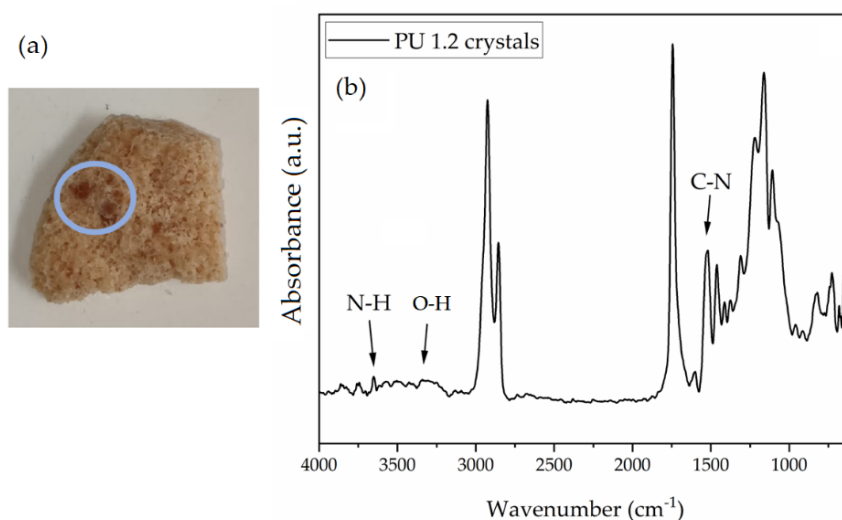


Figure 66. (a) PU 1.2, showing some the digital image of the PU crystals seen in its underside and their FTIR spectrum (105,107).

From Figure 66a, rather than unreacted NCO lumps, those are regions where higher density PU was formed, likely due to the excessive NCO present in this sample due to the higher NCO/OH ratio. The lumps not being solidified NCO is confirmed by the absence of a strong peak at 2200 cm⁻¹ in the FTIR spectrum (Figure 66b) characteristic N=C=O, according to (115,116) indicating that it is, in fact, not unreacted solidified MDI stuck to the polymeric matrix, but a different domain of PU of higher density. This could have happened as a bigger quantity of added Isocyanate might have caused a bigger local formation of polyurethane prior to the homogenization by the stirring, which might have also caused local regions of lower density PU in the polymeric matrix.

5.7 Composites

The composites used in this work were made with the same PU mixture described and sawdust of both raw and wood treated at the temperatures already discussed: 275 °C for the beech, 310 °C for the fir and 290 °C for the CV. Each combination of wood and polymer was also made in the three NCO/OH ratios

used in the synthesis of composites (0.8, 1.0, and 1.2). The composites were prepared according to what was described in the method sections. The mass of wood used of each wood percentage (2% and 5%) is listed in Table 14. The quantities of polyol and NCO are the same for the PU synthesis. Also, notice that since the wood percentage is based on the mass of the whole polymer, for each NCO/OH ratio a different mass will be used for each percentage.

Table 14. Quantity of wood used in each percentage for each NCO/OH ratio. Do note that the same quantities were used for all the three used species of wood.

NCO/OH ratio	2% wood (g)	5% wood (g)
0.8	0.2342	0.5855
1.0	0.2428	0.6070
1.2	0.2514	0.6285

Figure 67 exhibits the digital images of all the polymers and composites samples produced for this work. The samples in Figure 67 are labeled according to the kind of samples (PU, for the PU samples, and by the name of the wood, in the composites), wood thermal treatment (whether they are raw or their treatment temperature), wood percentage and NCO/OH ratio. The composites with treated CV were not made at the same time as the other samples, so they were inserted in the figure differently.



Figure 67. Digital images of all samples produced in this work.

5.7.1 FTIR, characterizations of the materials

5.7.1.1 Wood particle size selection

To use thermally treated wood sawdust as reinforcement material for PU composites, it is important to choose the best particle sizes. It is known that smaller particle sizes lead to bigger surface areas and better interactions between the reinforcement material and the PU matrix, they also contribute to more mechanically stable polymers than bigger sized particles by creating smaller pockets to house them in the polymeric matrix that present smaller matrix disturbance angles, resulting in smaller cracking diameters (117). The cracking mechanism and how it is affected by particle size is shown in Figure 68.

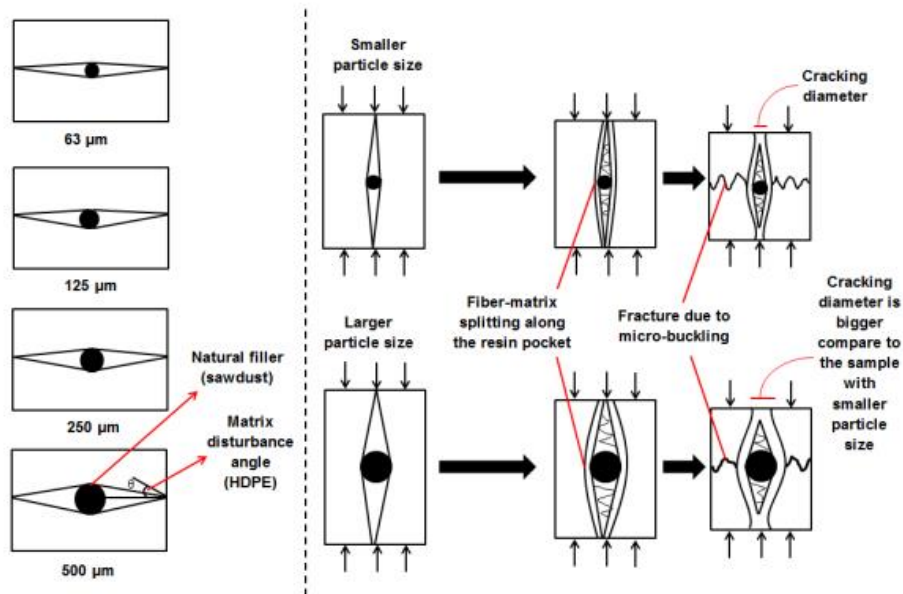


Figure 68.How particle size affects the polymeric matrix of a composite (117).

It was in the interest of the study to see which particle size would present the biggest amount of surface -OH groups. For that normalized ATR-FTIR spectra of the chosen samples were run and their -OH band were compared. Figure 69 shows the normalized FTIR spectra of beech treated at 275 °C, B275, samples in three different particle sizes (bigger than 500 μm, between 500 and 250 μm and smaller than 250 μm).

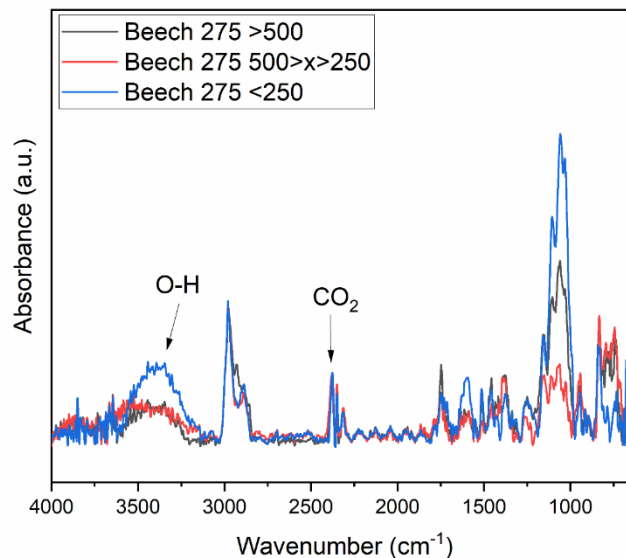


Figure 69. FTIR spectra of beech treated at 275 °C (B275) in different particle sizes (< 250 μm, 250-500 μm, > 500 μm) (105).

From FTIR spectra (Figure 69), it is possible to see that while all the three sample sizes show -OH, the smaller sample size, < 250 μm, shows the biggest -

OH band, indicating this that this particle size is the most indicate for a good interaction with the PU's isocyanate, thus a better interaction with the polymeric matrix.

Figure 70 shows the normalized FTIR spectra of F310 samples in the same particle sizes as the samples of beech.

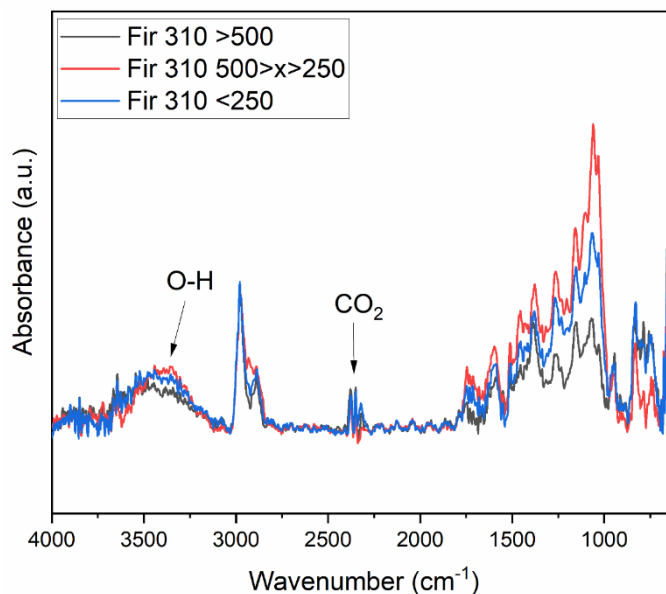


Figure 70. FTIR spectra of F310 in different particle sizes (< 250 μm, 250-500 μm, > 500 μm) (105).

In the case of fir the difference between the -OH bands in the FTIR spectra of all the three particles sizes is not big, with the particles bigger than 500 μm < x < 250 μm sample showing a slightly bigger -OH band. Despite that, the smaller particles were still chosen because they not only provide a bigger contact surface with the polymeric matrix but would also allow us to add a bigger quantity of reinforcement material into the polymer to produce the composite.

Figure 71 shows the normalized FTIR spectra of CV290 samples in two different particle sizes (between 500 μm and 250 μm and smaller than 250 μm), unfortunately, due to limitations of an international cotutelle, the particles bigger than 500 μm were not brought back to Brazil, where the FTIR spectra were ran, and there were no resources to bring them back in able time. The bigger than 500 μm particles, however, were never considered to be used due to the lack of a superior size limit in them, which could lead to heterogeneous and non-reproducible products.

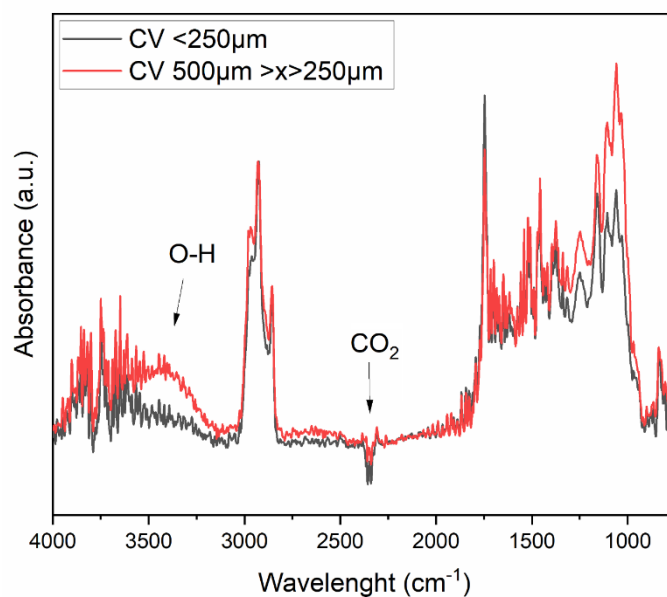


Figure 71. FTIR spectra of CV290 in different particle sizes, (< 250 µm, 250-500 µm, > 500 µm) (105).

Unlike the other woods tested, there is a considerable difference between the smaller and the intermediate particle size. This is likely caused because the high hardness of the wood helps to keep the particle size of its ground samples bigger even after 290 °C, consequently, the smaller particles are probably composed mostly of the more degraded fractions of the wood. Once again, despite the hardwood properties CV presents, its results are closer to the fir results, where the intermediate particle size also presented a bigger -OH band. Despite the FTIR spectra, the smaller than 250 µm particle size was also chosen for its already explained advantages on the polymeric matrix.

5.7.1.2 Preparation of PU

The composite samples were analyzed by FTIR spectra in the same conditions as done for the PU and the sawdust samples. To have a representative sample, pieces of the samples to be ran on the FTIR spectra were carefully picked from the different spots on the bottom of the composite, preferably reasonably near its geometrical center.

Figure 72 shows the FITR spectra of composites made with 2% (a) raw and (b) treated beech.

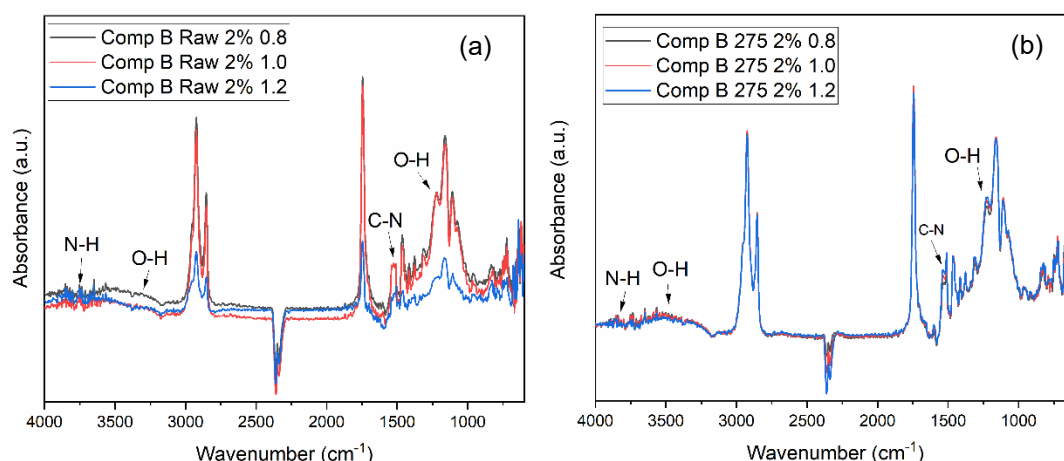


Figure 72. FTIR spectra of the composites made with 2% (a) raw and (b) treated beech. The CO₂ peak has been omitted for better visual clarity (105).

The N-H and C-N stretches, also seen in the FTIR spectra of PU (Figure 72), indicating that the PU was indeed synthesized.

At first sight, the FTIR spectra of the B275 samples are more similar to each other than the spectra of the raw wood samples. That might be related to the amorphous irregular nature of hemicelluloses, still present in the raw samples. The removal of hemicelluloses caused by thermal treatment led to the synthesis of more homogeneous composites, as the polymeric matrix bonds directly to cellulose, a more regular biopolymer.

Bigger -OH stretching bands (3500 cm⁻¹) are seen in the composites than the ones seen in the PU samples. That is likely due to the presence of wood particles, indicating the presence of unreacted -OH groups in the wood. While the B275 samples showed great homogeneity in their OH stretch band, in the raw samples, the Comp B Raw 2% 0.8 presented a bigger band, likely caused due to the lower quantity of NCO present to react with the hemicelluloses. The Comp B Raw 2% 1.0 and the Comp B Raw 2% 1.2, though, presented similar bands, which likely comes from, as it has already been said, the increased NCO/OH from 1.0 to 1.2 remains as excess, which forms the higher density PU lumps shown in the Figure 66. It can also be seen that the O-H bending peak at about 1400 cm⁻¹ increases slightly with the NCO/OH ratio.

Figure 73 presents the FITR spectra of the Composites made with 5% (a) raw, and (b) treated beech.

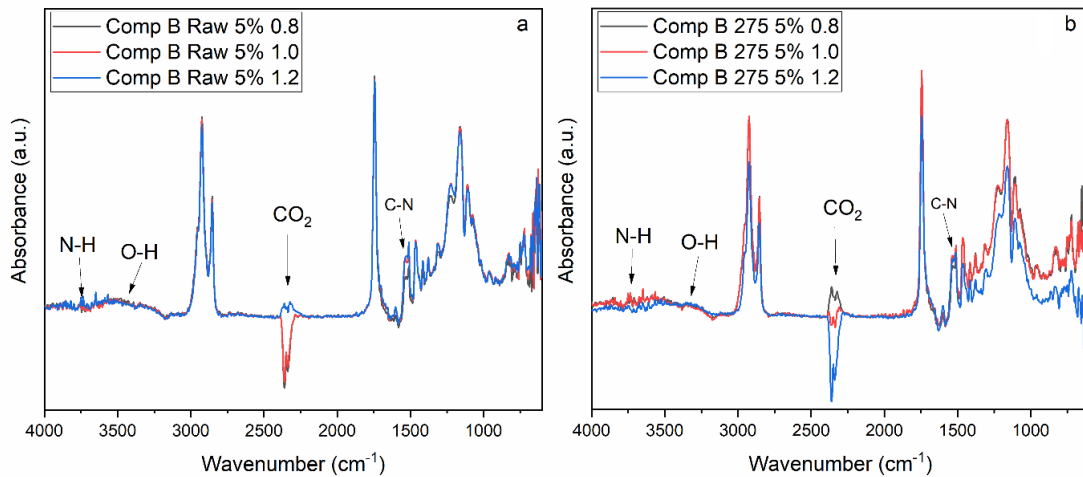


Figure 73. FTIR spectra of the composites made with 5% of (a) raw, and (b) treated beech (105).

Once again, the N-H and C-N stretches, also seen in the FTIR spectra of PU (Figure 73) indicate that the PU was indeed synthesized.

Different from the 2% beech, in this case, raw and treated wood samples are quite regular, with the spectra of the raw ones being more similar to each other this time. The bigger quantity of hemicelluloses present in the composites with raw wood caused by the bigger quantity of raw wood might have allowed bigger regularity in the samples. The C-N stretch in the raw wood composites show the same behavior as the composites and PU before, with a smaller peak for the 0.8 spectra and nearly identical peaks for the 1.0 and 1.2, for which an explanation has already been given. The same tendency is seen in the O-H bending, a lower peak for the 0.8, and bigger but nearly identical peaks for the higher ratio samples.

For B275, on the other hand, the 0.8 and 1.0 are nearly identical, except for the slightly bigger C-N stretch for the 1.0, which again is almost the same as in the 1.2. Other than that, the 5% 1.2 showed considerable differences when compared to all the other samples in the picture, especially in the 1500 cm⁻¹ to 1000 cm⁻¹ range, that could be because of the bigger quantity of reinforcement material, combined with the higher quantity of NCO was able to induce more reaction between the wood and the polymer itself, generating a more different product when compared to the other ones presented so far. That region of the spectrum shows peaks for both O-H bending and C-O stretching. Lower peaks in that region could indicate a more rigid molecular structure in the composite, that can be caused by the bigger degree of crosslinking that can be achieved

combining that NCO/OH ratio and that specific quantity of exposed cellulose from the B275 added to it.

Figure 74 presents the FTIR spectra of the Composites made with 2% of (a) raw, and (b) treated fir.

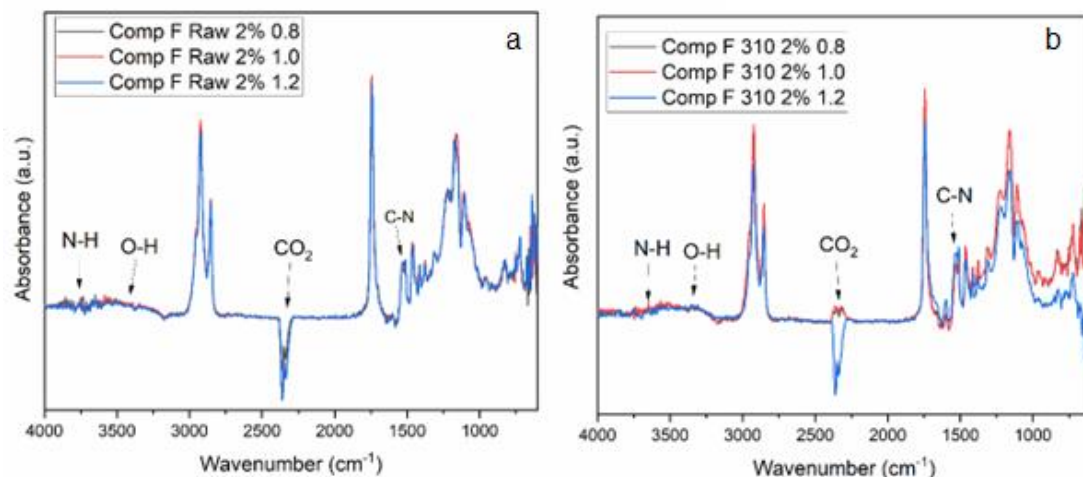


Figure 74. FTIR spectra of the composites made with 2% of (a) raw, and (b) treated fir (105).

Fir is a softwood, thus it has lower amounts of hemicelluloses (15). That can be seen on the raw fir spectra, in which, despite not having had heat treatment to degrade its hemicelluloses, which would ultimately reduce the size of the O-H stretch, it is still a little smaller when compared to the samples of raw beech. All the spectra were a lot like one another, indicating that the differences between the composite's properties are more due to the morphology and physical characteristics than to their chemistry. We see, once more, the same tendency happening with the C-N peaks on the raw fir spectra too, but this time the O-H bending seems nearly identical for all samples, instead of slightly increasing with the NCO/OH ratio, showing that the fir molecular structure doesn't allow much change in this regard.

The F310 2% showed the same tendency as the B275 5%, where the 0.8 and 1.0 ratios showed approximately the same spectra, but the 1.2 ratio showed big differences, especially 1500 cm^{-1} to 1000 cm^{-1} range of FTIR spectra, showing lower O-H bending and C-O stretching's than the other samples. As explained in Figure 74, that can indicate a more rigid structure for this specific sample, likely due to the NCO/OH ratio and the amount of surface cellulose's hydroxyl groups being optimal for a bigger formation of crosslinking. The fact that this has happened in the 2% samples for F310, but only in the 5% samples in the B275

samples could be caused because the lighter density of fir, specially treated fir, means a bigger quantity of material needs to be added to reach the same mass. Also, while hardwoods have vessels, bigger size could allow for a bigger access of the polymeric matrix into the wood structure. In softwood, most of the cells are tracheids and, while they are smaller than vessels, they are so much more numerous, and also bigger in size when compared to hardwoods tracheids (15), that the 2% of wood added was already enough to induce enough reaction on the surface of the wood for that to take place.

Figure 75 presents the FTIR spectra of the Composites made with 5% of (a) raw, and (b) treated fir.

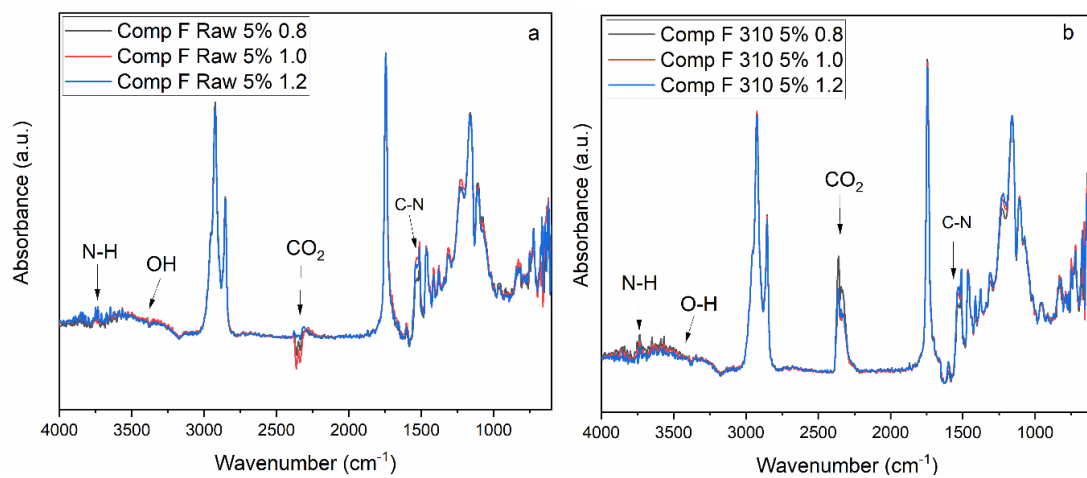


Figure 75. FTIR spectra of the composites made with 5% of (a) raw, and (b) treated fir (105).

Once again, we can notice high regularity in the raw fir FTIR spectra in Figure 75. One difference this time from the other raw samples is that both the C-N stretching, and the O-H bending are now slightly higher in the 1.0 ratio. That could be because the parity in the 5% of wood is enough to create enough crosslinking in the composite structure to begin decreasing the flexibility of its bonds in the 1.2 ratio, while the 1.0 ratio has enough NCO to promote a good amount of crosslinking and bonding to the hemicellulose, while keeping the crosslinking a little lower than the 1.2 ratio. The 0.8 ratio, again, showed the lowest C-N peak, as it has the lowest quantity of NCO to form the C-N bonds of PU.

Different from what happened with the F310 2% samples, the treated samples were homogenous, that was probably caused because the excess of exposed cellulose from the 5% of treated wood added to the mixture has made up for the factors that didn't allow the lowest NCO/OH ratios to form the same

product as the 1.2 ratio seen in the 2% samples. Now again, the C-N stretching and O-H bending increased slightly with the NCO/OH ratio. That could have happened due to the presence of water adsorbed inside the polymeric matrix, as will be seen in the DVS results.

Figure 76 presents the FTIR spectra of the Composites made with 2% of (a) raw, and (b) treated CV.

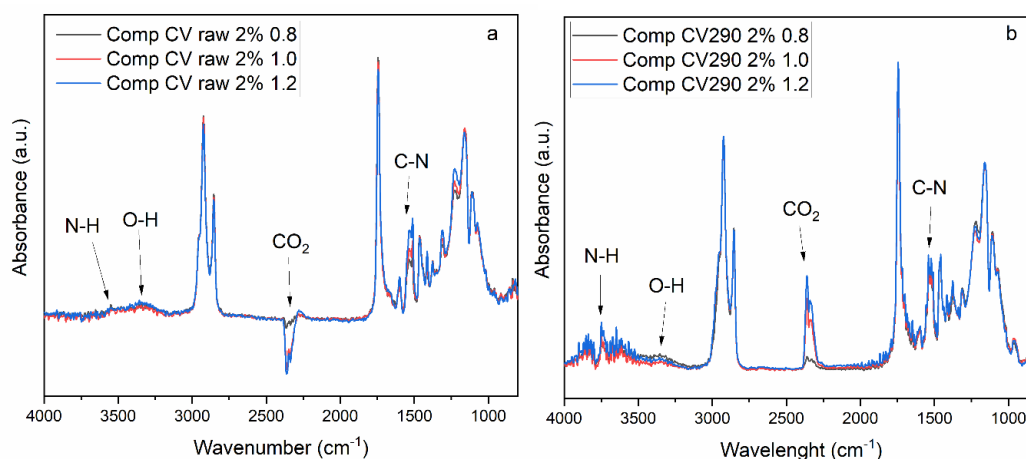


Figure 76. FTIR spectra of the composites made with 2% of (a) raw, and (b) treated CV (105).

Regarding the CV composites, there isn't much new to say that has not yet been said for the previous composites. One noticeable difference is that in both raw and treated 2% CV composites, the remaining -OH band at about 3400 cm⁻¹ is smaller, indicating a more intense formation of PU with the -OH of wood, shown in FTIR spectra. The C-N peak is much more visible with the treated CV, indicating that this kind of wood is more prone to react to NCO than both European woods studied. One other difference from the composites made from European woods is the C-N peak. While in those woods there was not much difference in this peak between the composites with NCO/OH ratio of 1.0 and 1.2, in the case of raw CV, specially, there is a clear scaling up in this peak, showing that raw CV richer in -OH to the point where the extra quantity of NCO present in the 1.2 ratio can actually produce more PU instead of remaining as excess. This higher assumed higher quantity of -OH groups was implied by its higher density mentioned in Table 8.

In the treated CV, however, the difference between the C-N peaks in the composites with 1.0 and 1.2 ratio is not too visible, showing that the increase in

surface area by the thermal treatment might not have exposed cellulose's -OH enough to make up for the loss of hemicelluloses OH.

Figure 77 presents the FTIR spectra of the Composites made with 5% of (a) raw, and (b) treated CV.

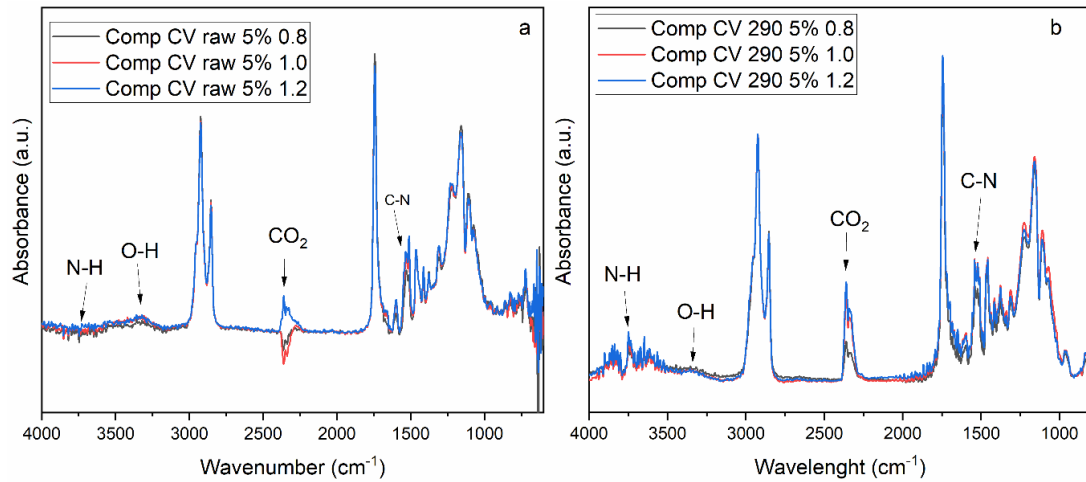


Figure 77. FTIR spectra of the composites made with 5% of (a) raw, and (b) treated CV. The CO₂ peak has been omitted for better visual clarity (105).

The bigger quantity of CV sawdust added didn't change much the samples' FTIR spectra. The C-N peak can be seen scaling up with the increase of the NCO Ratio for the raw wood composites as was seen in Figure 77, while for the treated wood composites the same happened again, with the 1.0 and 1.2 ratio composites showing little difference. This indicates that the increased quantity of wood might have caused the formation of higher density composites, without substantial changes to their chemistry.

5.8 Thermogravimetric Analysis (TGA)

5.8.1 PU

TGA and DTG curves of the PU obtained in this work are in Figure 78.

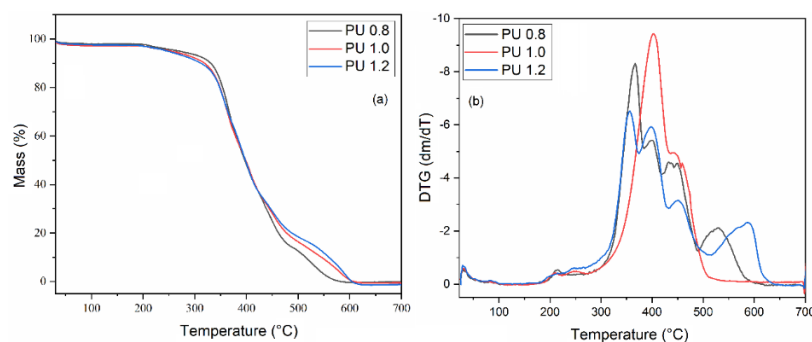


Figure 78. (a) TGA and (b) DTG curves of the PU samples.

In the TGA and DTG curves (Figure 78) it can be seen that, before 400 °C, all the three samples have similar thermal decomposition, with PU 0.8 showing a slightly lower mass loss between 200 °C and 400 °C, likely due to the sample with less isocyanate, it has fewer rigid segments to degrade at lower temperatures. They present essentially the same behavior from 300 °C to 400 °C, when it is reversed, and the PU 0.8 shows higher mass loss. That probably happens because this is the temperature of the soft segments' degradation, in which PU 0.8 is the richest. That is supported by the fact that PU 1.2, the one with the most NCO, thus the biggest amount of rigid segments has the lowest mass loss at this area (118).

One interesting thing to notice is that, while usual PU typically presents three degradation peaks in their DTG curves, representing the urethane bond rupture, breaking of rigid segments and breaking of soft segments, as the temperature increases, PU 0.8 and PU 1.2 presented each four different peaks in DTG curves. This may be caused by inequality in the amount of NCO and OH promoting crosslink formation, generating segments with intermediate rigidities and softness that degraded each at its own temperature. This behavior was not seen in the DTG curve of the PU 1.0, where only the usual three peaks were seen, which could have been caused by the equal quantities of NCO and OH having generated a more regular and less crosslinked PU.

Table 15 lists the T_{onset} , (T_{onset}), the temperature in which the polymers see lose 5% and 10% of mass (T_5 and T_{10} , respectively) values obtained from TGA curves (Figure 78a).

Table 15. Thermal properties of the PU samples.

Sample	T_{onset} (°C)	T_5 (°C)	T_{10} (°C)
PU 0.8	339.20	273.33	326.78
PU 1.0	332.30	254.62	314.26
PU 1.2	332.70	249.60	313.82

Table 15 shows that, in fact, PU 0.8 has the highest T_{onset} , even if just by a little. PU 1.0 showed a T_{onset} 0.4 lower than the PU 1.2, such a small difference could be caused by experimental error, but it can also be explained by the fact shown in Figure 66, which has shown that the PU 1.2 samples presented zones with higher density PU, that could also have created regions with slightly lower NCO concentration, resulting in localized softer segments that could degrade at

higher temperatures. Other than this, for both T_5 and T_{10} the temperatures decrease as the NCO/OH ratio and, by consequence, the rigidity of the PU segments increases.

5.8.2 Beech 2%, NCO/OH 0.8

The thermal stability of the composite samples was compared to that of the PU by TGA under synthetic air atmosphere. Figure 79 represents the TGA and DTG curves of the samples of PU, beech composites of both raw and treated wood at 2% at the NCO/OH ratio of 0.8.

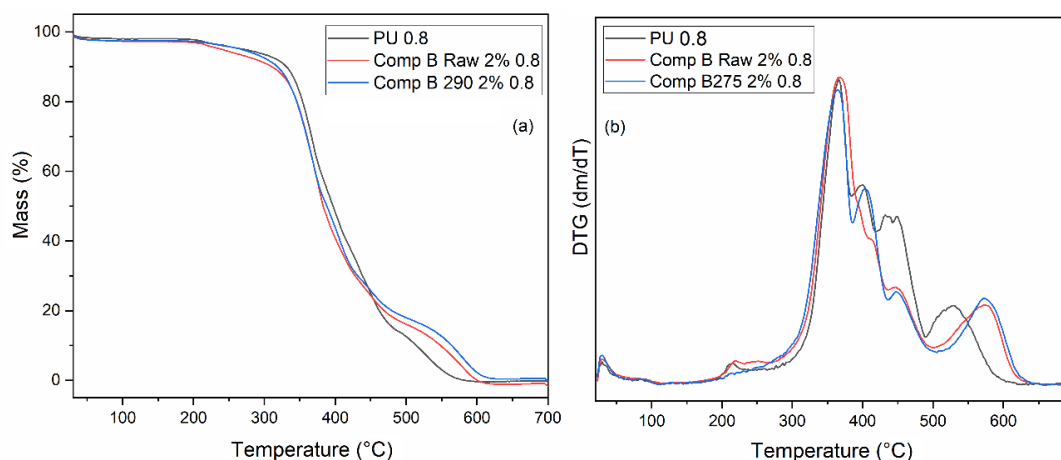


Figure 79. (a) TGA, and (b) DTG curves of the samples of PU, beech composites of both raw and treated wood at 2% at the NCO/OH ratio of 0.8.

On the TGA of the samples 0.8 samples (Figure 79a), we can see a relatively big separation between the mass loss of the four samples below 300 °C, with the PU showing a higher thermal stability, followed by Comp B275 2% 0.8 and Comp B Raw 2% 0.8, despite the difference being low. When the thermal degradation intensifies, at around 380 °C, the composite samples start behaving basically the same, while the mass loss for the PU keeps itself relatively lower until about 450 °C, when the behaviors reverse, the PU sample experiences the biggest mass loss of the samples, while the composite begin experience a lower mass loss rate, forming a shoulder on the plot, with the Comp B275 2% 0.8 showing the lowers mass loss of the three samples.

The thermal degradation of PU under air usually follow three basic steps: The breakage of the urethane bonds, followed by the degradation of the hard segments and finally the degradation of the soft segments (118). The increased quantity of urethane bonds formed by the addition of wood particles into the

mixture might be responsible for the composites' mass loss being slightly lower than then PU's and the wood might have promoted a bigger formation of hard segments, explaining why the composites' mass loss continues to be a little higher until about 450 °C. At this point, the PU probably keeps on degrading as a PU would with the degradation of its soft segments and the composites, while also experience this kind of degradation, also have wood particles, which have higher thermal degradation temperatures (15), which reverse the behaviors of the TGA curves. Also, since the Comp B275 2% 0.8 was already pre-thermally treated, it has less mass available to be lost at this temperature (15), making its thermal stability slightly higher at this temperature.

This time again, all the samples presented four peaks in DTG curves, likely for the reasons already discussed, but the peaks DTG curves for the composites have visible differences, especially in the degradation stem at about 400 °C, which is small for the raw composite and could be taken for a shoulder of the previous degradation peak. This can indicate that the lower quantity of NCO reacts differently with raw and treated wood -OH groups. The values of T_{onset} , T_5 , and T_{10} obtained from the TGA curves (Figure 79a) are shown in Table 16.

Table 16. Thermal properties of the samples of PU, beech composites of both raw and treated wood at 2% at the NCO/OH ratio of 0.8.

Sample	T_{onset} (°C)	T_5 (°C)	T_{10} (°C)
PU 0.8	339.2	272.33	326.78
Comp. B Raw 2% 0.8	335.0	242.20	318.92
Comp. B 275 2% 0.8	330,1	269.22	319.61

In these samples, PU 0.8 showed the highest T_{onset} , while the treated wood composite showed the lowest. By the way, T_{onset} is calculated, it can lead to confusing results, so the other two measured properties may lead to more comprehensible results. The Raw composite, though, showed the lowest T_5 and T_{10} of all samples, that probably because it has degradable hemicelluloses at these temperatures, causing a bigger mass loss. The treated wood composite presented the highest T_5 and T_{10} likely because, not only have its hemicelluloses already been previously degraded by the thermal treatment, but it might also have produced a smaller quantity of soft segments than the other two samples.

5.8.3 Beech 2%, NCO/OH 1.0

Figure 80 presents the TGA and DTG curves of the samples of PU, beech composites of both raw and treated wood at 2% at the NCO/OH ratio of 1.0.

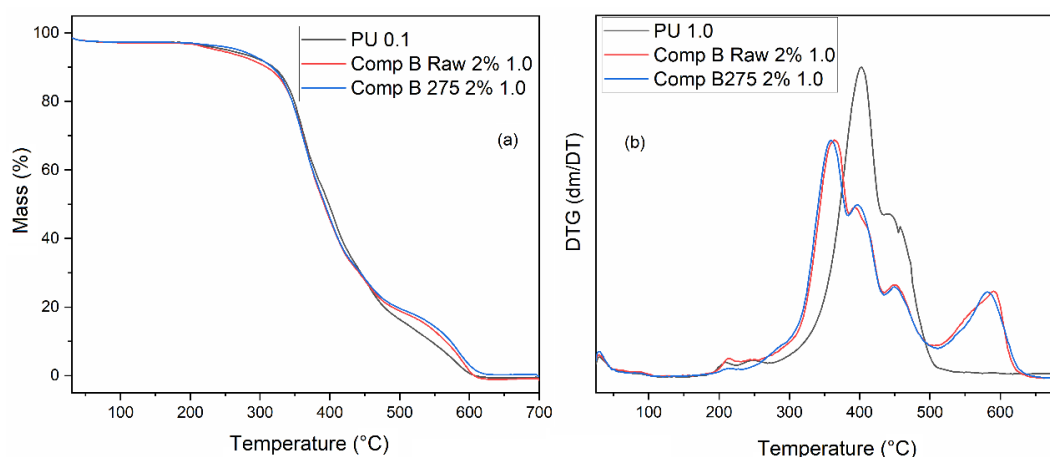


Figure 80. (a) TGA, and (b) DTG curves of the samples of PU, beech composites of both raw and treated wood at 2% at the NCO/OH ratio of 1.0.

The PU sample with NCO/OH ratio 1.0 show a quite different behavior, with the three samples behaving nearly the same at lower temperature, but with the Comp B 275 2% 1.0 having a slightly lower mass loss (Figure 80a). The even quantity of NCO and OH in this ratio, with the higher quantity of NCO, allowed a more uniform amount of urethane bonds to be formed in all samples, but with a higher amount of rigid segment being formed in the Comp B 275 2% 1.0 sample, due to the bigger quantity of exposed cellulose for the NCO to react to during the formation of the composite, PU hinge the higher mass losses to slightly higher temperatures. The degradation behavior of the samples remains similar, with a slightly lower mass loss for the PU 1.0 sample, likely due to a smaller number of hard segments present because of the absence of reinforcement material, until the reversal point, at about 450 °C, in which the degradation behavior reversed in the same way it did in the 0.8 samples, but with a lower separation between the samples. The lower mass loss of the PU 1.0 sample can be explained due to the higher NCO/OH ratio promoted the formation of more rigid segments, leaving a smaller number of soft segments to be degraded at that temperature. Once again, the observed degradation behavior reversal is likely due to the presence of wood, a material with higher degradation temperatures, and the treated samples presented the lowest mass loss at that temperature probably for the same reason explained for the 0.8 samples.

The DTG curve shows that, despite the differences shown in the composites' DTG curves from Figure 80b, in the samples with an NCO/OH ratio equal to 1.0, the peaks of the DTG curves are quite similar, indicating that the even quantities of NCO and OH don't show much preference to bonding to either treated or raw wood -OH groups. The values of T_{onset} , T_5 , and T_{10} obtained from the TGA curves (Figure 80a) are shown in Table 17.

Table 17. Thermal properties of the PU samples, beech composites of both raw and treated wood at 2% at the NCO/OH ratio of 1.0.

Sample	T_{onset} (°C)	T_5 (°C)	T_{10} (°C)
PU 1.0	332.3	254.62	314.26
Comp. B Raw 2% 1.0	331.6	242.25	311.82
Comp. B 275 2% 1.0	317.6	271.83	319.25

Table 17 shows a decrease in T_{onset} for the raw wood composite and a further decrease for the treated wood composite, which are hard to see in the sample's TG curves. The raw wood composite also showed the lowest T_5 and T_{10} , likely because of the presence of thermally degradable hemicelluloses at those temperatures, while the treated wood composite showed the highest temperatures, likely because its more easily degradable biopolymers had already been previously degraded in the thermal treatment.

5.8.4 Beech 2%, NCO/OH 1.2

Figure 81 represents the TGA curves of the samples of PU, beech composites of both Raw and treated wood at 2% at the NCO/OH ratio of 1.2.

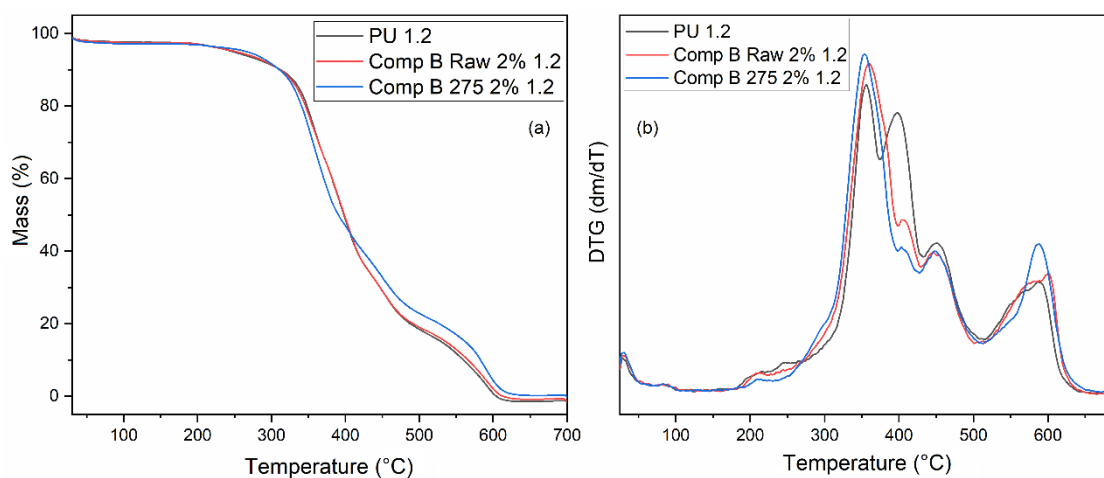


Figure 81. (a) TGA and (b) DTG curves of the PU samples, beech composites of both Raw and treated wood at 2% at the NCO/OH ratio of 1.2.

The 1.2 ratio samples behaved quite differently from the samples in other ratios. The PU 1.2 and Comp B Raw 2% 1.2 behaving nearly the same throughout all the TGA curves, with a lower degradation at first, likely for having less hard segments than the B275 composite samples, until about 400 °C. At this point, most of the hard segments of the Comp B275 2% 1.2 are most likely degraded, lowering its mass loss ratio. That, when considering the thermally treated wood present in it has higher thermal degradation temperatures, might explain why its mass loss is lower than that of the other two samples. Different from the other 0.8 and 1.0 samples, the PU 1.2 and the Comp B Raw 2% 1.2 still present similar profiles. It is likely that the excessive NCO present at this ratio, which, as already discussed, caused no big chemical differences in the polymer, but caused physical differences such as higher density, including the high-density lumps presented in Figure 66. This extra dense mass might be less thermally conductive, reducing the rate of thermal degradation until it was similar to that of the Comp B Raw 2% 1.2, whose raw wood present in it, while slowing down the thermal degradation, had enough degradable mass at lower temperatures (hemicelluloses) to separate its curve from the Comp B275 2%1.2.

The DTG curves show quite similar behaviors for all samples, especially past 450 °C. Also, the composites behave similarly in the whole temperature range, which is also like the PU 1.2 behavior, except for a big peak in DTG curve at about 400 °C, comparing the DTG curves of all beech composites so far, we can see that, despite the NCO/OH ratio of 0.8 resulting in quite different DTG curves, the other ratios, specially 1.0 produces more similar products. That could be expected since, as already explained, there are little differences between the products with NCO/OH ratio 1.0 and 1.2.

As observed on the FTIR spectra of the samples presented here, no big chemical difference should be expected. Table 18 lists the T_{onset} , T_5 and T_{10} values obtained from the TGA curves (Figure 81a).

Table 18. Thermal properties of the beech samples at 2% and 1.2 NCO/OH ratio.

Sample	T_{onset} (°C)	T_5 (°C)	T_{10} (°C)
PU 1.2	332.7	249.60	313.82
Comp. B Raw 2% 1.2	330.1	254.51	313.20
Comp. B 275 2% 1.2	322.8	266.84	311.51

The NCO/OH 1.2 ratio samples had thermal properties similar to the 1.0 ratio samples, as expected except that, while the treated wood composite presented a higher T_5 , is the one with the smallest T_{10} of the compared samples, even if just by a little. That could be caused because, while by the T_5 is higher for the treated wood composite, at T_{10} is likely that the degradation hemicelluloses and higher density PU caused by the bigger amount of NCO generates residues that stay adsorbed into the polymeric matrix in this range of temperature.

5.8.5 Fir 2%, NCO/OH 0.8

Figure 82 represents the TGA and DTG curves of the samples of PU, fir composites of both Raw and treated wood at 2 % at the NCO/OH ratio of 0.8.

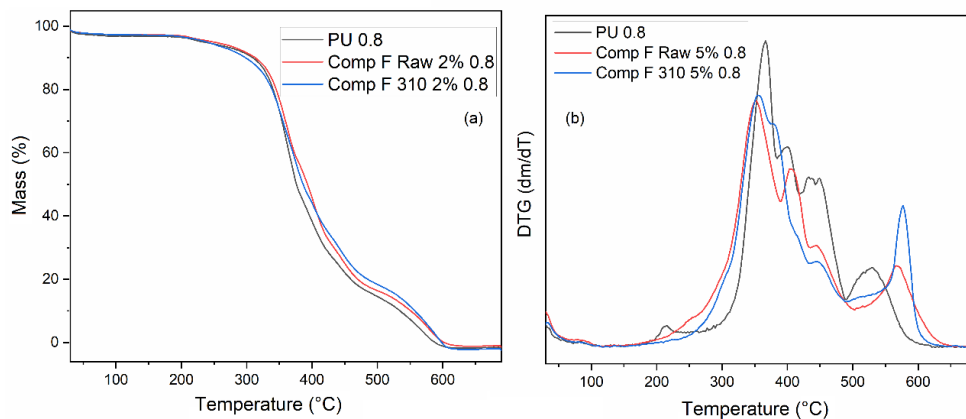


Figure 82. (a) TGA and (b) DTG curves of the samples of PU, fir composites of both Raw and treated wood at 2 % at the NCO/OH ratio of 0.8.

A first difference that can be easily spotted in TGA and DTG curves (Figure 82) compared to TGA and DTG curves of the beech samples (Figure 79) is that, thorough nearly all the TGA curves, the PU sample is the one with the biggest mass loss, except for the part immediately before the thermal degradation peaks up. Also different from the beech samples is that the raw fir sample, Comp F Raw 2% 0.8, has a lower mass loss than the treated fir samples up to about 400 °C. The PU 0.8 higher degradation can be explained because, different from the hardwood beech, the softwood fir has not only less hemicelluloses to be degraded at lower temperatures, but their hemicelluloses are also more resistant to thermal degradation, as already explained, making the composites have a slightly lower mass loss in the whole TGA curve. Comp F 310 2% 0.8, having had its hemicelluloses thermally degraded, has a close to behavior to the F Raw

sample, as both have no degradable mass, at that temperature (except, naturally, for the polymeric matrix, which is what makes up the whole PU 0.8 samples, causing its higher mass losses).

Past 400 °C, the fir hemicelluloses begin degrading, causing its mass loss to grow higher than that of the F 310 sample. At around 620 °C, the raw fir hemicelluloses degradation causes its mass loss gets closes to that of those two other samples and, eventually, the mass loss of the treated fir sample surpasses it. The hemicelluloses degradation in the raw wood samples should lead to the exposure of the wood's cellulose, leading to a product like the Comp F 310 2% 0.8. The reason why the Comp F 310 2% 0.8 ends up with a higher mass loss could be related to how the wood is treated. The thermal treatment in this work is done in a reactor, with a draw inert gas inlet and outlet, that allows residues formed in the treatment to be removed. When the wood is subjected to higher temperature as part of a composite, the residues might stay bonded to the polymeric matrix. One more possible explanation is because the thermal treatment of wood is done in N₂ atmosphere, while the TGA curves are performed under synthetic air atmosphere. The oxidizing atmosphere can lead to combustion byproducts for both hemicelluloses and cellulose in the Comp F Raw 2% 0.8, while in Comp F 310 2% 0.8 only cellulose combustion byproducts are possible, ultimately leading to a higher mass loss.

In the DTG curves, the treated wood composite presents the two first degradation peaks, at around 350 °C and 400 °C are much closer than all the other first two peaks seen in beech. That is likely caused by different kinds of hemicelluloses present in softwood (95) and then lack of self-catalyzation for their degradation, which is a peak that does not appear in the raw composite, meaning it could be some residue that was adsorbed into the porous treated wood structure previous to the TGA itself (different from the residue generation in the raw wood composite TGA curves), which allowed them to be readily degraded during the TGA. Table 19 presents the T_{onset}, T₅ and T₁₀ values obtained from the TGA curves (Figure 82a).

Table 19. Thermal properties of the fir samples at 2% and NCO/OH ratio of 0.8.

Sample	T _{onset} (°C)	T ₅ (°C)	T ₁₀ (°C)
PU 0.8	339.2	272.33	326.78
Comp. F Raw 2% 0.8	334.4	242.20	316.84
Comp. F 310 2% 0.8	332.3	264.30	321.96

In this case, the PU 0.8 presented the highest T_5 of all samples, likely due to the least number of rigid segments to be degraded at that temperature. The T_5 of the composites cannot be explained only by that, it also probably has influences of hemicelluloses degradable at lower temperatures, which is why the raw composite has a lower T_5 than the treated wood composite. The same arguments can explain the tendencies seen for the T_{10} .

5.8.6 Fir 2%, NCO/OH 1.0

Figure 83 represents the TGA and DTG curves of the samples of PU, fir composites of both Raw and treated wood at 2 % at the NCO/OH ratio of 1.0.

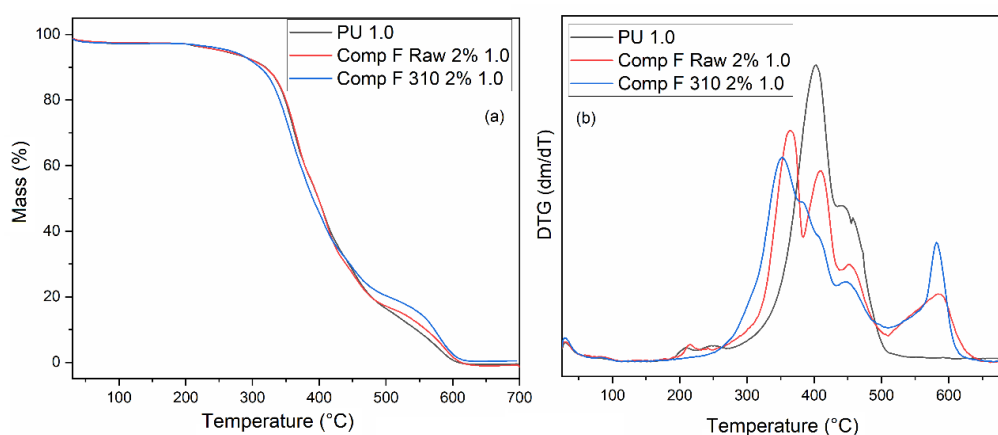


Figure 83. (a) TGA and (b) DTG curves of the samples of PU, fir composites of both Raw and treated wood at 2 % at the NCO/OH ratio of 1.0.

In this case, the PU 1.0 behavior of TGA curves is closely related to that of the Comp F Raw 2% 1.0 for most of the curve, with both presenting lower mass losses than the Comp F 310 2% 1.0 up to 400 °C. That happens likely because the exposed cellulose of the treated sample promoted the formation of more rigid segments, causing a bigger mass loss at lower temperatures, while the pure polymeric matrix that is the PU 1.0 sample and raw composites, in which the matrix is bonded to the weaker and amorphous hemicelluloses have bigger quantities of soft segments, whose degradation take place at higher temperatures.

As usual up to now, the curves behaviors change at 400 °C, with PU 1.0 having the highest mass loss, followed by Comp F Raw 2% 1.0, as its raw wood particles thermally degrade less at that temperature and the treated wood particles in the Comp F 310 2% 1.0 lose even less mass, as their more easily thermally degradable components have already been removed by the thermal

treatment itself. Also, the composites samples might present fewer soft segments to be degraded at those higher temperatures.

On Figure 84 we see a sharp increase in mass loss near 600 °C in the Comp F 310 2% 0.8, making its mass loss lower than that of Comp F Raw 2% 0.8, which was attributed to the generation of residues in the raw wood composite. The increased amount of NCO in the NCO/OH ratio of 1.0 might have promoted the formation of more PU in all samples, whose degradation made up for the formation of those residues.

The DTG curves for the treated wood composite has again presented the same two peaks at 350 °C and 400 °C seen in the DTG curves (Figure 83), indicating it can be actually small quantities of residues that got adsorbed into the porosity of the wood, but this time presenting what seem to be five peaks instead of the four peaks that have been seen so far in this work. Table 20 shows the T_{onset} , T_5 and T_{10} values obtained from the TGA curves (Figure 83a).

Table 20. Thermal properties of the fir samples at 2% and 1.0 NCO/OH ratio.

Sample	T_{onset} (°C)	T_5 (°C)	T_{10} (°C)
PU 1.0	332.3	254.62	326.57
Comp. F Raw 2% 1.0	334.3	257.00	319.25
Comp. F 310 2% 1.0	321.0	266.90	311.46

In Table 20, the T_5 of the raw composite was slightly higher than the PU 1.0, that can be caused because, despite the presence of degradable hemicelluloses to increase the mass loss in the composite, the wood mass itself can have pushed the T_5 a little bit higher. The absence of hemicelluloses caused by the intense thermal treatment of the wood left less degradable mass available at that temperature. As for the T_{10} , the addition of raw and specially treated wood has increased the quantity of rigid segments in the polymeric matrix, explaining the tendency seen in Table 20.

5.8.7 Fir 2%, NCO/OH 1.2

Figure 84 represents the TGA and DTG curves of the samples of PU, fir composites of both Raw and treated wood at 2 % at the NCO/OH ratio of 1.2.

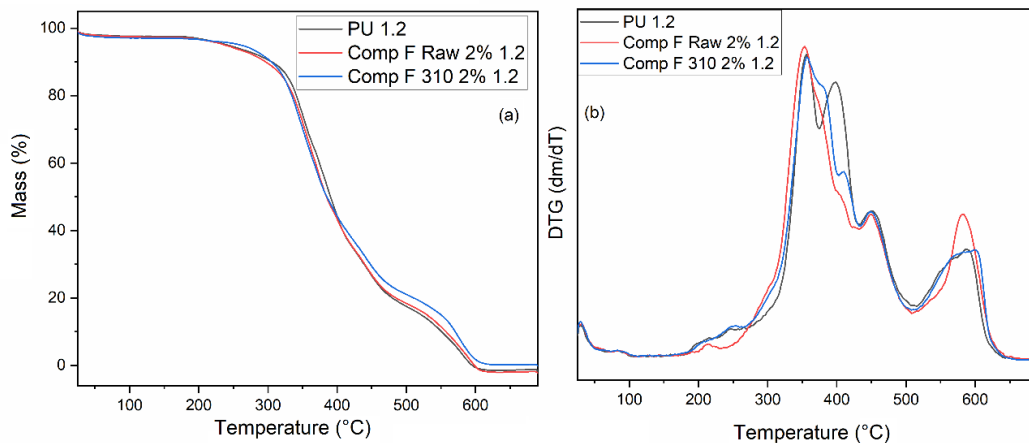


Figure 84.(a) TGA and (b) DTG curves of the samples of PU, fir composites of both Raw and treated wood at 2 % at the NCO/OH ratio of 1.2.

In the TGA and DTG curves of the NCO/OH ratio of 1.2 we can see that, before 400 °C turning point, the PU 1.2 is the sample that presents the least mass loss, while during the mass loss happening from 300 °C to 400 °C, the composite samples follow each other closely, something they did not do in the other fir samples seen up to now. This could be happening because the excessive isocyanate presents as a result of the NCO/OH ratio 1.2, together with the wood present on the composites could create enough rigid segments in the Comp F Raw 2% 1.2 to make it nearly equivalent to the total that is usually formed on the samples with treated samples, where the polymeric matrix bonding to the exposed cellulose usually created more rigid segments. Yet, the excessive isocyanate on the pure PU only creates higher density areas and lumps on the sample. Past the 400 °C, as usual, the mass loss tendencies are changing and the Comp F 310 2% 1.2 starts degrading at the lowest mass loss among the three samples, likely because of the presence of treated wood and not as many soft segments as the other samples.

The TGA and DTG curves of PU 1.2 and Comp F Raw 2% 1.2 follow a tendency seen in the Beech 2% 1.2 samples, with both curves being close. As explained in the proper section, that could be caused because the higher density PU formed by the NCO/OH ratio of 1.2 might make it less thermally sensible and make the TGA curve like that of the F raw composite, with raw wood, which are less thermally sensible than PU, to degrade. It is also interesting to notice that at 700 °C seem to generate more residue than the other samples.

As observed on the FTIR spectra (Figures 65 and 74) of the samples presented here, no big chemical difference should be expected, except for the Comp F 310 2% 1.2 sample.

The DTG curves of these samples have shown again five peaks decomposition for the treated wood composite, with two peaks real close, at about 350 °C 400 °C, previously assumed to be adsorbed thermal treatment residues, resulting in all the 2% treated fir composites to present DTG curves peaks, instead of the four peaks seen in the other composites in this work. Table 21 shows the T_{onset} , T_5 and T_{10} values obtained from the TGA curves (Figure 84a).

Table 21. Thermal properties of the fir samples at 2% and 1.2 NCO/OH ratio.

Sample	T_{onset} (°C)	T_5 (°C)	T_{10} (°C)
PU 1.2	332.7	249.60	313.82
Comp. F Raw 2% 1.2	329.4	244.73	303.89
Comp. F 310 2% 1.2	319.9	271.85	311.57

The presence of degradable hemicelluloses in the raw wood composite can be seen in the lower T_5 presented by this sample when compared to the treated wood polymer, and the effect can be seen, though at a smaller scale, in those samples' T_{10} .

One effect that can be seen in most the TGA curves presented so far is that the PU samples show lower mass losses up to about 400 °C to 450 °C, at which point its mass loss increases, leaving the raw and more pronouncedly the treated composite presenting lower mass loss. That can have happened probably because before those temperatures, the polymeric matrix and wood fractions that are degradable at lower temperatures (mostly on raw wood composites) are being degraded concurrently, but past this point, only the hardly degradable fractions of wood, such as lignin and other residues, remain in the composites, decreasing the overall mass loss in the TGA curves. Since the PU samples do not have any wood in their composition, they end up presenting the highest mass loss as higher temperatures.

5.8.9 Beech 5%, NCO/OH 0.8

Figure 85 presents the TGA and DTG curves of the samples of PU and beech composites of both Raw and treated wood at 5% at the NCO/OH ratio of 0.8

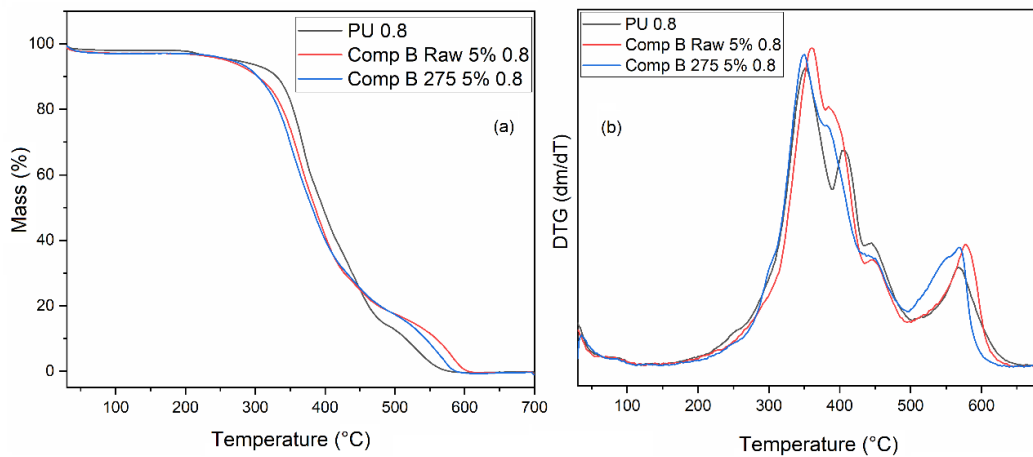


Figure 85. (a) TGA and (b) DTG curves of the samples of PU, beech composites of both Raw and treated wood at 5% at the NCO/OH ratio of 0.8.

The bigger quantity of wood sawdust added into the mix to prepare the composites has led to a bigger separation between the TGA curves of the composites and the PU, which now shows a much lower mass loss than seen in the other samples in which it had the lowest mass loss. Also, the composite samples showed similar behavior, the Comp B275 5% 0.8 showing slightly higher mass loss. This time, the point in which the mass loss tendency is reversed is at about 450 °C, instead of the 400 °C seen in all of the samples with 2% of wood, likely because of the increased amount of wood, both raw and treated, promoted a bigger formation urethane bonds and rigid segments, leading to an increased mass loss at lower temperatures up to the point where the wood itself begins to degrade, which is the point where the composites mass loss become lower than that of the PU 0.8.

Figure 85a shows the first TGA curve in which the raw wood composite mass loss is lower than that of the treated wood. That is likely caused because the higher quantity of wood has led to a bigger generation of hemicelluloses' degradations residues that stay adsorbed in the wood's structure. As these residues had already have been previously removed in the thermal treatment the sample underwent.

The DTG curves of samples were all similar, with both composites showing peaks similar to those 350 °C and 400 °C seen in the fir composites DTG curves, which in this case could be caused by the hardwood's hemicelluloses being degraded at lower temperatures. Another evidence that is due to a different degradation mechanism from what happened with the fir samples, those 5%

beech samples present only four degradation peaks, instead of the 5 peaks present 2% treated fir composites. Table 22 presents the T_{onset} , T_5 and T_{10} values obtained from the TGA curves (Figure 85a).

Table 22. Thermal properties of the beech samples at 5% and 0.8 NCO/OH ratio.

Sample	T_o (°C)	T_5 (°C)	T_{10} (°C)
PU 0.8	339.2	272.33	326.78
Comp. B Raw 5% 0.8	326.1	259.56	304.08
Comp. B 275 5% 0.8	316.9	266.84	304.27

The increased quantity of wood had a clear impact on the mass loss of the composites, which are now visibly higher than that of the PU 0.8 sample. For the composites, the T_5 was lower with the raw wood, likely due to the presence of hemicelluloses. The treated composite had a lower T_5 than the PU 0.8 likely because of a higher quantity of hard segments caused by the reaction with the treated wood. While both effects contribute to higher mass losses, we can see in the figure 86 that despite the slightly higher T_{10} of the treated wood composite, it can be seen that in most of the TGA curves the treated wood composite presents a slightly higher mass loss, by the reasons already discussed.

5.8.10 Beech 5%, NCO/OH 1.0

Figure 86 shows the TGA and DTG curves of the samples of PU and beech composites of both Raw and treated wood at 5% at the NCO/OH ratio of 1.0

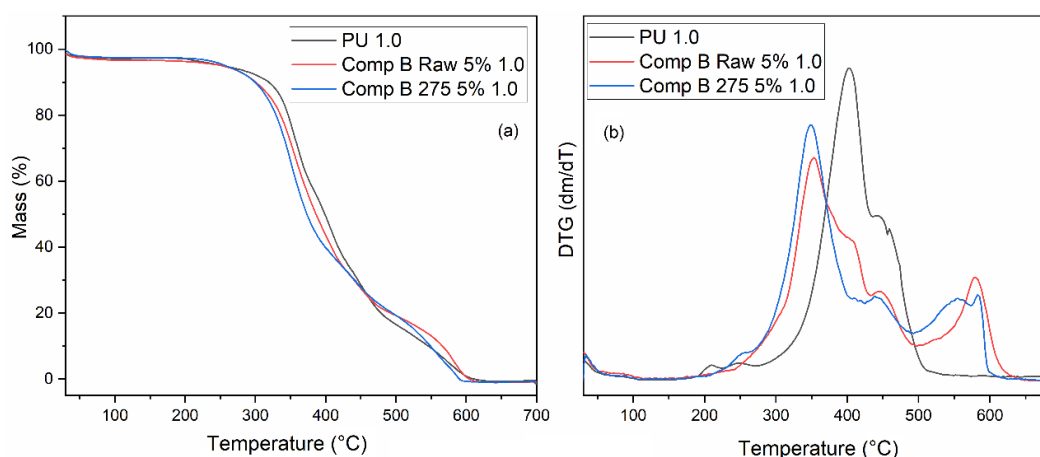


Figure 86. (a) TGA and (b) DTG (b) curves of the samples of PU, beech composites of both Raw and treated wood at 5% at the NCO/OH ratio of 1.0.

As was the case with previous samples, the higher quantity of wood has increased the separation between the PU and the composites' TGA curves, again

with the PU having the lowest mass loss until about the previously mentioned inversion point of about 450 °C, when it starts having the highest mass loss of the three samples in the plot. Again, the treated wood composite was showing the highest mass losses, with the raw wood composite between the two other samples until the inversion point. That likely happens for the reasons mentioned above.

The DTG curves, while similar to those in the previous figure 86, didn't show a small peak at 400 °C, presenting instead, one 4th peak at around 600 °C that has not been seen in other samples. Apart from that, the samples behaved as expected from the already analyzed results. Table 23 lists the T_{onset} , T_5 and T_{10} values obtained from the TGA curves (Figure 86a).

Table 23. Thermal properties of the beech samples at 5% and 1.0 NCO/OH ratio.

Sample	T_o (°C)	T_5 (°C)	T_{10} (°C)
PU 1.0	332.3	254.62	326.57
Comp. B Raw 5% 1.0	322.1	254.37	301.56
Comp. B 275 5% 1.0	317.6	259.47	301.64

The T_5 and T_{10} values followed the same tendencies observed in the previously analyzed samples in Table 23 and the values can be explained using the same line of thought.

5.8.11 Beech 5%, NCO/OH 1.2

Figure 87 presents the TGA and DTG curves of the samples of PU and beech composites of both Raw and treated wood at 5% at the NCO/OH ratio of 1.2.

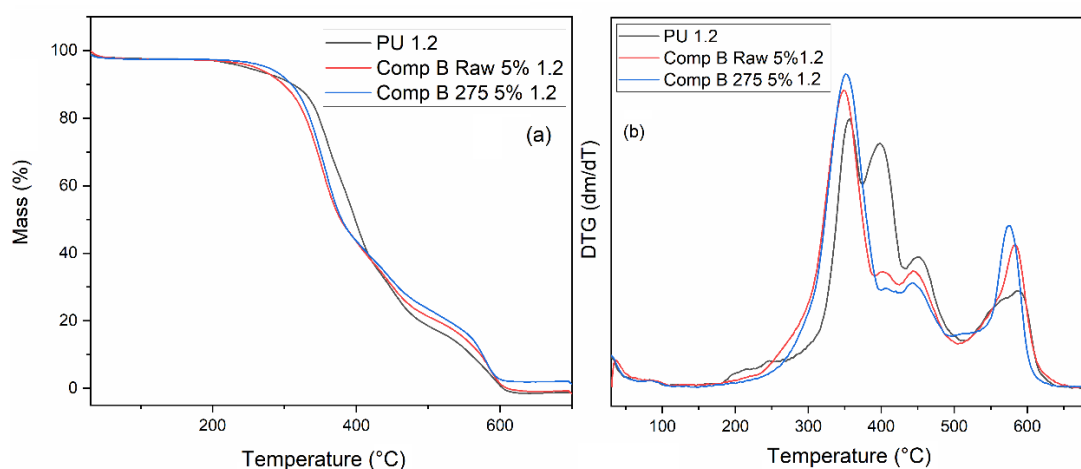


Figure 87. (a) TGA and (b) DTG curves of the samples of PU, beech composites of both Raw and treated wood at 5% at the NCO/OH ratio of 1.2.

The raw wood composite showed slightly higher mass losses than the treated wood composite, with both having higher mass losses than the PU which might be caused by the presence of harder segments in the composites, as well as more mass available to be degraded at lower temperatures on them. This time, the inversion point happened at about 450 °C, a little higher than for the other samples and, past this point, the PU presented the higher mass loss among the tree samples.

The DTG curves again didn't show the small pair of peaks seen in the equivalent 0.8 treated wood composite, but also didn't present the 4th degradation peak at 600 °C, as it was seen in the equivalent 1.0 treated wood composite. This results in only three actual degradation peaks for this sample, not considering the tiny peak at about 400 °C. Table 24 shows the T_{onset} , T_5 and T_{10} values obtained from the TGA curves (Figure 87a).

Table 24. Thermal properties of the beech samples at 5% and 1.2 NCO/OH ratio.

Sample	T_o (°C)	T_5 (°C)	T_{10} (°C)
PU 1.2	332.7	249.60	313.82
Comp. B Raw 5% 1.2	317.3	261.97	299.20
Comp. B 275 5% 1.2	317.7	269.33	309.22

In most previous TGA curves we've shown so far, the degradation behavior of all three samples is nearly the same up to about 300 °C after which the composites start degrading and the PU goes some more degrees without any major degradation, in the case of the 5% composites, that is. In the case of these samples, we can see the curves separate early in the TGA curves, that is reflected in the data shown in Table 24, where the difference in temperatures is higher than the ones we have seen so far. In this case, the treated wood composite shows higher temperatures than the raw wood composite in all the measured parameters, indicating it is an overall more thermally stable sample, thought by the TGA curves it generates more residues than the other samples, which is not environmentally desirable.

Overall, except for samples in the NCO/OH ratio 0.8, despite the 5% TGA curves not showing much difference from the 2% TGA curves, the DTG curves were noticeably different, with the composites showing short intermediate peaks while the PU shows big intermediate peaks. That can indicate that the 5% amount of wood resulted in less segments with intermediate softness and hardness,

probably because the bigger availability of hardwood hydroxyl favored the formation of soft segments.

5.8.12 Fir 5%, NCO/OH 0.8

Figure 88 represents the TGA and DTG curves of the samples of PU and fir composites of both Raw and treated wood at 5% at the NCO/OH ratio of 0.8

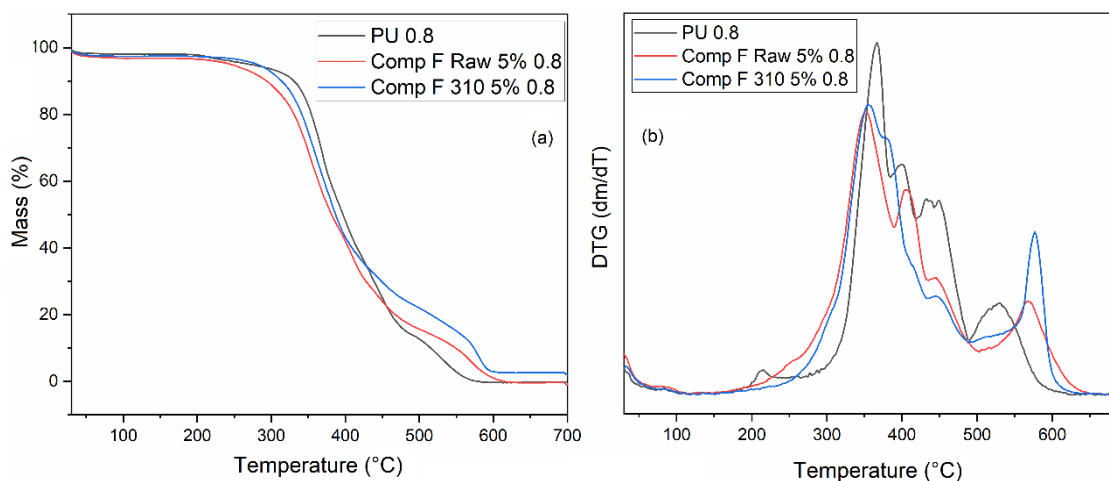


Figure 88.(a) TGA and (b) DTG curves of the samples of PU, fir composites of both Raw and treated wood at 5% at the NCO/OH ratio of 0.8.

The 5% fir samples also show the same curve separation seen in the 5% beech samples, but with the raw wood composite having higher mass losses than the treated composite in the whole TGA curves. As softwood hemicelluloses are more temperature resistant, the presence of hemicelluloses alone cannot explain this behavior, so it can be inferred that the presence of hemicelluloses not only helps increase the mass loss at lower temperatures, but also leads to the formation of more rigid segments. These rigid segments are also present in the treated wood composite, but since it no longer has hemicelluloses to be degraded at that temperature, its resulting mass loss is lower. This sample also has an inversion point at nearly 400 °C where the PU mass loss becomes the highest.

One more difference compared to the 5% beech samples is that the peaks of DTG curves are more like those of the PU, at least as far as the 0.8 NCO/OH ratios go. The Treated wood composite presented the small pair of DTG curves peaks at around 350 °C and 400 °C also seen in the 2% fir samples and the 5% treated beech at 0.8 ratio, which has been attributed to small quantities of thermal degradation residues getting adsorbed into the porous structure of the treated

wood before the progress of the TGA eliminates it. Table 25 shows the T_{onset} , T_5 and T_{10} values obtained from the TGA curves (Figure 88a).

Table 25. Thermal properties of the fir samples at 5% and 0.8 NCO/OH ratio.

Sample	T_{onset} (°C)	T_5 (°C)	T_{10} (°C)
PU 0.8	339.2	272.33	326.78
Comp. F Raw 5% 0.8	322.3	247.08	294.05
Comp. F 310 5% 0.8	319.1	281.83	314.29

The TGA curves separation makes itself notice in this table too. The combination of hemicelluloses and rigid segments present in the raw wood composite causes it to have higher T_5 and T_{10} than the treated wood composite, which has no hemicelluloses. DTG curves (Figure 88b) show that the softwood and its hemicelluloses favor the formation of segments of intermediate rigidities, as it is more like the DTG curve of the PU than the 5% beech DTG curves were, presenting more noticeable intermediate peaks at least with regard to the NCO/OH ratio 0.8.

5.8.13 Fir 5%, NCO/OH 1.0

Figure 89 presents the TGA and DTG curves of the samples of PU and fir composites of both Raw and treated wood at 5% at the NCO/OH ratio of 1.0.

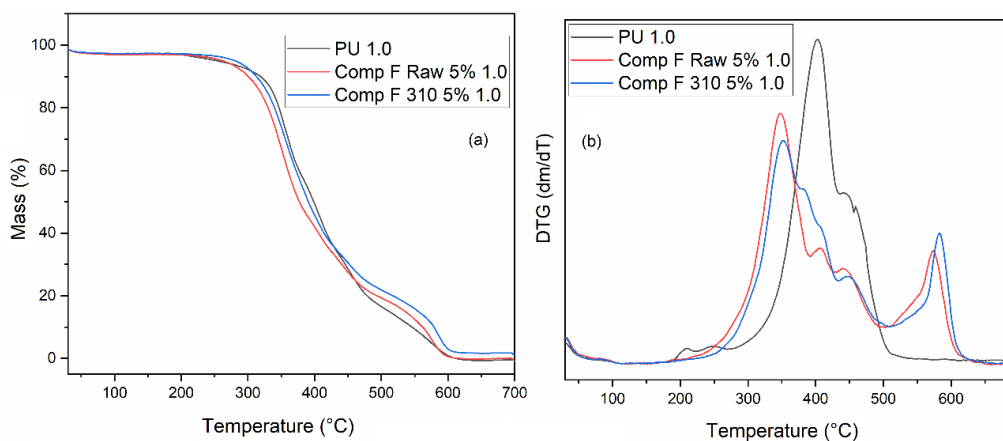


Figure 89. (a) TGA and (b) DTG curves of the samples of PU, fir composites of both Raw and treated wood at 5% at the NCO/OH ratio of 1.0.

The TGA curves of the samples in the Figure 89a follow the same tendencies seen in the previous figure, and it can be interpreted in the same way, including the inversion point at about 450 °C. Different from the equivalent 0.8 samples, though, the DTG curves are again noticeably different from the PU DTG curve, as seen with the 5% beech composites except by the NCO/OH ratio 0.8,

showing that the increased quantity of wood, be it hard or soft wood, disfavors the formation of intermediate rigidity segments. This can be seen by the small intermediate peaks in the DTG curves, which also showed the already mentioned pair of peaks at 350 °C and 400 °C that have already been explained. Table 26 presents the T_{onset} , T_5 and T_{10} values obtained from the TGA curves (Figure 89a).

Table 26. Thermal properties of the fir samples at 5% and 1.0 NCO/OH ratio.

Sample	T_{onset} (°C)	T_5 (°C)	T_{10} (°C)
PU 1.0	332.3	254.62	326.57
Comp. F Raw 5% 1.0	315.0	264.39	301.74
Comp. F 310 5% 1.0	319.1	281.83	314.32

Table 26 shows this time a considerable difference in the T_5 between the raw and the treated composites, with a difference of 17.44 °C, with a difference of 12.51 °C in the T_{10} , though the PU 1.0 had still the highest T_{10} .

5.8.14 Fir 5%, NCO/OH 1.2

Figure 90 represents the TGA and DTG curves of the samples of PU and fir composites of both Raw and treated wood at 5% at the NCO/OH ratio of 1.2.

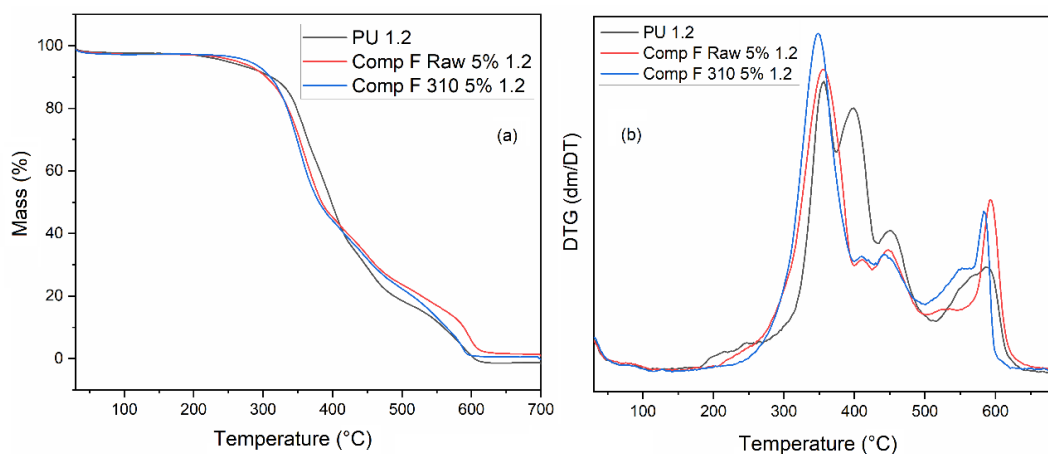


Figure 90. (a) TGA and (b) DTG curves of the samples of PU, fir composites of both Raw and treated wood at 5% at the NCO/OH ratio of 1.2.

In TGA and DTG curves (Figure 90) can be seen that, different from what happened to the other 5% fir composites, the raw composite now presents slightly lower mass loss than the treated composite, but still closely following its behavior up to the inversion point at 400 °C, when it, while still have lower mass loss, doesn't follow the treated composite behavior closely anymore. This could be caused by the excessive quantity of this NCO/OH ratio has created a bigger quantity of rigid segments on the treated composite to the point that it

compensates for the raw wood composite mass loss due to hemicelluloses degradation. As with the sample Comp B Raw 5% 0.8, the lower mass loss in the raw composite at higher temperatures are likely residues of hemicelluloses degradation that good adsorbed into the wood structure and could not have been removed in the studied temperature.

Again, it can be seen the addition of wood disfavoring the formation of intermediate rigidity segments, with the intermediate DTG peaks being much smaller than the rigid and soft segment peaks. Table 26 shows the T_{onset} , T_5 and T_{10} values obtained from the TGA curves (Figure 90a).

Table 27. Thermal properties of the fir samples at 5% and 1.2 NCO/OH ratio.

Sample	T_{onset} (°C)	T_5 (°C)	T_{10} (°C)
PU 1.2	332.7	249.60	313.82
Comp. F Raw 5% 1.2	319.9	264.36	306.73
Comp. F 310 5% 1.2	317.1	281.93	312.07

The values presented in Table 27 confirm that this time the treated composite presents higher mass losses compared to the raw composite, which is likely happening by the reasons already explained above.

5.8.15 CV 2%, NCO/OH 0.8

Due to time and location constraints, the treated CV composites samples had their TGA done in Brazil, at UnB, in a considerably different and more aged equipment than the rest of the samples, which were done in France. The difference of equipment has noticeable impacts in the sample's TGA and DTG curves, resulting in PU TGA and DTG curves that were quite different from the ones obtained in France. The PU TGA and DTG curves are, thus, omitted in the CV section to avoid confusion.

Figure 91 represents the TGA and DTG curves of the samples CV composites of both Raw and treated wood at 2% at the NCO/OH ratio of 0.8.

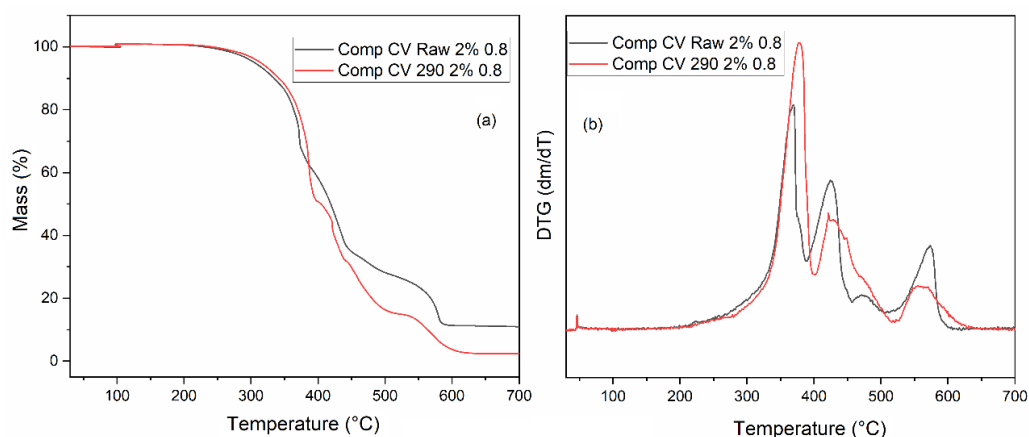


Figure 91. (a) TGA and (b) DTG (b) curves of the samples CV composites with both Raw and treated wood at 2% at the NCO/OH ratio of 0.8.

One thing that can be easily noticed in the TGA curves (Figure 91a) is the more irregular nature of the curves, including a regression in the TGA curves at around 100 °C. This will, unfortunately, also be seen in the next TGA curves.

As seen in the previous TGA curves, an inversion of behavior happens at about 400 °C, with the treated wood composite presenting higher mass loss values past this point. Also, similarly to the previous TGA results, the raw wood composite has a lower mass loss before 400 °C, likely related to the less thermally stable components of the CV having already been degraded by the thermal treatment itself. It can also be noticed that a higher formation of residue in the raw wood composite, in relatively higher quantities when compared to the other samples, is likely caused by the residues in the treated wood having been carried away by the N₂ in the treatment itself, while the residues of the raw wood decomposition remained in the polymeric matrix.

Regarding the DTG curves, they are both close in behavior, but the treated wood composite presented a higher first peak, caused by the sudden increase in thermal degradation at 400 °C, as well as a smaller final peak, possibly related to the lower formation of residues in this sample. It can also be seen a better separation between the 2nd and 3rd degradation peaks in the raw wood, indicating that the treated wood might present a higher structural regularity, which might have been caused by its polymeric matrix bonding to the cellulose, a regular polymer, rather than to hemicellulose, an irregular polymer. Table 28 lists the T_{onset}, T₅ and T₁₀ values obtained from the TGA curves (Figure 91a).

Table 28. Thermal properties of the CV samples at 2% and 0.8 NCO/OH ratio.

Sample	T _{onset} (°C)	T ₅ (°C)	T ₁₀ (°C)
Comp. CV Raw 2% 0.8	343.79	305.11	334.53
Comp. CV 290 2% 0.8	325.49	314.28	341.82

The CV composites presented a T_{onset} close to that of the other composites at the same NCO/OH ratio, but higher T₅ and T₁₀. It has previously explained, CV is more thermally stable than the other woods studied, as it is some wood from the Cerrado, needing more protection against higher temperatures and fire than the European woods, causing its composites to lose less mass at lower temperatures.

5.8.16 CV 2%, NCO/OH 1.0

Figure 92 represents the TGA and DTG curves of the samples CV composites of both Raw and treated wood at 2% at the NCO/OH ratio of 1.0.

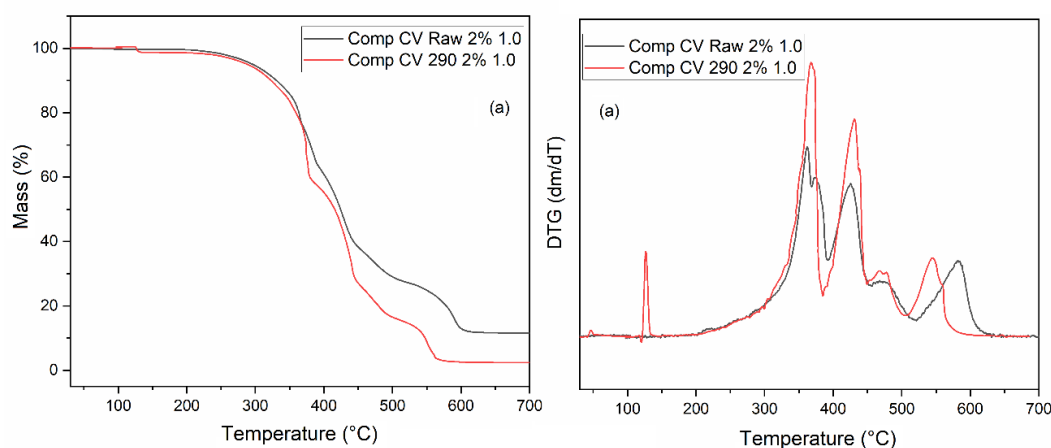


Figure 92. (a) TGA and (b) DTG curves of the samples CV composites with both Raw and treated wood at 2% at the NCO/OH ratio of 1.0.

The TGA and DTG curves (Figure 92) show a close behavior to what was seen in Figure 91, but since the treated wood composite presents a slightly lower mass loss at the first part of the TGA curves, the mass loss inversion did not show up at 400 °C, but the rapidly increasing mass loss near that temperature can still be seen, as well as the higher quantity of residue present in the raw wood composite. The lack of this inversion point might be explained by the increased number of rigid segments present in the polymeric matrix.

A bigger separation of the 2nd and 3rd peak of the treated wood DTG curve is seen this time, as well as the 1st peak in the raw wood DTG curve showing a small bipartition, indicating that a new thermodegradation stage is close to

appearing. Table 28 shows the T_{onset} , T_5 and T_{10} values obtained from the TGA curves (Figure 92a).

Table 29. Thermal properties of the CV samples at 2% and 1.0 NCO/OH ratio.

Sample	T_{onset} (°C)	T_5 (°C)	T_{10} (°C)
Comp. CV Raw 2% 1.0	336.52	269.43	331.12
Comp. CV 290 2% 1.0	343.94	288.69	323.07

The lower T_{onset} , T_5 and T_{10} presented by these samples may be related to the increasing amount of NCO resulting in a higher quantity of rigid segments, leading to more degradation at lower temperatures.

5.8.17 CV 2%, NCO/OH 1.2

Figure 93 represents the TGA and DTG curves of the samples CV composites of both Raw and treated wood at 2% at the NCO/OH ratio of 1.2.

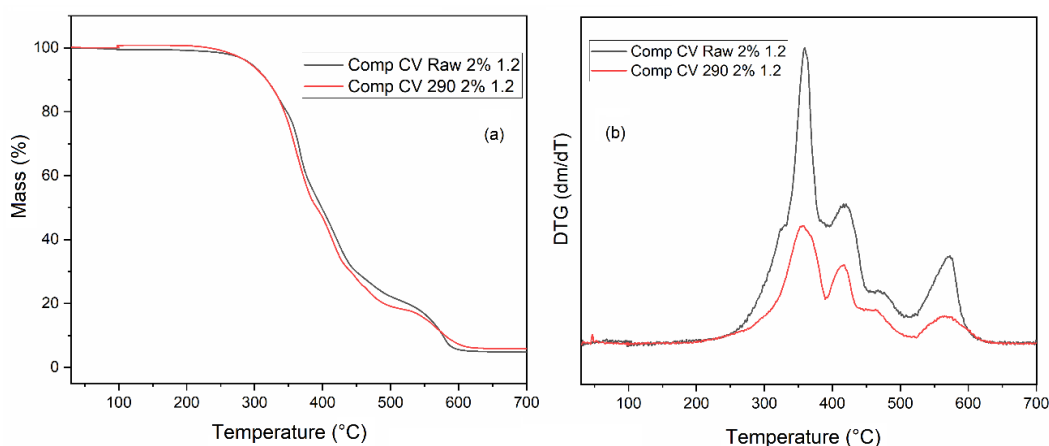


Figure 93. (a) TGA and (b) DTG curves of the samples CV composites with both Raw and treated wood at 2% at the NCO/OH ratio of 1.2.

In TGA and DTG curves (Figure 93), there is no longer a bipartition of the 1st and 2nd peaks of the DTG curve for the raw wood. Instead, a prominent 2nd peak can be seen, with the 1st peak appearing to be just a shoulder on the other peak. Also, the residue formation seen in the other CV composites up to now are not seen. It is likely that the products of the raw CV with NCO are more volatile and do not get stuck inside the polymeric matrix as much as the thermal degradation residues of the wood itself.

Other than the differences pointed in the previous paragraph, the thermal degradation behavior of both composites does not show other major changes.

The values of T_{onset} , T_5 , and T_{10} obtained from the TGA curves (Figure 93a) are shown in Table 30.

Table 30. Thermal properties of the CV samples at 2% and 1.2 NCO/OH ratio.

Sample	T_{onset} (°C)	T_5 (°C)	T_{10} (°C)
Comp. CV Raw 2% 1.2	329.08	299.53	322.64
Comp. CV 290 2% 1.2	318.92	293.85	317.75

These samples follow the tendency of the raw composite T_5 being lower than the T_5 fir the treated wood composites, probably for the reasons already discussed. A difference in behavior, though, is that, just like in the previous samples, the T_{10} is higher for the raw composite. While in the 1.0 composites it could be explained by the clear amount of residue produced by the degradation of hemicelluloses in raw wood, the hemicellulose PU might still produce residues that result in a higher T_{10} , but that are volatile enough to be dragged away by the TGA gas, resulting in much less residue formation.

5.8.18 CV 5%, NCO/OH 0.8

Figure 93 represents the TGA and DTG curves of the samples CV composites of both Raw and treated wood at 5% at the NCO/OH ratio of 0.8.

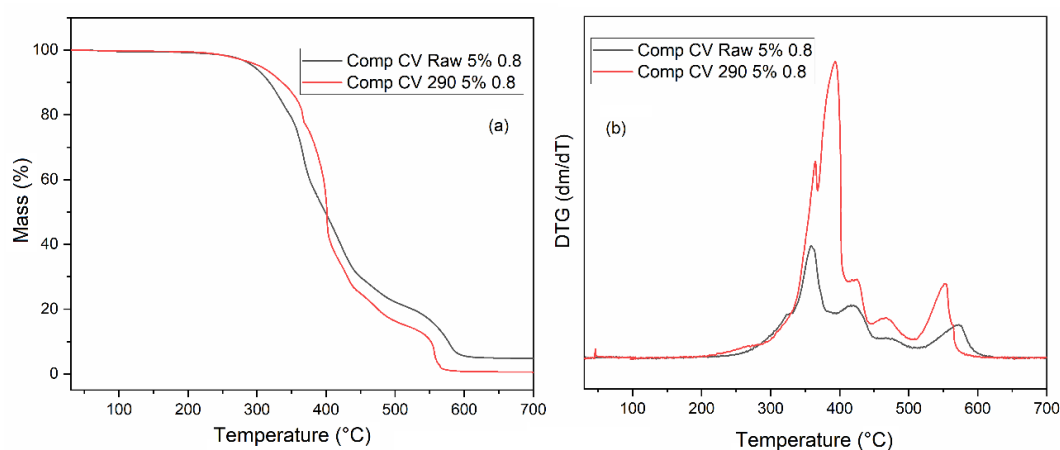


Figure 94. (a) TGA and (b) DTG curves of the samples CV composites with both Raw and treated wood at 5% at the NCO/OH ratio of 0.8.

This time, the treated wood composite showed a principle of more degradation step, even though it is a minor one. The increased amount of wood in the composites also increased the separation between the raw and treated wood composite, while still retaining the inversion point at around 400 °C already seems in many samples and the bigger generation of residue by the raw wood.

The values of T_{onset} , T_5 , and T_{10} obtained from the TGA curves (Figure 94a) are shown in Table 31.

Table 31. Thermal properties of the CV samples at 5% and 0.8 NCO/OH ratio.

Sample	T_{onset} (°C)	T_5 (°C)	T_{10} (°C)
Comp. CV Raw 5% 0.8	343.22	294.851	318.36
Comp. CV 290 5% 0.8	337.64	304.92	336.51

This table shows again the same tendency of the treated wood having higher T_5 and T_{10} , with both values being lower than the equivalent 2% composite, indicating that the contribution of the polymeric matrix for the overall thermal properties of the composite.

5.8.19 CV 5%, NCO/OH 1.0

Figure 95 shows the TGA and DTG curves of the samples CV composites of both Raw and treated wood at 5% at the NCO/OH ratio of 1.0.

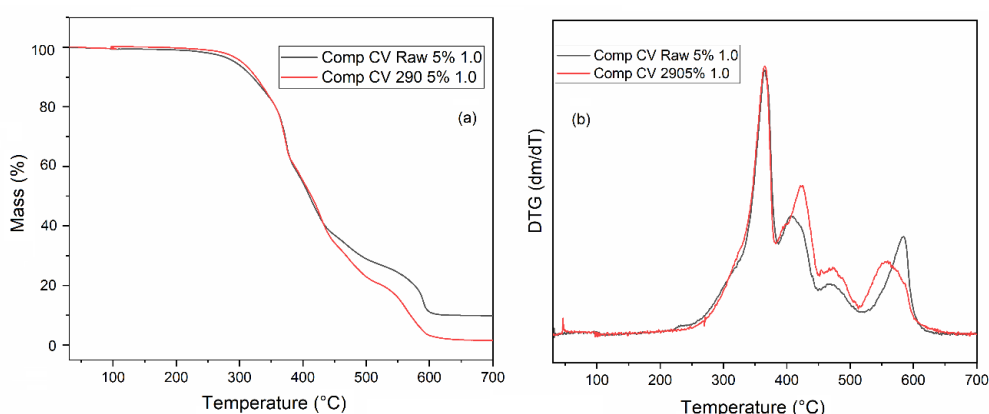


Figure 95. (a) TGA and (b) DTG curves of the samples CV composites with both Raw and treated wood at 5% at the NCO/OH ratio of 1.0.

The TGA curve of the CV 5% NCO/OH composites do not show much difference from the other composites, except for the absence of a clear inversion point at 400 ° C, with both TGA curve having quite similar behaviors, which can even be seen in their DTG curve. Again, the raw wood composite showing a bigger generation of thermal degradation degree. The values of T_{onset} , T_5 , and T_{10} obtained from the TGA curves (Figure 95a) are presented in Table 32.

Table 32. Thermal properties of the CV samples at 5% and 1.0 NCO/OH ratio.

Sample	T_{onset} (°C)	T_5 (°C)	T_{10} (°C)
Comp. CV Raw 5% 1.0	328.22	293.79	321.14
Comp. CV 290 5% 1.0	332.12	304.73	326.38

The CV 5% 1.0 composites show no difference from the tendencies seen so far, with both T_5 and T_{10} being lower for the raw wood composite.

5.8.20 CV 5%, NCO/OH 1.2

Figure 96 represents the TGA and DTG curves of the samples CV composites of both Raw and treated wood at 5% at the NCO/OH ratio of 1.2.

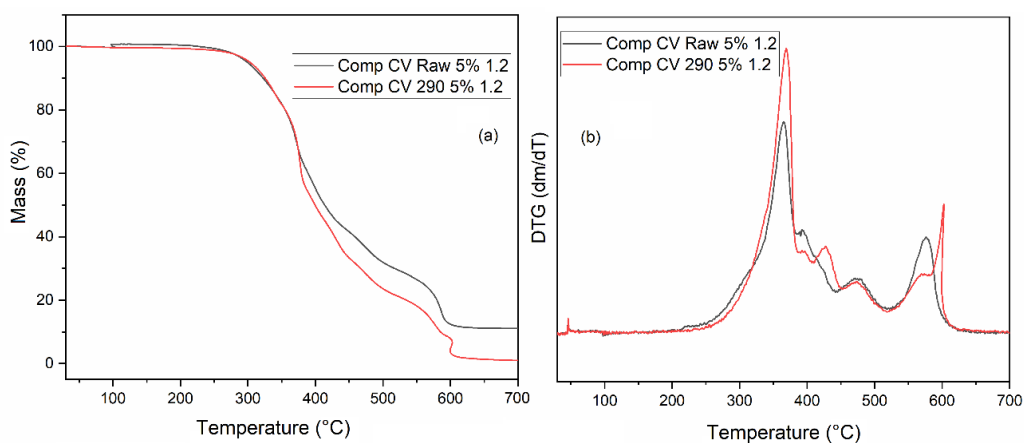


Figure 96. (a) TGA and (b) DTG curves of the samples CV composites with both Raw and treated wood at 5% at the NCO/OH ratio of 1.2.

Rather than what was seen in TGA curves of the equivalent 2% composites, the nigger formation of residue was observed in now. That is possibly do the increased amount of wood in the sample. Other than that, the TGA curves of both samples are quite similar, showing mostly a difference in the second and final peaks. Other than this, no bigger differences have been observed from the other TGA and DTG curves. The values of T_{onset} , T_5 , and T_{10} obtained from the TGA curves (Figure 96a) are presented in Table 33.

Table 33. Thermal properties of the CV samples at 5% and 1.2 NCO/OH ratio.

Sample	T_{onset} (°C)	T_5 (°C)	T_{10} (°C)
Comp. CV Raw 5% 1.2	326.06	299.53	232.64
Comp. CV 290 5% 1.2	319.96	303.39	326.11

The properties listed on Table 33 also show good correlation with the previously seen T_5 and T_{10} , with T_5 for the raw wood being lower.

Overall, it could be noticed that:

- for beech, the increase in the wood quantity increased the raw wood composite T_5 but increased both T_5 and T_{10} for the treated wood and that increase

of the NCO/OH ratio presents a small increase in the raw wood T_5 , even though no tendency was found for T_{10} ;

- for fir, the increase in NCO/OH ratio increased the T_5 for the treated wood composites at 2%, having neglectable affects at 5%. Also, the T_5 for raw wood increased to 5% wood content;

- for CV, no tendency was easily noticed.

5.9 Dynamic mechanical analysis (DMA)

Dynamic mechanical analysis (DMA) tests were performed using a Q800 DMA Instrument manufactured by TA Instruments in New Castle, DE, USA. The experiments utilized a three-point bend fixture. Samples labeled as PU 0.8, PU 1.0, and PU 1.2 were prepared by cutting specimens with dimensions approximately 5.0 mm × 9.0 mm × 5.0 mm (length × width × thickness). Each specimen was initially cooled down to 0 °C, then heated to 150 °C at a heating rate of 3 °C·min⁻¹ under an iso-strain mode, 1 Hz and 14 μm of frequency and amplitude were employed, respectively. Two replicates of each sample were cut out. Each replicate was tested individually, and the results represent the average of the trials.

DMA is a technique used for studying a material's behavior under various conditions such as stress, temperature, frequency, and other parameters. It encompasses both the analysis of the material's response, and the instrument used to conduct the tests. It is a popular method for analyzing viscoelastic properties of flexible PU foams. (119). Additionally, DMA is alternatively referred to as Dynamic Mechanical Thermal Analysis (DMTA). DMA quantifies both stiffness and damping characteristics, typically reported as storage modulus (modulus) and loss tangent (tan delta), respectively.

The results presented in Figure 97 and 98, and in Table 34 represent storage modulus (E) at 25 °C and 100 °C, it also shows the glass transition temperature T_{g1} and T_{g2} which shows that the polyurethane is a condensation polymer which contains two molecules that come together and react with one another. From Table 34 the storage modulus shows not much of a change at room temperature and at 100 °C therefore, no matter the ratio of the of this polymer PU 0.8, PU 1.0, and PU 1.2 they are all comparable. T_{g1} in Table 34 indicates the

lower temperature which is the soft segment of the polymer while T_{g2} shows the higher temperature which is the hard segment of the polymer. PU 1.2 exhibits the maximum degree of flexibility within its soft segment while PU 1.0 has the strongest stiffness with the highest T_{g2} . Generally, the transition temperatures of PU 0.8 are seen to be lower than those of the other two samples.

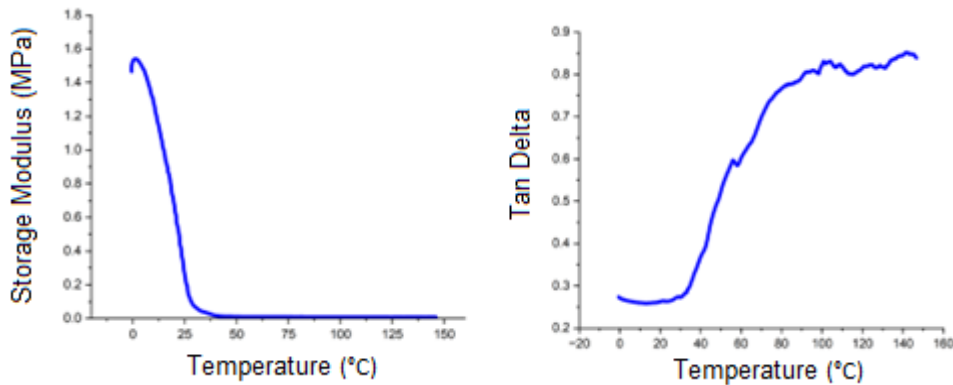


Figure 97. Storage modulus and $\tan \delta$ plotted as a function of temperature.

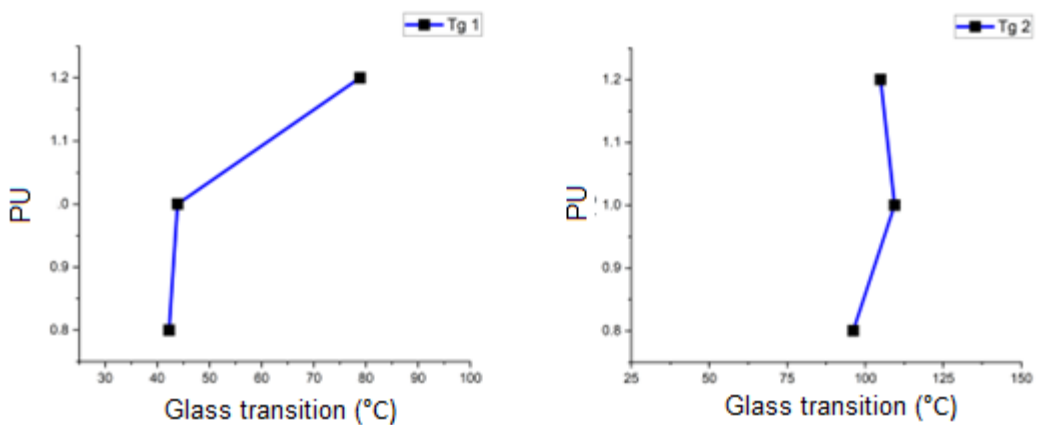


Figure 98. Diagram showing the T_{g1} and T_{g2} .

Table 34. DMA results of PU samples.

Sample	E at 25 °C (MPa)	E at 100 °C (MPa)	Tan δ T_{g1} (°C)	Tan δ T_{g2} (°C)
PU 0.8	0.30±0.06	0.012±0.003	42.25±22.13	96.15±3.04
PU 1.0	0.36±0.08	0.030±0.010	43.90±5.23	109.45±26.09
PU 1.2	0.39±0.03	0.024±0.012	78.85±8.27	104.90±8.77

5.10 Dynamic vapor sorption (DVS)

DVS analyses were performed to measure the sample's interaction with water. Unfortunately, a failure in the equipment made it not possible to run the analyses in all the samples, so the composites with treated beech and fir at 5%,

all the CV composites and the woods themselves were not analyzed by this technique and will be left to be analyzed in future works.

5.10.1 PU

Figure 99 shows the DVS curves of the PU samples.

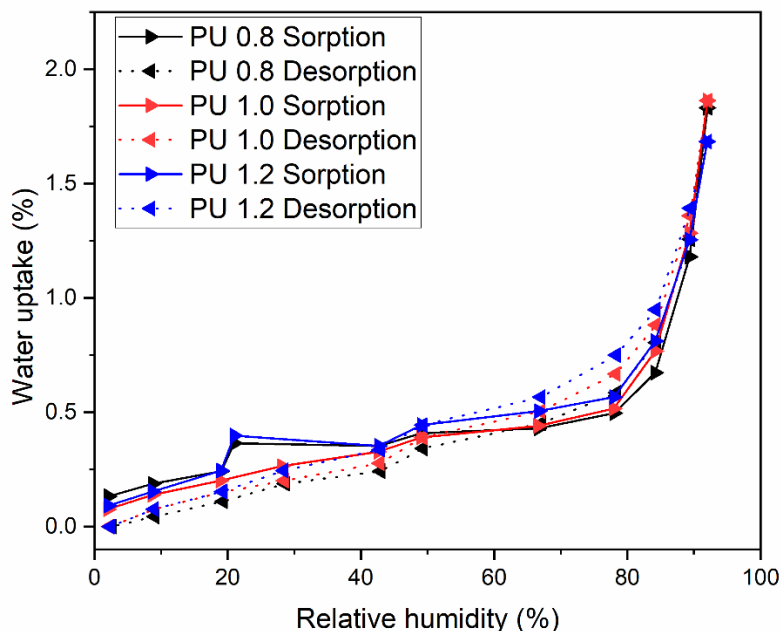


Figure 99. DVS curves of the PU samples.

DVS curves (Figure 99) show that all the PU samples have little hygroscopicity, with the maximum water uptake being only at 1.83%, 1.86% and 1.68% for the PU 0.8, PU 1.0 and PU 1.2 respectively. The low hygroscopicity was already expected as it is a hydrophobic material.

The shape of the DVS curve is characteristic for materials who have weaker interactions with water than the water interacts with itself, and the hysteresis seen in all the three curves indicates the presence of mesopores (pore size between 2 nm and 50 nm) in which the capillary condensation of water can occur (120). The types of DVS curves are shown in Figure 100.

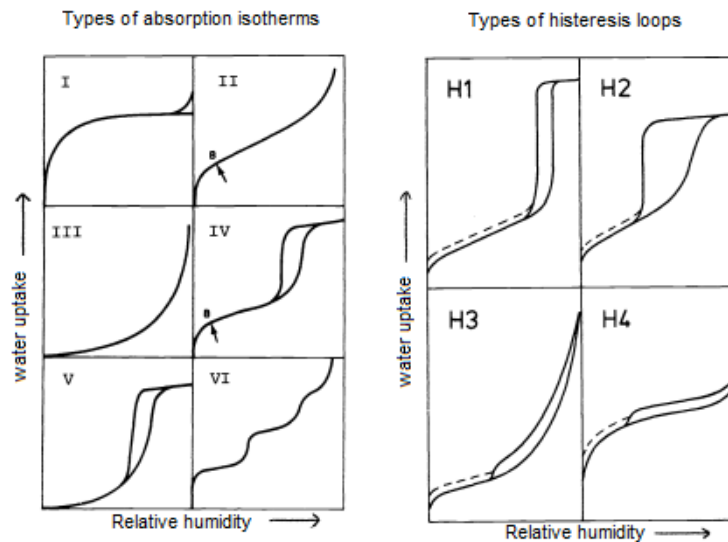


Figure 100. Types of absorption isotherms and hysteresis loops (120). Adapted figure.

Comparing the PU DVS curves with the curves from the literature, it may appear that they are similar to the type III curve, with an H3 hysteresis loop, characteristic of samples with slit-like pores. The dashed lines in the hysteresis loops are seen when the sample presents micropores, indicating their presence in the PU samples.

It is also interesting to notice that of the three PU samples, only the PU 1.0 sample did not present a sudden increase in water uptake at around 21% relative humidity in the sorption phase.

While we know from other DVS experiments performed in the laboratory that heat-treated wood is a hydrophobic material and that the hygroscopicity of a material decreases as the temperature of light pyrolysis treatment increases, for example, from 190 °C to 225 °C (121,122). It has also been seen that higher treatment temperatures might in fact increase the wood's hygroscopicity by increasing its porosity and allowing for capillary condensation within the product (123), to the point that charcoal is considered a hygroscopic material due to its adsorbent nature caused by its high porosity (124).

5.10.2 Beech 2% 0.8

Figure 101 shows the DVS curves of the PU 0.8 and the beech composite samples at 2% and 0.8 NCO/OH ratio.

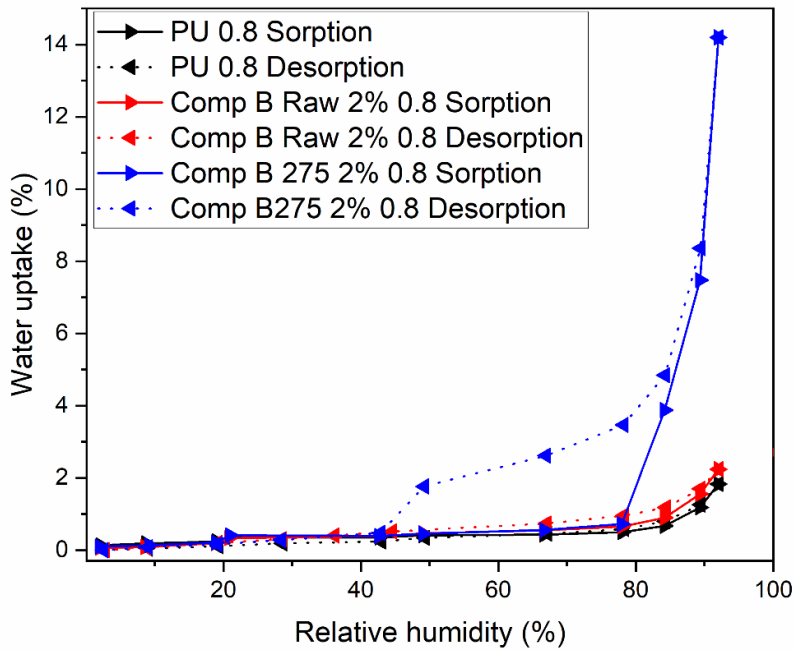


Figure 101. DVS curves of the PU 0.8 and the beech composite samples at 2% and 0.8 NCO/OH ratio.

The first thing to notice in DVS curves (Figure 101) is that while both the raw wood composite and the PU have low and similar maximum water uptakes (2.24% and 1.83%, respectively), the treated wood composite's is 14.19%, nearly ten times higher, this difference will be seen in all the other treated wood composites, probably caused by the fact that the treatment temperatures used in this works are closer to the temperature of carbonization than to light pyrolysis, but still retaining the hygroscopic cellulose's -OH groups made more available for the increased porosity. By the DVS curves of the PU, it can be seen that the polymeric matrix of composites is hydrophobic, and the addition of raw wood, which is highly hygroscopic, only increased the water uptake in 0.41%. That probably happened because, despite the raw wood hygroscopicity, the wood's surface is completely covered by the hydrophobic matrix and the little increase in water uptake is most likely caused by an increase in microporosity in the final product, which caused a small increase in water adsorption by micropore filling. From the literature, it is known that treated wood is also hydrophobic (15), and the works of Bengang *et al.* (2023) (123) showed that the water uptake of wood decrease with the increasing thermal treatment temperature to a certain limit. This drastic increase in water uptake is likely due to the increase in mesoporosity in the sample because, as previously explained, after the micropore filling and

monolayer adsorption in the sample, liquid-like water can condense inside mesopores and smaller macropores in a process called capillary condensation, which could cause a much bigger increase in water uptake compared to the micropore filling.

The increased hygroscopicity is in accordance with the works of Dias Junior *et al.* (2016) (125), who have shown that the charcoal hygroscopicity increases with the treatment temperature. The higher porosity and hygroscopicity of the woods treated at high temperatures used in this works might explain the increase of mesoporosity in the final composite. It is known that the reaction of isocyanate and water in PU generates CO₂ (63), which causes the polymer's porosity. The Higher availability of water caused the increased porosity might expose the isocyanate to bound water that was previously inaccessible in the depths of the wood structure, leading to a higher CO₂ formation, ultimately causing a higher water uptake in the treated wood composite samples. The total water uptake, however, is still relatively low when compared with hygroscopic materials, such as raw wood.

5.10.3 Beech 2% 1.0

Figure 102 shows the DVS curves of the PU 1.0 and the beech composite samples at 2% and 1.0 NCO/OH ratio.

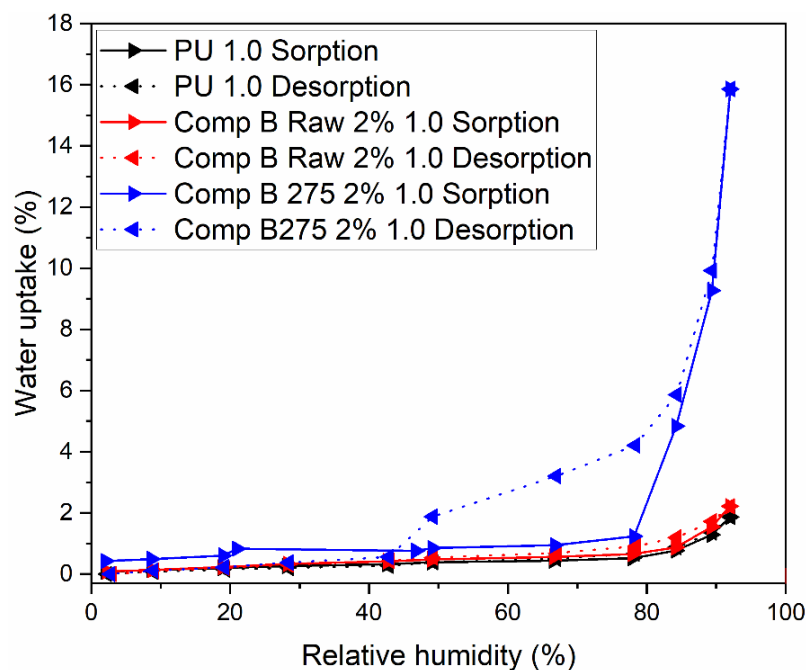


Figure 102. DVS curves of the PU 1.0 and the beech composite samples at 2% and 1.0 NCO/OH ratio.

Once again, the uptake of the Comp B275 2% 1.0 (15,86%) is much higher than the uptake of the PU 1.0 and Comp B Raw 2% 1.0 (1.86% and 2.21%, respectively), likely for the same reasons discussed for the Figure 101.

5.10.4 Beech 2% 1.2

Figure 103 shows the DVS curves of the PU 1.2 and the beech composite samples at 2% and 1.2 NCO/OH ratio.

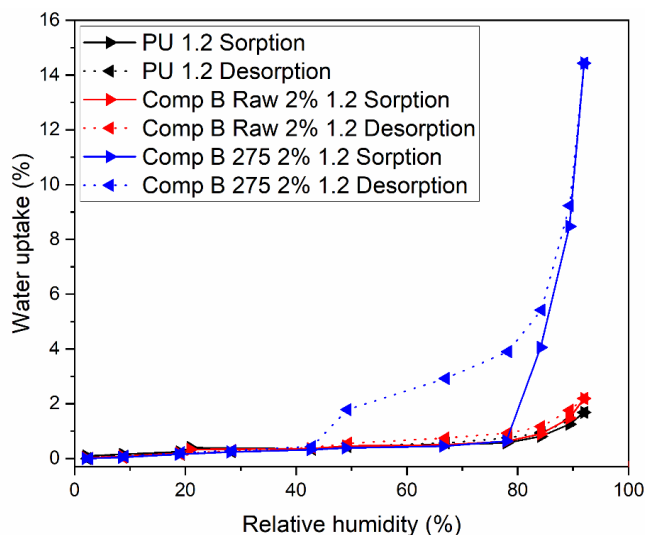


Figure 103. DVS curves of the PU 1.2 and the Beech composite samples at 2% and 1.2 NCO/OH ratio.

In this NCO/OH ratio, the Comp B 275 2% 1.2's water uptake is 14.43%, lower than the Comp B 275 2% 1.0's by 1.43%, while the raw wood composite had a maximum water uptake of 2.19%, lower than the equivalent sample with the 1.0 NCO/OH ratio.

For the composites of 2% beech, the 1.0 sample had the highest total water uptake by around 10%, that could have been caused by the even quantity of NCO and OH not causing as much crosslinking than the other two NCO/OH ratios, which favors the formation of a polymeric matrix with a slightly higher mesoporosity which, as discussed, causes a higher water uptake in the sample by causing capillary condensation of water in them (120). The other two samples, PU and Comp B Raw 2%, didn't show any clear tendency of this kind.

5.10.5 Fir 2% 0.8

Figure 104 shows the DVS curves of the PU 0.8 and the fir composite samples at 2% and 0.8 NCO/OH ratio.

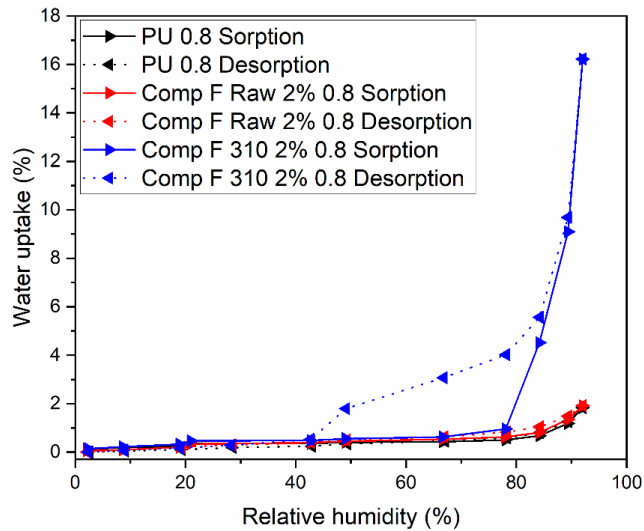


Figure 104. DVS curves of the PU 0.8 and the fir composite samples at 2% and 0.8 NCO/OH ratio.

In the case of the 2% fir composites and 0.8 NCO/OH ratio, the maximum water uptake of the raw and the treated wood samples are 1.91% and 16.22%, respectively. The treated wood sample is higher than the equivalent beech sample, by 2,03% but the raw wood sample is lower by 0.33%. The higher water uptake in the treated fir sample indicates that the added softwood better contributes to the formation of mesopores than the hardwood.

5.10.6 Fir 2% 1.0

Figure 105 shows the DVS curves of the PU 1.0 and the fir composite samples at 2% and 1.0 NCO/OH ratio.

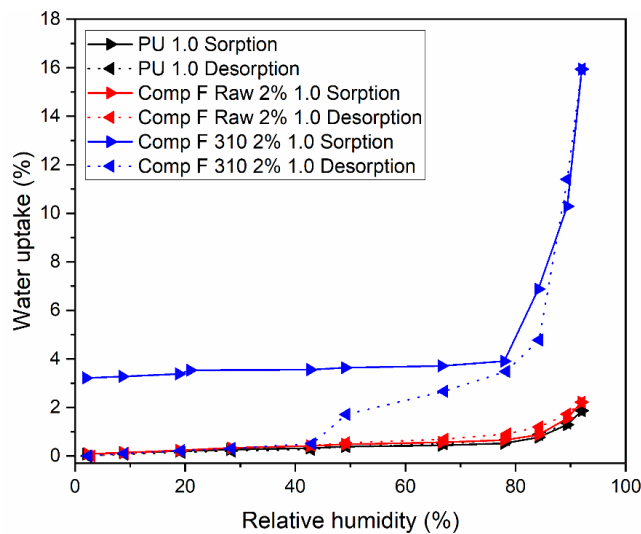


Figure 105. DVS curves of the PU 1.0 and the fir composite samples at 2% and 1.0 NCO/OH ratio.

From DVS curves (Figure 105), it can be seen that different from the other samples so far, the Comp F 310 2% 1.0 has a higher initial water uptake, at 3.21%, meaning the morphology of the sample can trap a higher quantity of water adsorbed in it at room humidity, which is actually higher than the maximum water uptake of all the PU and raw wood composite samples. The maximum water uptake of this sample is 15.94%, 1.75% higher than the equivalent beech composite sample this time. The raw wood composite, however, is nearly the same as that of the equivalent beech sample, being 0.08% lower, a value that could be attributed to experimental error.

5.10.4 Fir 2% 1.2

Figure 106 shows the DVS curves of the PU 1.2 and the fir composite samples at 2% and 1.2 NCO/OH ratio.

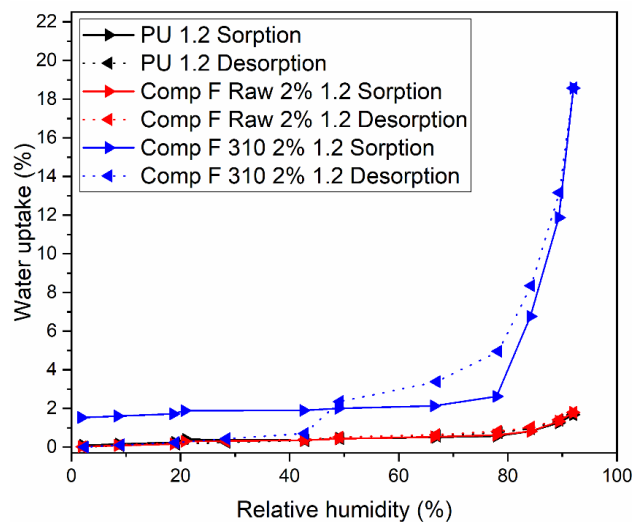


Figure 106. DVS curves of the PU 1.2 and the fir composite samples at 2% and 1.2 NCO/OH ratio.

In DVS curves (Figure 106), the treated wood sample, Comp F 310 2% 1.2 also has an initial water uptake considerably higher than the other samples in the plot, at 1.52%, which likely happened again, due to water adsorbed into the samples structure prior to the DVS curves. The maximum uptake for the samples is 2.01%, for Comp F Raw 2% 1.2 and 18.57, for Comp F 310 2% 1.2, the highest water uptake of the composites with 2% of wood.

Table 35 lists the maximum water uptakes of all DVS curves of polymers and composites with 2% of both raw and treated wood.

Table 35. Maximum water uptakes of the composite samples with 2% of wood.

		Water uptake (%)	
		Fir	Beech
Treated			
NCO/OH Ratio	0.8	16.22	14.19
	1.0	15.94	15.86
	1.2	18.57	14.43
Raw			
NCO/OH Ratio	0.8	2.01	2.24
	1.0	1.75	2.21
	1.2	1.91	2.19

The higher water uptake of each NCO/OH ratio is highlighted.

Table 35 shows that the water uptakes of the treated fir composites increased with the NCO/OH ratio, while the treated beech had a higher uptake in the 1.0 NCO/OH ratio. The treated fir composites also presented higher water uptakes than the treated beech in all the NCO/OH ratios. The water uptake of the raw beech composites decreases with the increasing NCO/OH ratio, which raw fir didn't show any clear tendency. Also, the raw fir composites showed higher water uptakes than the raw fir in all the NCO/OH ratios.

The treated fir samples presenting higher water uptakes is also in accordance to the works of Dias Júnior *et al.* (2016) (125), who has shown that the increasing treatment temperature increases the hygroscopicity of charcoal.

As explained at the beginning of this session, an equipment failure made it impossible to carry out this analysis on all samples with 5% wood.

5.10.5 Beech 5% 0.8

Figure 106 shows the DVS curves of the PU 0.8 and the Comp B Raw 5% and 0.8 NCO/OH ratio.

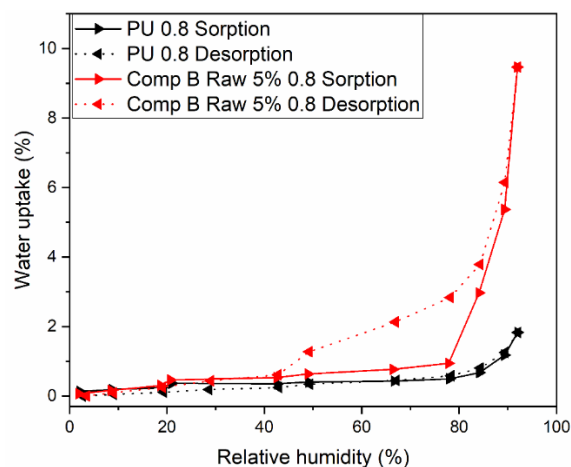


Figure 107. DVS curves of the PU 0.8 and the Comp B Raw 5% and 0.8 NCO/OH ratio.

DVS curves (Figure 107) show that with 5% of wood, the water uptake increases considerably when compared to the composites with 2% of raw wood, having reached 9.46%. Despite this high increase, likely caused by the increase of mesoporosity in the polymeric matrix (120), the value remains lower than water uptake of the treated wood composites with 2% of wood, which allows us to infer that the 5% treated wood composites would have higher water uptake values.

5.10.6 Beech 5% 1.0

Figure 107 represents the DVS curves of the PU 1.0 and the Comp B Raw 5% 1.0.

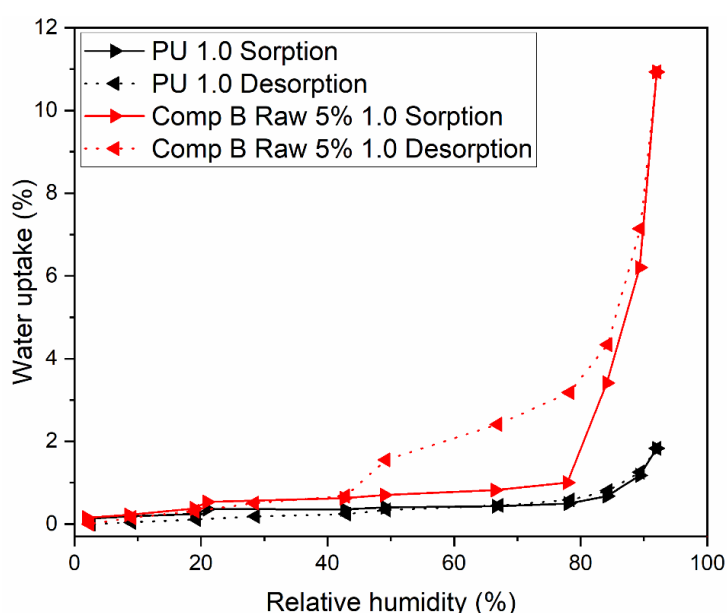


Figure 108. DVS curves of the PU 1.0 and the Comp B Raw 5% and 1.0 NCO/OH ratio.

As seen in the Figure 108, the Comp B Raw 5% 1.0 also had a much higher water uptake than the equivalent 2% composite, at 10.93%, 1.46% higher than the Comp B Raw 5% 1.0, likely due to a slightly higher mesoporosity (120).

5.10.7 Beech 5% 1.2

DVS curves of the PU 1.2 and the Comp B Raw 5% 1.2 are presented in Figure 109.

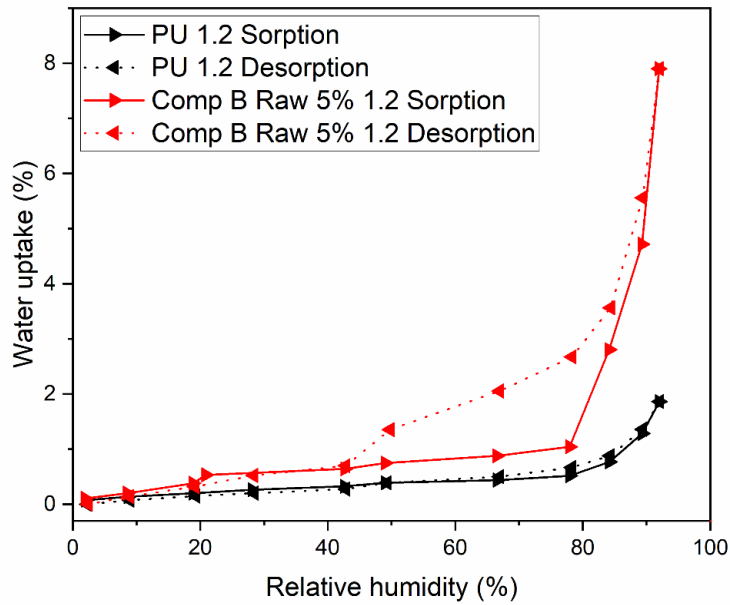


Figure 109. DVS curves of the PU 1.2 and the Comp B Raw 5% and 1.2 NCO/OH ratio.

In the Comp B Raw 5% 1.2, the water uptake, despite also clearly higher than the equivalent 2% composite, its maximum water uptake is 7.90%, being lower than the previous composite by 3.03%, similar to what was seen with the 2% treated beech composites, where the 1.0 ratio showed the highest water uptake, having a decrease in the 1.2 sample, which was still higher than that of the 0.8 sample.

5.10.8 Fir 5% 0.8

DVS curves of the PU 0.8 and the Comp B Raw 5% 0.8 are presented in Figure 110.

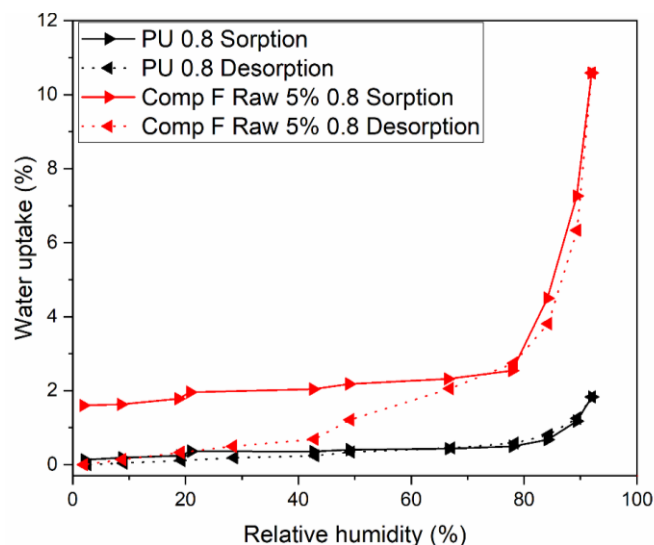


Figure 110. DVS curves of the PU 0.8 and the Comp F Raw 5% and 0.8 NCO/OH ratio.

The composite in DVS curves (Figure 110) has also presented a higher initial water uptake at 1.60%, similar to the initial water uptake of, Comp F 310 2% 1.2, though a little higher. Its maximum uptake, 10.58%, is 1.12% higher than the equivalent beech composite.

5.10.9 Fir 5% 1.0

Figure 111 shows the DVS curves of the PU 1.0 and the Comp F Raw 5% 1.0.

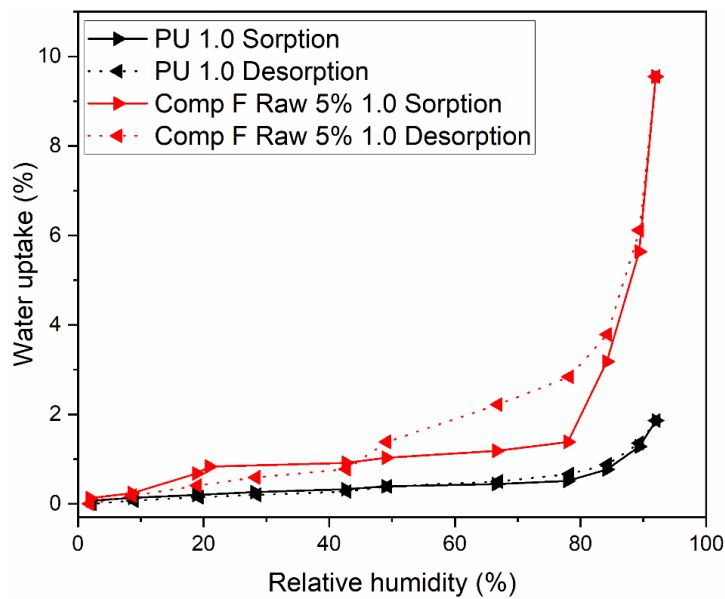


Figure 111. DVS curves of the PU 1.0 and the Comp F Raw 5% and 1.0 NCO/OH ratio.

In the DSV curves (Figure 111) unlike the DVS curves in Figure 105, the composite presents a low initial water uptake. With a maximum water uptake of 9.55%, it has reached a lower uptake than the sample Comp F Raw 5% 0.8, by 1.03%.

5.10.10 Fir 5% 1.2

Figure 112 shows the DVS curves of the PU 1.2 and the Comp F Raw 5% 1.2.

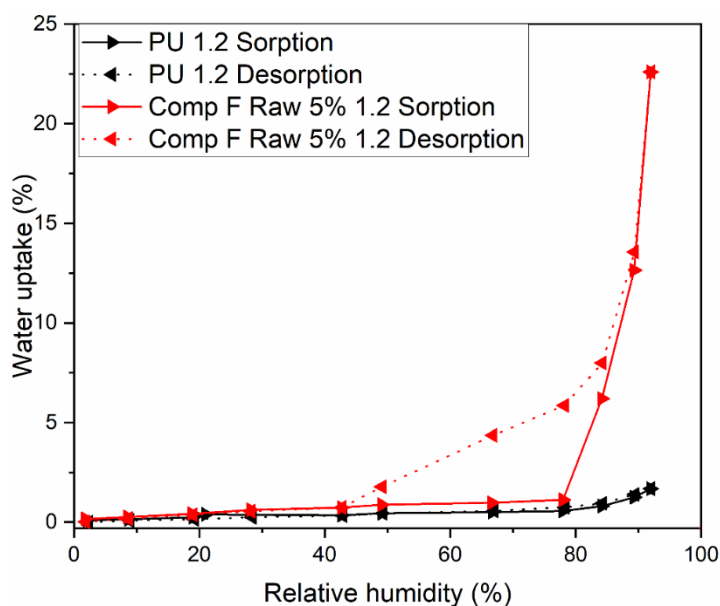


Figure 112. DVS curves of the PU 1.2 and the Comp F Raw 5% and 1.2 NCO/OH ratio.

At a maximum water uptake of 22.6%, the Comp F Raw 1.2 sample presented not only a higher uptake than the equivalent beech sample but also the highest water uptake of all samples tested by DVS in this work, including the treated wood composites, which had reached considerably higher water uptakes when compared to the equivalent raw wood composites at 2%. Despite the failure in the equipment prevented the DVS analyses of the composites with 5% of wood treated, and by the behavior already observed, it can be inferred that they would present higher water uptakes than the raw wood composites.

Unfortunately, the CV samples could not be analyzed because of the mentioned failure in the DVS equipment, but it can be inferred by the previous results that the treated CV composites would have a water uptake between those of the treated fir and treated beech.

5.11 Conclusions

The properties of the used vegetable oil were close to the ones measured in previous works by the author, indicating a certain reproducibility in the results.

The epoxide and polyol have been confirmed by FTIR and ^1H NMR spectroscopy, though the polyol was better seen in the FTIR spectrum and the OH index calculated, 85.57 mg KOH/g, was low as expected for a polyol made from a vegetable oil with few unsaturations, but it is still possible that the reaction has been incomplete.

The PU synthesized with the three different NCO/OH ratio have shown real similar FTIR spectra, especially the ones with 1.0 and 1.2 ratio, indication that past 1.0, the excessive isocyanate added remains as excess, without greatly altering the chemistry of the product. This was further confirmed by the presence of PU lumps on the PU 1.2 sample, which are probably higher density PU lumps formed before the homogenization of the mixture by the mechanical stirring, this has probably led to localize less density PU regions in the sample too.

For the composites, particle sizes smaller than 250 μm were chosen not only for the literature data indicating that they create more mechanically resistant composites, but also because the FTIR data of the ground wood at different particle sizes have shown a greater abundance of surface -OH in treated beech and, even though the surface -OH of fir and CV were not the highest in the smallest particle sizes, the results were close enough for them to still be chosen.

The composites' FTIR spectra, for most parts, showed the same tendency seen in the PU samples, with the C-N peak being nearly equal in the samples with NCO/OH ratio of 1.0 and 1.2, but being smaller for the 0.8 ratio, with no big differences being shown the wood content and thermal treatment of the wood, except for the CV composites.

In the raw CV composites, both 2% and 5% raw wood composites showed noticeable differences between the C-N peak of the 1.0 and 1.2 NCO/OH ratio samples and didn't show as much residual -OH as the other samples. This might indicate that this wood is rich enough in hemicelluloses to induce a bigger formation of PU, causing the excessive NCO in the 1.2 NCO/OH ratio to be a reagent instead of an excess, this richness in hemicelluloses might be what causes the higher density of the wood when comparing to the other two species studied. This tendency, though, was not observed in the treated CV composites, probably caused by the loss of hemicellulose in the thermal treatment.

Regarding the TGA and DTG curves, the PU 1.0 sample presented the three usual degradation peaks described in the literature, representing the breaking of urethane bonds, breaking of rigid segments and breaking of soft segments. PU 0.8 and 1.2 both showed 4 degradation peaks, indicating that the uneven quantity of NCO and OH might have caused crosslinking that resulted in segments of intermediate rigidity and softness.

In most cases, the addition of wood to the PU caused the intermediate peaks to decrease, showing the presence of wood favors the formation of rigid and soft segments rather than the intermediate rigidities. Though this effect is not too noticeable in the 2% wood samples, it is easy to see in the 5% wood samples, especially at the 1.0 and 1.2 NCO/OH ratios. That might be caused because the increased presence of -OH that is “fixated” in the wood particles favors the formation of hard segments more than the flexible -OH groups in the polyol.

The 2% added wood in the composite didn't change much the TGA curves of the samples in both beech and fir, but the 5% addition caused a great separation between the PU, raw composite and treated composite samples.

One more thing to notice in the TGA curves is that in all of them, the PU sample, which is usually the one with less mass loss at lower temperatures, likely to the presence of fewer hard segments, at 400 °C to 450 °C has a behavior inversion and starting have higher mass loss values that likely happens because at that point the wood present in the composites prevents them from losing as much mass as the PU.

The results obtained by DMA analysis showed that the storage modulus was the same for all PU at room temperature, regardless of the molar ratio. However, at a temperature of 100 °C, PU with ratios 0.8 and 1.2 showed differences, but it is considered that they are comparable. With respect to T_{g1} is the lower temperature which is the soft segment of the polymer while T_{g2} is related to the higher temperature which is the hard segment of the polymer. PU 1.2 exhibits the maximum degree of flexibility within its soft segment while PU 1.0 has the strongest stiffness with the highest T_{g2} .

The DVS curves for the PU showed pretty similar results, with less than 2% of water uptake, which was expected as the polymeric matrix is hydrophobic.

The addition of raw wood at 2% did little to change the water uptake, but the composites with treated wood showed considerably higher water uptakes. That was probably caused by the intense treatment temperature, higher than the usual light pyrolysis used in thermal treatments, left the wood, especially fir, closer to charcoal than to thermally treated wood. The temperature treatment, though, was not high enough to destroy the celluloses, which was more exposed by the increased porosity caused by the treatment. This has also exposed bond water to the celluloses, that reacted with the isocyanate, creating composites with

higher porosity, leading to a higher water uptake, with treated fir showing the highest uptake as, according to the works of Dias Júnior *et al.* (2016) (125), the hygroscopicity of charcoal increased with the treatment temperature.

The samples with 5% raw wood all presented a much higher water uptake than the 2% raw composites. That could have been caused by the water adsorbed into the hygroscopic wood itself reacting with the isocyanate and leading to a higher mesoposity.

Despite the failure in the DVS equipment not allowing the analysis to be run on the 5% treated wood composites, it is possible to infer that the maximum water uptakes could be higher than those of the composites with 5% raw wood.

The CV composites couldn't not be analyzed by the DVS for the same reason, but they would not behave differently from the other composites, especially the composites of fir, since this wood has had closer results to fir than to beech.

Chapter 6

General Conclusions

6.1 General Conclusions

This work has made use of different indirect techniques to assert the best temperature to degrade the sample's hemicellulose with as little damage as possible to the cellulose. Many tests carried out allowed us to infer the correct temperatures to be 275 °C for beech, 310 °C for fir and 290 °C for CV, all those temperatures are higher than what is usually done, which is a light pyrolysis to induce some degradation of the wood's hemicelluloses, making it more resistant to xylophage fungi and other threats.

While the thermal treatments and wood fractioning done for beech and fir have match close results to the hemicelluloses content found in literature for those woods, the sparse data on CV wood made it not possible to follow the exact same line of thought as used for the European woods. Still, the same treatments were run as they presented satisfactory results.

The thermal treatments of both beech and fir led to expected results considering the hard and softwood nature, respectively, with softwood being more resistant to thermal degradation due to the fewer amount of hemicelluloses present in the biopolymer composition. Carvoeiro, on the other hand, despite literature data showing it presents hardwood characteristics, such as vessels, presented lower mass loss values, more similar to those of fir, a softwood. That can be explained as, being a tree from the Cerrado biome, it needs to be more naturally resistant to higher temperatures, as its biome is known for its seasonal fires.

These treated woods were weighted, had their density measured, sieved and the best particle size to use on the composites were determined by measuring the size of the -OH band in the normalized FTIR spectrum of each particle size, indicating that the smallest particle size (<250 µm) was the best not only for having the biggest amount of exposed -OH, but also having larger surface area and causing less tension in the polymeric matrix

The synthesis PU began with the epoxidation of MKO, previously done by the author, after which the epoxide was reacted with glycerol, using $\text{BF}_3(\text{Et}_2\text{O})$ as catalyst and ethyl ether as solvent. The polyol formation was confirmed by both FTIR and ^1H NMR spectra.

After the OH content of the polyol was determined, PU foams made with three different NCO/OH ratios synthesized and confirmed by FTIR and ^1H NMR spectra, though the difference between the PU 1.0 and PU 1.2 was diminutive, and the PU 1.2 presented localized high density PU regions, which had been previously assumed to be regions of unreacted NCO, but were proven by FTIR spectra to be high density PU.

The composites synthesis were confirmed by FTIR spectra, though the difference between equivalent composites were also small, with the difference in the C-N peaks in nearly all samples being considerably small, specially between the 1.0 and 1.2 ratio samples, except for the raw CV composites, which seemed to have enough hemicelluloses and cellulose to make the extra CNO from the 1.2 NCO/OH ratio into an actual reagent, instead of just excess. This different behavior did not happen with the treated wood CV composites.

The TGA and DTG curves showed great similarities between the composites made with raw and treated wood, with most of them presenting lower mass losses for the raw woods composite up to about 400 °C, presumably the point where thermal treatment happening inside the TGA equipment catches up with the treatment done on the Shimadzu oven. Overall, the increase in wood quantity and NCO/OH did not greatly affect the thermal properties of the composites, except for small increases in T_5 for raw wood composites

Another noticeable thing about the sample's DTG curves is that, while the PU 0.8 and 1.2 clearly presented 4 degradation peaks, the PU 1.0, in which there is an even quantity of -OH and NCO presented only 3, with but a principle of a 4th degradation peak, indicating a bigger regularity in int polymeric matrix, while both other PU for crosslinking that increase the complexity of the structure.

The results obtained by DMA analysis showed that the storage modulus don't present considerable results while compared to PU. PU 1.2 exhibits the maximum degree of flexibility within its soft segment while PU 1.0 has the strongest stiffness with the highest T_{g2} . The DMA results showed that all the PU samples are comparable in terms of storage modulus regardless of their NCO/OH ratio.

The DVS curves of the PU resulted in very little water uptake, and so did the 2% raw wood composites. The 2% treated wood composites, however shoed much bigger water uptakes, likely caused by the intense thermal treatment has

allowed the NCO to access bond water in the wood cellulose's now accessible due to the higher porosity of the material, which has resulted in the formation of enough CO₂ to give the composite a considerable amount of mesoporosity.

The 5% raw composites also showed considerably increased water uptake than the 2% raw wood composite, that is likely caused by isocyanate reacting to the water bond to the raw wood from its own hygroscopicity, allowing for the formation of enough mesoporosity to drive the water uptakes higher. Unfortunately, due to failure of the equipment, it was not possible to keep conducting the DVS analysis, but the acquired data allows us to infer that that the composites with 5% treated wood would have presented a much greater water uptake.

Chapter 7

Future works perspectives

- The BET analysis should be done both the polymers, composites and wood samples to calculate their porosity.
- The DVS of the rest of the samples should be done, as well as the DVS of the wood samples.
- The thermal treatments done in this work were made in 5 °C intervals, it would be interesting to run the treatment degree by degree to find the exact temperature for the hemicelluloses degradation.
- Alkaline treatments to remove hemicelluloses from the wood should be attempted and the resulting product should be used to make composites, and their properties should be compared to composites with thermally removed hemicelluloses.
- Other species of wood, both Brazilian and European should be tested.

Chapter 8

References

1. Upcycling plastic polymers into single-walled carbon nanotubes from a magnesia supported iron catalyst. *Carbon*. 2023 Nov 1;215:118492.
2. Idris SN, Amelia TSM, Bhubalan K, Lazim AMM, Zakwan NAMA, Jamaluddin MI, et al. The degradation of single-use plastics and commercially viable bioplastics in the environment: A review. *Environmental Research*. 2023 Aug 15;231:115988.
3. Breves AB. Modificação química dos óleos da polpa e da amêndoa da macaúba (*Acrocomia aculeata* (Jacq.) Lood. ex Mart) para a obtenção de epóxidos [Internet] [Master thesis]. University of Brasília; 2018 [cited 2024 Mar 13]. Available from: <http://repositorio2.unb.br/jspui/handle/10482/33218>
4. Garrison TF, Kessler MR. 3 - Plant Oil-Based Polyurethanes. In: Madbouly SA, Zhang C, Kessler MR, editors. *Bio-Based Plant Oil Polymers and Composites* [Internet]. William Andrew Publishing; 2016 [cited 2023 Nov 30]. p. 37–54. Available from: <https://www.sciencedirect.com/science/article/pii/B9780323358330000037>
5. Datta J, Głowińska E. Chemical modifications of natural oils and examples of their usage for polyurethane synthesis. *Journal of Elastomers & Plastics*. 2014 Feb 1;46(1):33–42.
6. Narine S, Kong X, Bouzidi L, Sporns P. Physical Properties of Polyurethanes Produced from Polyols from Seed Oils: I. Elastomers. *JAOCS, Journal of the American Oil Chemists' Society*. 2007 Dec 1;84:55–63.
7. Sharmin E, Zafar F, Akram D, Alam M, Ahmad S. Recent advances in vegetable oils based environment friendly coatings: A review. *Industrial Crops and Products*. 2015 Dec 15;76:215–29.
8. Statista [Internet]. [cited 2024 Mar 30]. Vegetable oils consumption worldwide 2023/24. Available from: <https://www.statista.com/statistics/263937/vegetable-oils-global-consumption/>
9. Amaral FP do [UNESP. Estudo das características físico-químicas dos óleos da amêndoa e polpa da macaúba [*Acrocomia aculeata* (Jacq.) Lodd. ex Mart]. 2007 Dec 17 [cited 2023 Dec 28]; Available from: <http://hdl.handle.net/11449/90468>
10. Souza F, Rodrigues F, Rodrigues L. EXTRAÇÃO ARTESANAL E CARACTERIZAÇÃO DO ÓLEO DE MACAÚBA (*Acrocomia aculeata*) EM DOIS ESTÁGIOS DE MATURAÇÃO | ENCICLOPEDIA BIOSFERA. *Enciclopedia Biosfera* [Internet]. 2013 Jul 1 [cited 2024 Mar 22];9(16). Available from: <https://conhecer.org.br/ojs/index.php/biosfera/article/view/3438>
11. Pimenta TV, Andrade MHC, Antoniassi R. Extração, neutralização e caracterização dos óleos do fruto da macaúba (*Acrocomia aculeata*) [Internet]. 2012 [cited 2024 Mar 22]. Available from: <https://www.embrapa.br/busca-de-publicacoes/>

/publicacao/946318/extracao-neutralizacao-e-caracterizacao-dos-oleos-do-fruto-da-macauba-acrocomia-aculeata

12. Zou G, Liang Z, Na X, Wang X, Chang Z, Yang Y, et al. Study of stress wave attenuation characteristics of particle ceramic embedded polyurethane composites. *Materials Today Communications*. 2023 Dec 1;37:107057.
13. Lopes MDM, Pádua M de S, Carvalho JPRG de, Simonassi NT, Lopez FPD, Colorado HA, et al. Natural based polyurethane matrix composites reinforced with bamboo fiber waste for use as oriented strand board. *Journal of Materials Research and Technology*. 2021 May 1;12:2317–24.
14. Kuranchie C, Yaya A, Bensah YD. The effect of natural fibre reinforcement on polyurethane composite foams – A review. *Scientific African*. 2021 Mar 1;11:e00722.
15. Rowell RM, editor. *Handbook of Wood Chemistry and Wood Composites*. 2nd ed. Boca Raton: CRC Press; 2012. 703 p.
16. Chang LC, Sain M, Kortschot M. Improvement in Compressive Behavior of Alkali-treated Wood Fibre-reinforced Bio-based Polyurethane Foams. *Cellular Polymers*. 2014 May 1;33:139–58.
17. Ben ZY, Samsudin H, Yhaya MF. Glycerol: Its properties, polymer synthesis, and applications in starch based films. *European Polymer Journal*. 2022 Jul;175:111377.
18. Calderon MJP, Dumancas GG, Gutierrez CS, Lubguban AA, Alguno AC, Malaluan RM, et al. Producing polyglycerol polyester polyol for thermoplastic polyurethane application: A novel valorization of glycerol, a by-product of biodiesel production. *Heliyon* [Internet]. 2023 Sep 1 [cited 2023 Nov 30];9(9). Available from: [https://www.cell.com/heliyon/abstract/S2405-8440\(23\)06699-9](https://www.cell.com/heliyon/abstract/S2405-8440(23)06699-9)
19. Machmudah S, Diono W, Kanda H, Goto M. Hydrolysis of Biopolymers in Near-Critical and Subcritical Water. In: *Water Extraction of Bioactive Compounds*. 2017. p. 69–107.
20. Ono K, Erhard A. *Ullmann's Encyclopedia of Industrial Chemistry*. In 2011.
21. Holtzaple MT. HEMICELLULOSES. In: *Encyclopedia of Food Sciences and Nutrition*. 2003. p. 3060–71.
22. Bryant ND, Pu Y, Tschaplinski TJ, Tuskan GA, Muchero W, Kalluri UC, et al. Transgenic Poplar Designed for Biofuels. *Trends Plant Sci*. 2020 Sep;25(9):881–96.
23. Ajuong E, Pinion LC. Degradation of Wood*. *Shreir's Corrosion*. 2010 Dec 31;2439–46.

24. Fu Z, Zhou Y, Gao X, Liu H, Zhou F. Changes of water related properties in radiata pine wood due to heat treatment. *Construction and Building Materials*. 2019 Sep 4;227:116692.
25. Lin BJ, Silveira EA, Colin B, Chen WH, Lin YY, Leconte F, et al. Modeling and prediction of devolatilization and elemental composition of wood during mild pyrolysis in a pilot-scale reactor. *Industrial Crops and Products*. 2019 May 10;131:357–70.
26. Bellon KR da R, Monteiro PHR, Klitzke RJ, Auer CG, Andrade AS de. BEHAVIOR OF THERMALLY MODIFIED WOOD TO BIODETERIORATION BY XYLOPHAGE FUNGI. *CERNE*. 2020 Dec 16;26:331–40.
27. Richa L, Colin B, Pétrissans A, Wolfgram J, Wallace C, Quirino RL, et al. Catalytic torrefaction effect on waste wood boards for sustainable biochar production and environmental remediation. *Environmental Pollution*. 2024 Jan 15;341:122911.
28. Zhou X, Li W, Mabon R, Broadbelt LJ. A Critical Review on Hemicellulose Pyrolysis. *Energy Technology*. 2017;5(1):52–79.
29. Abdo M, Flity H, Terrei L, Zoulalian A, Mehaddi R, Girods P, et al. An alternative wood pyrolysis model based on TGA and cone calorimeter tests. *Thermochimica Acta*. 2024 Jan 1;731:179646.
30. SHAFIZADEH F, CHIN PPS. Thermal Deterioration of Wood. In: *Wood Technology: Chemical Aspects* [Internet]. AMERICAN CHEMICAL SOCIETY; 1977 [cited 2024 Mar 22]. p. 57–81. (ACS Symposium Series; vol. 43). Available from: <https://doi.org/10.1021/bk-1977-0043.ch005>
31. Tian Y. Multi-distributed activation energy model for wood pyrolysis: modelling strategy applied to experimental kinetics of different particle sizes. *Universit'e Paris-Saclay*; 2021.
32. Prakash N, Karunanithi T. Kinetic Modeling in Biomass Pyrolysis – A Review. 2008;4(12):1627–36.
33. Burra KRG, Gupta AK. Modeling of biomass pyrolysis kinetics using sequential multi-step reaction model. *Fuel*. 2019 Feb 1;237:1057–67.
34. Lin YY, Chen WH, Colin B, Lin BJ, Leconte F, Pétrissans A, et al. Pyrolysis kinetics of potassium-impregnated rubberwood analyzed by evolutionary computation. *Bioresource Technology*. 2021 Jan 1;319:124145.
35. Carrier M, Loppinet-Serani A, Denux D, Lasnier JM, Ham-Pichavant F, Cansell F, et al. Thermogravimetric analysis as a new method to determine the lignocellulosic composition of biomass. *Biomass and Bioenergy*. 2011 Jan;35(1):298–307.
36. Matos PRR de. Utilização de óleos vegetais como bases lubrificantes. 2011 Jun 29 [cited 2024 Mar 22]; Available from: <http://repositorio2.unb.br/jspui/handle/10482/8755>

37. Chemistry (IUPAC) TIU of P and A. IUPAC - fatty acids (F02330) [Internet]. [cited 2024 Mar 22]. Available from: <https://goldbook.iupac.org/terms/view/F02330>
38. Sommerfeld M. Trans unsaturated fatty acids in natural products and processed foods. *Prog Lipid Res.* 1983;22(3):221–33.
39. Evaristo A, Grossi J, Carneiro A, Pimentel L, Motoike S, Kuki K. Actual and putative potentials of macauba palm as feedstock for solid biofuel production from residues. *Biomass and Bioenergy.* 2016 Feb 1;85:18–24.
40. Noreen A, Zuber M, Tabasum S, Zahoor AF. Bio-based polyurethane: An efficient and environment friendly coating systems: A review. *Progress in Organic Coatings.* 2016 Feb 1;91:25–32.
41. Rustan A, Drevon C. Fatty Acids: Structures and Properties. In 2005.
42. Voet D, Voet JG, Pratt CW. Fundamentos de Bioquímica - 4.ed.: A Vida em Nível Molecular. Artmed Editora; 2014. 1200 p.
43. Silva L, Fortes I, Sousa F, Pasa V. Biokerosene and green diesel from macauba oils via catalytic deoxygenation over Pd/C. *Fuel.* 2016 Jan 15;164:329–38.
44. del Río J, Evaristo A, Marques G, Martin-Ramos P, Martín-Gil J, Gutiérrez A. Chemical composition and thermal behavior of the pulp and kernel oils from macauba palm (*Acrocomia aculeata*) fruit. *Industrial Crops and Products.* 2016 Feb 6;84:294–304.
45. Navarro-Díaz H, Gonzalez S, Irigaray B, Vieitez I, Jachmanián I, Hense H, et al. Macauba oil as an alternative feedstock for biodiesel: Characterization and ester conversion by the supercritical method. *The Journal of Supercritical Fluids.* 2013 Jan 1;93.
46. <https://www.conab.gov.br/ultimas-noticias/5157-com-novo-recorde-producao-de-graos-na-safra-2022-23-chega-a-322-8-milhoes-de-toneladas> [Internet]. 2023 [cited 2024 Mar 23]. Available from: <https://www.conab.gov.br/ultimas-noticias/5157-com-novo-recorde-producao-de-graos-na-safra-2022-23-chega-a-322-8-milhoes-de-toneladas>
47. Fortes I, Baugh P. Pyrolysis–GC/MS studies of vegetable oils from Macauba fruit. *Journal of Analytical and Applied Pyrolysis.* 2004 Aug 1;72:103–11.
48. Melo PG de. Produção e caracterização de biodieseis obtidos a partir da oleaginosa macaúba (*Acrocomia aculeata*) [Internet]. Universidade Federal de Uberlândia; 2012 [cited 2024 Mar 23]. Available from: <https://repositorio.ufu.br/handle/123456789/17363>
49. Dos Santos RCM, Gurgel PC, Pereira NS, Breves RA, De Matos PRR, Silva LP, et al. Ethyl esters obtained from pequi and macaúba oils by transesterification with homogeneous acid catalysis. *Fuel.* 2020 Jan;259:116206.

50. Moreira SLS, Imbuzeiro HMA, Silvert C, Dietrich OHS, Pimentel LD, Fernandes RBA. Above- and below-ground carbon accumulation in cultivated macauba palm and potential to generate carbon credits. *Journal of Cleaner Production*. 2020 Aug 20;265:121628.
51. Moreira SLS, Pires CV, Marcatti GE, Santos RHS, Imbuzeiro HMA, Fernandes RBA. Intercropping of coffee with the palm tree, macauba, can mitigate climate change effects. *Agricultural and Forest Meteorology*. 2018 Jun 15;256–257:379–90.
52. Carvalho KJ de, Souza AL de, Machado CC. Macaúba - *Acrocomia aculeata* (Jacq.) Lood. ex Mart.: ecologia, manejo, silvicultura e tecnologia da macaúba. 2011 [cited 2024 Mar 24]; Available from: <http://www.bibliotecaflorestal.ufv.br/handle/123456789/11140>
53. McNutt J, He Q. Development of biolubricants from vegetable oils via chemical modification. *Journal of Industrial and Engineering Chemistry*. 2016 Feb 1;36.
54. Silva LN, Cardoso CC, Pasa VMD. Synthesis and characterization of esters from different alcohols using Macauba almond oil to substitute diesel oil and jet fuel. *Fuel*. 2016 Feb 15;166:453–60.
55. Evaristo AB, Grossi JAS, Pimentel LD, de Melo Goulart S, Martins AD, dos Santos VL, et al. Harvest and post-harvest conditions influencing macauba (*Acrocomia aculeata*) oil quality attributes. *Industrial Crops and Products*. 2016 Jul 1;85:63–73.
56. Penha FM, Rezzadori K, Proner MC, Zin G, Fogaça LA, Petrus JCC, et al. Evaluation of permeation of macauba oil and *n*-hexane mixtures through polymeric commercial membranes subjected to different pre-treatments. *Journal of Food Engineering*. 2015 Jun 1;155:79–86.
57. Rehghunadhan A. POLYURETHANE POLYMERS. 2017.
58. Borowicz M, Paciorek-Sadowska J, Isbrandt M. Synthesis and application of new bio-polyols based on mustard oil for the production of selected polyurethane materials. *Industrial Crops and Products*. 2020 Nov;155:112831.
59. Zhang R, Shi Q, Hu P, Ji J, Suo Z. Influence of castor oil-based bio-oil on the properties and microstructure of asphalt binder. *Construction and Building Materials*. 2023 Dec 8;408:133564.
60. Martinović N, Polak T, Ulrih NP, Abramovič H. Mustard Seed: Phenolic Composition and Effects on Lipid Oxidation in Oil, Oil-in-Water Emulsion and Oleogel. *Industrial Crops and Products*. 2020 Nov 15;156:112851.
61. Paraskar PM, Prabhudesai MS, Kulkarni RD. Synthesis and characterizations of air-cured polyurethane coatings from vegetable oils and itaconic acid. *Reactive and Functional Polymers*. 2020 Nov 1;156:104734.

62. Polyurethane Polymers: Composites and Nanocomposites - 1st Edition | Elsevier Shop [Internet]. 2017 [cited 2024 Mar 24]. Available from: <https://shop.elsevier.com/books/polyurethane-polymers-composites-and-nanocomposites/thomas/978-0-12-804065-2>
63. Clayden J, Greeves N, Stuart W. Organic Chemistry - Jonathan Clayden; Nick Greeves; Stuart Warren - Oxford University Press [Internet]. second edition. 2012 [cited 2024 Mar 24]. Available from: <https://global.oup.com/academic/product/organic-chemistry-9780199270293?cc=us&lang=en&>
64. Mokhtari C, Malek F, Manseri A, Caillol S, Negrell C. Reactive jojoba and castor oils-based cyclic carbonates for biobased polyhydroxyurethanes. *European Polymer Journal*. 2019 Apr 1;113:18–28.
65. Bagnato G, Iulianelli A, Sanna A, Basile A. Glycerol Production and Transformation: A Critical Review with Particular Emphasis on Glycerol Reforming Reaction for Producing Hydrogen in Conventional and Membrane Reactors. *Membranes (Basel)*. 2017 Mar 23;7(2):17.
66. Quispe CAG, Coronado CJR, Carvalho Jr. JA. Glycerol: Production, consumption, prices, characterization and new trends in combustion. *Renewable and Sustainable Energy Reviews*. 2013 Nov 1;27:475–93.
67. Attarbachhi T, Kingsley MD, Spallina V. New trends on crude glycerol purification: A review. *Fuel*. 2023 May 15;340:127485.
68. Vasiliev VV, Morozov EV. Advanced Mechanics of Composite Materials (Third edition). In: Vasiliev VV, Morozov EV, editors. *Advanced Mechanics of Composite Materials (Third Edition)* [Internet]. 3rd ed. Boston: Elsevier; 2013 [cited 2024 Jan 9]. p. 1–27. Available from: <https://www.sciencedirect.com/science/article/pii/B9780080982311000017>
69. Thyavihalli Girijappa YG, Mavinkere Rangappa S, Parameswaranpillai J, Siengchin S. Natural Fibers as Sustainable and Renewable Resource for Development of Eco-Friendly Composites: A Comprehensive Review. *Frontiers in Materials* [Internet]. 2019 [cited 2024 Jan 10];6. Available from: <https://www.frontiersin.org/articles/10.3389/fmats.2019.00226>
70. Azzouzi D, Rabahi W, Seddiri F, Hemis M. Experimental study of the fibres content effect on the heat insulation capacity of new vegetable composite plaster-pea pod fibres. *Sustainable Materials and Technologies*. 2020 Apr 1;23:e00144.
71. Magnusson M. A study of alternative Polyurethane films with hemicelluloses. Preparation, characterization and methods [Internet] [Bachelor of science thesis]. Chalmers University of Technology; 2017. Available from: <https://odr.chalmers.se/server/api/core/bitstreams/b86fe661-7f1a-41ca-8cb1-7e63c2f177e2/content>
72. Editora Interciência [Internet]. 2006 [cited 2024 Mar 24]. LUBRIFICANTES E LUBRIFICAÇÃO INDUSTRIAL. Available from:

//www.editorainterciencia.com.br/index.asp?pg=prodDetalhado.asp&idprod=145

73. CPM - Programa de Certificação de Pessoal de Manutenção, Senai. 1997;
74. Mang T, Dresel W. *Lubricants and Lubrication*. 2007. 1 p.
75. Yu Q, Huang G, Cai M, Zhou F, Liu W. In situ zwitterionic supramolecular gel lubricants for significantly improved tribological properties. *Tribology International*. 2015 Nov 1;95.
76. Suhane A, Sarviya RM, Siddiqui AR. Prospects of Vegetable Oils as Lubricant in Crop Cutter and Harvesting Machines. *Materials Today: Proceedings*. 2018 Jan 1;5(9, Part 3):20513–7.
77. Salimon J, Salih N, Yousif E. Chemically modified biolubricant basestocks from epoxidized oleic acid: Improved low temperature properties and oxidative stability. *Journal of Saudi Chemical Society*. 2011 Jul 1;15:195–201.
78. Chen X, Xu R, Xu Y, Hu H, Pan S, Pan H. Natural adsorbent based on sawdust for removing impurities in waste lubricants. *J Hazard Mater*. 2018 May 15;350:38–45.
79. Zainal NA, Mohd Zulkifli NW, Gulzar M, Masjuki HH. A review on the chemistry, production, and technological potential of bio-based lubricants. *Renewable and Sustainable Energy Reviews*. 2018 Feb 1;82:80–102.
80. Mène-Saffrané L. Vitamin E Biosynthesis and Its Regulation in Plants. *Antioxidants*. 2018 Jan;7(1):2.
81. Bart JCJ, Gucciardi E, Cavallaro S. *Biolubricants science and technology*. Cambridge, UK: Woodhead Publishing Limited; 2013. 1 p. (Woodhead Publishing series in energy).
82. Rios Í, Cordeiro J, Arruda T, Rodrigues F, Uchoa A, Luna FM, et al. Chemical modification of castor oil fatty acids (*Ricinus communis*) for biolubricant applications: An alternative for Brazil's green market. *Industrial Crops and Products*. 2019 Dec 1;145:112000.
83. Nagy K, Kerrihard A, Beggio M, Craft B, Pegg R. Modeling the impact of residual fat-soluble vitamin (FSV) contents on the oxidative stability of commercially refined vegetable oils. *Food Research International*. 2016 Mar 1;84.
84. Maiorano G, Angwech H, Di Memmo D, Wilkanowska A, Mucci R, Abiuso C, et al. Effects of intramuscular Vitamin E multiple injection on quality, oxidative stability and consumer acceptability of meat from *Laticauda* lambs fed under natural rearing conditions. *Small Ruminant Research*. 2016 May 1;139.
85. Fritsche S, Wang X, Jung C. Recent Advances in our Understanding of Tocopherol Biosynthesis in Plants: An Overview of Key Genes, Functions,

and Breeding of Vitamin E Improved Crops. *Antioxidants* (Basel). 2017 Dec 1;6(4):99.

86. Kumar R, Hu F, Hubbell CA, Ragauskas AJ, Wyman CE. Comparison of laboratory delignification methods, their selectivity, and impacts on physiochemical characteristics of cellulosic biomass. *Bioresource Technology*. 2013 Feb 1;130:372–81.
87. Comitato R, Ambra R, Virgili F. Tocotrienols: A Family of Molecules with Specific Biological Activities. *Antioxidants* (Basel). 2017 Nov 18;6(4):93.
88. Miyake Y, Yokomizo K, Matsuzaki N. Rapid determination of iodine value by ¹H nuclear magnetic resonance spectroscopy. *J Amer Oil Chem Soc*. 1998 Jan 1;75(1):15–9.
89. Andrade Breves R, Ajiola D, de Vasconcelos Vieira Lopes R, Quirino RL, Colin B, Petrissans A, et al. Bio-Based Polyurethane Composites from Macauba Kernel Oil: Part 1, Matrix Synthesis from Glycerol-Based Polyol. *Journal of Composites Science*. 2024 Sep;8(9):363.
90. Leveneur S, Zheng J, Taouk B, Burel F, Wärnå J, Salmi T. Interaction of thermal and kinetic parameters for a liquid-liquid reaction system: Application to vegetable oils epoxidation by peroxy-carboxylic acid. *Journal of the Taiwan Institute of Chemical Engineers*. 2014;45(4):1449–58.
91. Rubio M, Ramírez-Galicia G, López-Nava LJ. Mechanism formation of peracids. *Journal of Molecular Structure: THEOCHEM*. 2005 Aug;726(1–3):261–9.
92. Rocha TLAC, Schuster RH, Jacobi MM, Samios D. Estudo da modificação química de polidienos do tipo SBR e BR. *Polímeros*. 2004 Dec;14:318–21.
93. ASTM D1193-06(2018) 15.3.2018 | technical standard | MyStandards [Internet]. 2018 [cited 2024 Mar 24]. Available from: https://www.mystandards.biz/standard/astm-d1193-06_2018-15.3.2018.html
94. International Standard. ISO 6886: Animal and vegetable fats and oils - determination of oxidative stability (accelerated oxidation test) [Internet]. 2016 [cited 2024 Mar 30]. Available from: <https://www.iso.org/standard/41434.html>
95. Blaschek H, Ezeji T. Chapter 7 Science of Alternative Feedstocks - FarmDoc - University ... [Internet]. 2012 [cited 2024 Mar 24]. Available from: <https://www.yumpu.com/en/document/view/5881789/chapter-7-science-of-alternative-feedstocks-farmdoc-university->
96. Su P. Sorption of metal ions to wood, pulp and bark materials. [Turku]: Abo Akademi; 2012.
97. Ruxanda B, Teacă C, Spiridon I. Chemical modification of beech wood: Effect on thermal stability. *BioResources*. 2008 Jun 30;3.

98. Mária F, Elena O, Illa A. Comparative study of hemicelluloses extraction from beech and oak wood. *Wood Research*. 2013 Jan 1;58:543–54.
99. Kučerová V, Lagana R, Hýrošová T. Changes in chemical and optical properties of silver fir (*Abies alba* L.) wood due to thermal treatment. *Journal of Wood Science*. 2019 Dec 1;65.
100. Senila L, COSTIUG S, Becze A, Kovacs E, Kovacs E, Alexandra-Daniela S, et al. BIOETHANOL PRODUCTION FROM ABIES ALBA WOOD USING ADAPTIVE NEURAL FUZZY INTERFERENCE SYSTEM MATHEMATICAL MODELING. *Cellulose Chemistry and Technology*. 2020 Feb 20;54:53–64.
101. Júnior SB, Yared JAG, de Sousa VG, Narducci TS, Salomão R de P, Martorano LG. Tachigali vulgaris na Amazônia: retrospectiva de pesquisas com plantios experimentais. 2021;
102. Faria MCG de, Neto C de M e S, Lima PAF, Chagas MP, Filho MT, Junior CRS. Brazilian cerrado species: wood characteristics. *Bioscience Journal*. 2020 May 25;36(4):1335–52.
103. matthews james, Himmel michael, Crowley M. Conversion of cellulose I α to I β via a high temperature intermediate (I-HT) and other cellulose phase transformations. *Cellulose*. 2012 Feb 1;19:297–306.
104. Shaikh H, Anis A, Poulouse A, Al-Zahrani S, Madhar N, Alhamidi A, et al. Isolation and Characterization of Alpha and Nanocrystalline Cellulose from Date Palm (*Phoenix dactylifera* L.) Trunk Mesh. *Polymers*. 2021 Jun 7;13:1893.
105. Pavia D.P L GM, Kriz GS, Vyvyan JR. Introdução à espectroscopia . Tradução da quarta edição norte americana. 4th Nort American. Vol. single volume. cengage Learning; 2010.
106. Monteavaro LL, da Silva EO, Costa APO, Samios D, Gerbase AE, Petzhold CL. Polyurethane networks from formiated soy polyols: Synthesis and mechanical characterization. *Journal of the American Oil Chemists' Society*. 2005;82(5):365–71.
107. Quirino RL, Da Silva TF, Payne A, De V. V. Lopes R, Paterno LG, Sales MJA. Synthesis and Thermomechanical Properties of Polyurethanes and Biocomposites Derived from Macauba Oil and Coconut Husk Fibers. *Coatings*. 2015 Sep;5(3):527–44.
108. Arjunan V, Anitha R, Thirunarayanan S, Mohan S. Simulations on the structure, vibrations and electronic properties of 1,2-epoxy-3-phenoxy propane and 1,2-epoxy-3-(p-tolyloxy)propane by FT-IR, FT-Raman, FT-NMR and DFT methods. *Chemical Data Collections*. 2017 Dec;11–12:139–67.
109. Sideridou I, Vouvoudi E, Papadopoulos G. Epoxy polymer Hxtal NYL-1™ used in restoration and conservation: Irradiation with short and long

wavelengths and study of photo-oxidation by FT–IR spectroscopy. *Journal of Cultural Heritage*. 2015 Oct 1;18.

110. Popescu R, Diana C, Dinca OR, Marinescu A, Stefanescu I, Roxana I. Discrimination of vegetable oils using NMR spectroscopy and chemometrics. *Food Control*. 2015 Feb 1;48:84–90.
111. Erhan S, Sharma B, Liu Z, Adhvaryu A. Lubricant Base Stock Potential of Chemically Modified Vegetable Oils. *Journal of agricultural and food chemistry*. 2008 Oct 1;56:8919–25.
112. Lopes R de VV. Poliuretanas obtidas a partir dos óleos de linhaça (*Linum usitatissimum* L.) e maracujá (*Passiflora edulis* Sims f. *flavicarpa* Degener). 2015 Sep 24 [cited 2024 Mar 25]; Available from: <http://repositorio2.unb.br/jspui/handle/10482/18544>
113. Traquisa. Technical data sheet for castor oil [Internet]. 2023. Available from: https://www.traquisa.com/contenido/fichas/Technical-data-sheet-of-blown-Castor-oil-75_85-p.pdf
114. ASTM D5155-96 - Standard Test Methods for Polyurethane Raw Materials Determination of the Isocyanate Content of Aromatic Isocyanates [Internet]. [cited 2024 Apr 7]. Available from: <https://standards.iteh.ai/catalog/standards/astm/8b23690e-3889-41c6-b693-d698240ce1f6/astm-d5155-96>
115. Dai Z, Jiang P, Lou W, Zhang P, Bao Y, Gao X, et al. Preparation of degradable vegetable oil-based waterborne polyurethane with tunable mechanical and thermal properties. *European Polymer Journal*. 2020 Oct 5;139:109994.
116. Durand S, D'Orlando A, Mougnyard L, Bourmaud A, Beaugrand J. Combining infrared and Raman spectra to assess MDI localization in novel flax-reinforced automotive composites. *Composites Part C: Open Access*. 2023 Oct;12:100382.
117. Jaya H, Omar MF, Md Akil H, Arifin Ahmad Z, Zulkepli NN. Effect of Particle Size on Mechanical Properties of Sawdust-High Density Polyethylene Composites under Various Strain Rates. *BioResources*. 2016 Jun 20;11(3):6489–504.
118. Coutinho FMB, Delpech MC. Degradation profile of films cast from aqueous polyurethane dispersions. *Polymer Degradation and Stability*. 2000 Jan;70(1):49–57.
119. Saidpour H, Razmara M, Arunachalam S. DMA Investigation on Polyurethane. In Mepco Schlenk Engineering College, Sivakasi, India; 2008 [cited 2024 Apr 1]. Available from: <http://hdl.handle.net/10552/1027>
120. Sing KSW. Reporting physisorption data for gas/solid systems with special reference to the determination of surface area and porosity (Provisional). *Pure and Applied Chemistry*. 1982 Jan 1;54(11):2201–18.

121. Kamdem P, Pizzi AP, Jermannaud A. Durability of heat-treated wood. *Holz als Roh- und Werkstoff*. 2002 Feb 1;60:1–6.
122. Tjeerdsma BF, Boonstra MJ, Militz H. Thermal modification of non-durable wood species 2. Improved wood properties of thermal treated wood. In 98-06-14/19 Maastricht, The Low Countries; 1988 [cited 2024 Mar 31]. Available from: <https://www.irg-wp.com/irgdocs/details.php?928f2680-9e22-45f9-b0a1-0ddd090af5f0>
123. Zhang B. Hydrophobation du Bois traité thermiquement et stabilité en milieu humide. *Panneaux de particules, colles et finitions écocompatibles*. [Thèse docotoral]. Université de Lorraine; 2023.
124. Costa LJ, de Castro VR, Trugilho PF, Lana AQ, Oliveira AC, Lima MDR, et al. Physical–chemical properties and hygroscopicity of Brazilian metallurgical charcoal. *Wood Sci Technol* [Internet]. 2024 Feb 1 [cited 2024 Mar 31]; Available from: <https://doi.org/10.1007/s00226-024-01529-2>
125. Dias Júnior AF, Pirola LP, Takeshita S, Lana AQ, Brito JO, Andrade AM de. HIGROSCOPICITY OF CHARCOAL PRODUCED IN DIFFERENT TEMPERATURES. *CERNE*. 2016 Dec;22:423–30.

Chapter 9

Annex

Discontinued work results

9.1 Polyol T1 synthesis

Figure 113 shows the FTIR spectra obtained from the attempt to synthesize a polyol called Polyol P1.

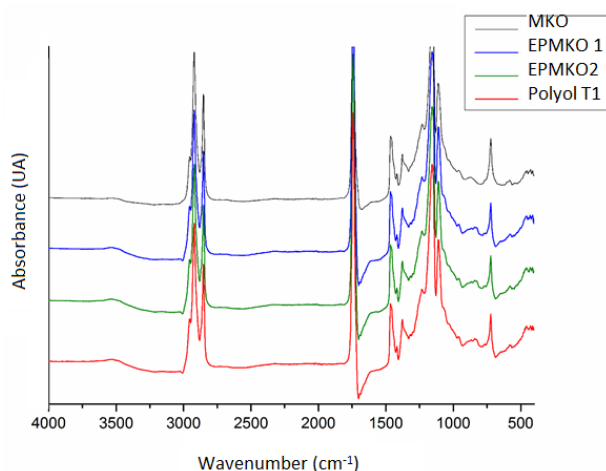


Figure 113. FTIR spectra obtained from the attempt to synthesize a polyol called Polyol P1 (105).

FTIR spectra (Figure 113) show 2 different epoxide samples, which were plotted in this figure, despite being identical, because both were used to try and synthesize the polyol but, as can be seen, there is no difference between the epoxides and the polyol, with the apparent peak 3500 cm⁻¹ being likely due to residual water in the product.

9.2 Polyol using zinc as a catalyst

Figure 114 presents the FTIR spectra obtained from the attempt to synthesize a polyol using zinc chloride as catalyst.

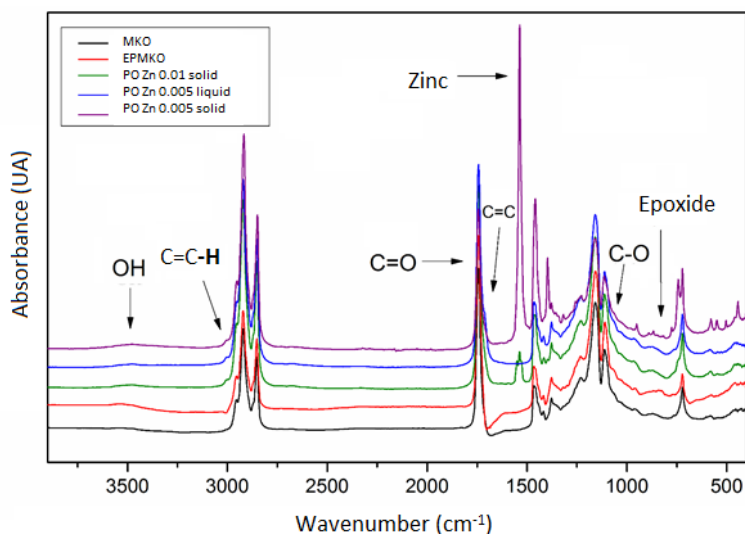


Figure 114. FTIR spectra obtained from the attempt to synthesize a polyol using zinc chloride as catalyst (105).

First, it is possible that the polyol was not formed, except for a very small band seen in the PO Zn 0.005 solid sample. The Zn 0.005 product was biphasic product, with a paste like solid. This solid phase presented what seen to a small quantity of -OH but, as seen in the FTIR spectra, the sample solid nature also had zinc stuck in it, so it is most likely that the -OH seen it just residual water stuck in the product.

9.3 α -tocopherol acetate additivation

Table 36 shows that the epoxidation increases the oxidative stability of the MKO in over 100%. The addition of α -tocopherol acetate to MKO, while it did increase the products oxidative stability, the stability gains were small, needing 20% (v/v) of α -tocopherol acetate to reach a better result equivalent to the epoxidations, showing that, while a promising way to increase a vegetable oil's oxidative stability, the stability gains are small and might not be adequate for some applications.

Table 36. Results of oxidative stability caused by the addition of α -tocopherol.

Sample	Oxidative stability (min)
MKO	31.51
EPMKO	72.00
TCMKO5	35.76
TCMKO10	44.08
TCMKO15	63.90
TCMKO20	79.83

DECLARAÇÃO DE ORIGINALIDADE DE DISSERTAÇÃO DE MESTRADO OU TESE DE DOUTORADO

Declaro que a presente dissertação/tese é original, elaborada especialmente para este fim, não tendo sido apresentada para obtenção de qualquer título e que identifique e cito devidamente todas as autoras e todos os autores que contribuíram para o trabalho, bem como as contribuições oriundas de outras publicações de minha autoria.

Declaro estar ciente de que a cópia ou o plágio podem gerar responsabilidade civil, criminal e disciplinar, consistindo em grave violação à ética acadêmica.

Brasília (dia de (mês) de (ano))

Assinatura do/a discente: Rodolfo ex. Breves

Programa: PPGQ (programa de pós-graduação em química)

Nome completo: Rodolfo Afonso de Breves

Título do Trabalho: Produção de material com portos por espuma de poliestireno e fibras de madeira tratadas termicamente

Nível: () Mestrado Doutorado

Orientador/a: Boles